Tuning the structural and magnetic properties of Sr_2FeReO_6 by substituting Fe and Re with valence invariant metals

Dissertation

zur Erlangung des Grades

„Doktor der Naturwissenschaften”

am Fachbereich Chemie, Pharmazie und Geowissenschaften

der Johannes Gutenberg-Universität Mainz

Alexandra Jung

geb. in Limburg

Mainz, 2006

Table of contents

1. Introduction

In the present era, called the “information age”, the storage of a constantly increasing amount of information on magnetic storage devices is a demanding task. Since the discovery of the “giant magnetoresistance” (GMR) effect by Grünberg and Baibich [1,2] and the introduction of GMR based magnetic read heads to the market in 1998, the areal density of data recorded with magnetic media increased by about 100 % per year. [3] The discovery of the GMR effect is the technological keystep to miniaturised data storage in mobile multimedia systems.

Magnetoresistance in general is the change of the electrical resistance of a conductor upon application of a magnetic field. The “giant magnetoresistance” effect (GMR) was discovered on Fe/Cr multilayers. [1,2,4,5] The coupling of metallic ferromagnetic (Fe) layers across non ferromagnetic metallic (Cr) layers induces an antiferromagnetic coupling between the successive Fe layers. The resistance of this multilayer system depends on the relative alignment of the Fe spins in different layers to each other. Without application of an external magnetic field, two successive Fe layers are antiparallel arranged. Majority electrons of one Fe layer cross the Cr interlayer but they are scattered at the Cr/Fe layer interface because they would be minority electrons in the next Fe layer. (Fig. 1) Application of a magnetic field large enough to align the spins in consecutive Fe layers parallel to the magnetic field (usually several Tesla) drastically reduces the resistivity of the multilayer system. Now, the majority electrons of one Fe layer are hardly scattered at the boundary to the next Fe layer because they are also majority electrons there. (Fig. 1)

Fig. 1 Scattering paths of electrons in simple GMR multilayers, FM1 and FM2 represent the two ferromagnetic layers, NM represents the non ferromagnetic layer. [5]

For the application of the GMR effect in magnetic read-heads, magnetic field sensors and field strength sensors, GMR multi-layer devices are built in a different way. A soft magnetic metallic layer is separated from a hard magnetic metallic layer by a non-magnetic metallic layer which inhibits coupling between the ferromagnetic ones. Thus, the magnetization of the spins in the soft ferromagnetic layer can be aligned parallel to a low magnetic field whereas high magnetic fields are needed to align the spins in the hard magnetic layer.

However, it is not possible to construct high density “random access memory” devices on the basis of GMR elements as the metallic GMR devices exhibit a low absolute resistivity. Consequently, the relative change of the resistivity upon application of a magnetic field is rather low (5-20 %). [4-6] Thus, the significant read-out of information at low working current is not given in GMR based RAMs. This problem was overcome by exchanging the non-ferromagnetic metallic layer separating the ferromagnetic metallic layers by an insulating layer, e.g. Al_2O_3. If this insulating interlayer is sufficiently thin (1-2 nm), electrons of the ferromagnetic layers can cross the Al_2O_3 tunneling barrier. The tunneling probability and the current flow depend on the relative orientation of the spins in the ferromagnetic layers to each other. Owing to the spin polarized band structure of ferromagnets, the spin direction of the conduction band of the ferromagnetic metallic layers depends on the direction of the external magnetic field. In the case of parallel alignment of the spins in two consecutive layers, the metallic spin states at the Fermi level (E_F) have the same orientation in both layers, e.g. spin down. (Fig. 2) A spin down electron of the ferromagnetic layer 1 (FM1) can tunnel into the ferromagnetic layer 2 (FM2) because FM2 offers empty spin down states at E_F. In case of an antiparallel arrangement, the spin down electrons of FM1 can not tunnel into FM2 because the FM2 spin down band is completely filled with electrons. (Fig. 2) Thus, the spin dependent tunneling of the spin polarized electrons of the ferromagnetic layers through the tunneling barrier determines the resistivity of the TMR device. Alignment of the ferromagnetic layers parallel to an applied magnetic field drastically decreases the resistivity of the device compared to the resistivity in case of antiparallel arrangement of the layers without magnetic field. This extrinsic effect is called “tunneling magnetoresistance” (TMR). The relative change of the resistance of a multilayer TMR device (ΔR/R) depends on the amount of spin polarization of the two layers (P1 and P2):

$$\frac{\Delta R}{R} = \frac{P_1 P_2}{1 - P_1 P_2}\,.$$

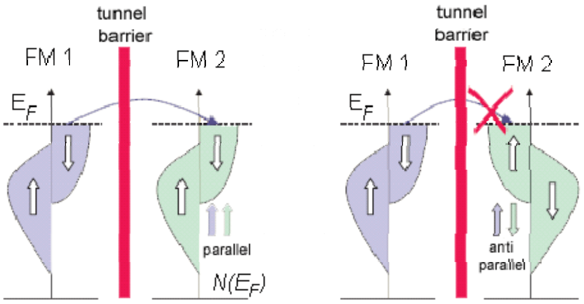

Fig. 2 Scheme of the tunnelling magnetoresistance effect of a TMR device in parallel (left) and in antiparallel (right) orientation. [5]

Based on TMR multilayer systems, fast and high density “magnetic random access memory” (MRAM) devices can be constructed to allow non-volatile magnetic data storage. The high absolute resistivity and high TMR effect of the TMR devices (> 50 %) enable the easy distinguishability of the two states (parallel and antiparallel corresponding to low and high resistivity, respectively) at a low working current.

However, the main disadvantage of the TMR devices is their multi-layer structure. [7,8] Building up extended arrays of multi-layer TMR elements is limited by the physical boundary conditions of thin layer technology. One possible solution to this problem is the use of materials exhibiting the "powder magnetoresistance" effect (PMR) in magnetoelectronic devices. [9,10] The PMR effect was discovered by Hwang et al. on $La_{0.67}Sr_{0.33}MnO_3$ in 1996. [11] This compound shows a large negative "colossal magnetoresistance" at very high magnetic field in the vicinity of T_C in single crystalline as well as polycrystalline samples. However, the polycrystalline samples additionally present a PMR effect of 20 % at low magnetic field (5 kOe) and 77 K (T_C = 240 K). In contrast to the intrinsic CMR effect, the PMR effect is extrinsic. It originates from the spin dependent tunneling of the charge carriers from one particle to the next one across the grain boundary. (Fig. 3) In other words, the electrons are localized within micrometer-size ferromagnetic particles which are separated by tunnel barriers. Without application of a magnetic field, the resulting magnetization of the individual particles is randomly distributed. Thus, electrons generally can not tunnel from one particle to another because the contiguous particle does not offer empty states near E_F in the appropriate spin direction. In a sufficiently large magnetic field, the electron spins align parallel to the magnetic field direction. Consequently, the metallic spin direction offering empty states near E_F is the same in every particle and electrons can tunnel from particle to particle. The PMR effect of a compound can be improved by introduction of insulating particles into the grain boundaries of the PMR material. This was first proven with samples of ferromagnetic CrO_2 particles diluted with insulating Cr_2O_3 particles. The measured MR effect increases from 29 % to 50 % at 5 K. [9,12] Generally, large magnetoresistance ratios are associated to large contact resistances between the particles in PMR materials.

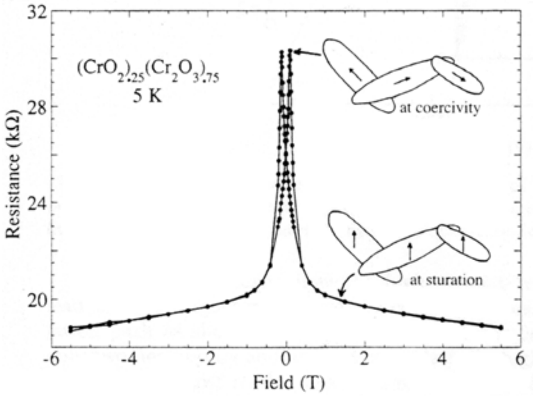

Fig. 3 PMR effect at the example of $(CrO_2)_{0.25}(Cr_2O_3)_{0.75}$. [9]

Thus, materials offering a large PMR effect at room temperature could be the solution to the problem of layer quality in TMR devices. [10] The difficulty of growing next to perfect layers of ferromagnetic metals and non-magnetic insulators could be overcome by using a ferromagnetic metallic powder with insulating barriers between the individual particles of the powder.

The essential features of materials exhibiting a large negative low-field magnetoresistance in polycrystalline samples are (i) a spin polarized half-metallic band structure and (ii) a wide existence range of the ferromagnetic phase up to temperatures at least two times above working temperature. [13-16] The first requirement corresponds to a band structure which is insulating in one spin direction and metallic in the other. In the insulating spin direction the electrons are localized at one/several atoms leading to a local magnetic moment at the corresponding atoms. In the metallic spin direction, the first requirement corresponds to a saddle point (the so-called van Hove-instability) (Fig. 4) close to the Fermi level. [16,17] The second requirement ensures that the PMR effect of a compound is large at room temperature. In the PMR materials studied up to now, the magnetoresistance effect depends on the temperature and is largest well below T_C (usually several hundred K below).

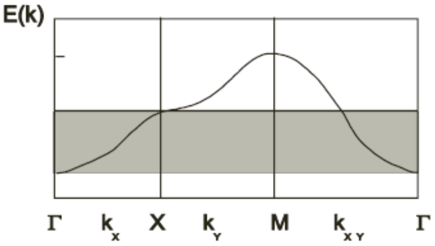

Fig. 4 Scheme of a band structure with a saddle point (van Hove-singularity) at point X. Occupied states are shaded in grey. [16]

This band model approach provides a practical tool for a systematic variation of magnetization, Curie temperature and PMR effect of the compound under consideration by specifying the relative energies of the van Hove-singularity and the Fermi level. The coincidence of van Hove-singularity and E_F can be achieved by adjusting the electron count of this compound to its optimum value by “doping” the parent compound with elements providing a different number of valence electrons.

The discovery of the powder magnetoresistance effect at room temperature and low magnetic fields in polycrystalline samples of the ferrimagnetic double perovskites Sr_2FeMoO_6 and Sr_2FeReO_6 has indicated the potential of compounds from the so-called double perovskite group for spintronic application. [18,19] The extreme flexibility of the double perovskite structure type in terms of symmetry and elements involved allows the substitution of Sr, Fe, Re and Mo by a wide variety of metal cations without risk of a phase separation. Therefore, the double perovskites Sr_2FeReO_6 and

Sr_2FeMoO_6 offer the possibility of varying the electron count of the parent compound systematically by means of "doping".

Double perovskites have the general formula $A_2MM'X_6$ where A represents a large electropositive ion, M and M' represent small transition metal or main group ions and X is commonly an oxide or a halide ion. [20-23] The ideal double perovskite structure can be described as a rock-salt arrangement of corner sharing MO_6 and $M'O_6$ with the A^{x+} cations situated in the 12-coordinate voids between the octahedra. (Fig. 5) The symmetry of the double perovskite can be estimated by means of the perovskite tolerance factor *t*. [24] The tolerance factor is an empiric equation which describes the interrelation between the perovskite structure and the associated ionic radii. For perovskites of the general formula AMX_3

$$t = \frac{r(A) + r(X)}{\sqrt{2}\left[r(M) + r(X)\right]}.$$

For $A_2MM'O_6$ double perovskites

$$t = \frac{r(A) + r(O)}{\sqrt{2}\left[\frac{r(M) + r(M')}{2} + r(O)\right]}.$$

The double perovskite is expected to crystallize in ideal cubic symmetry for $0.89 \le t \le 1$. Tetragonally or monoclinic distorted double perovskites are reported for $0.8 < t < 0.89$. Values $t < 0.8$ lead to crystallization in the illmenite structure type whereas $t > 1$ enforces hexagonal stacking.

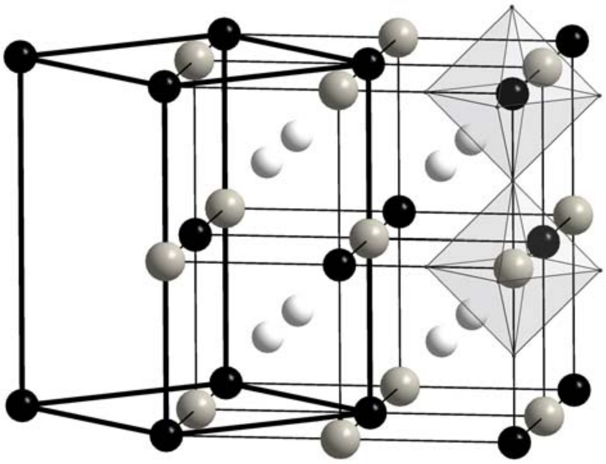

Fig. 5 Crystal structure of the double perovskite $A_2MM'O_6$; M (black), M' (dark grey), A (light grey), and O (corners of the octahedra); the cubic unit cell is drawn in thin black lines, the tetragonal unit cell in thick black lines.

In the ideal double perovskite the oxygen atoms are located on the connection line of the M and M' cations, i.e. the metal cations are bridged by their common oxygen atoms. This situation is valid for highly symmetric double perovskites in cubic or (partially) in tetragonal symmetry. Further reduction of symmetry (tetragonal or monoclinic) leads to a reduction of the M–O–M’ bond angle by tilting of the MO_6 and $M'O_6$ octahedra. Subsequently, the oxygen atoms are not located on the direct connection line of the M and M’ cations any more. Therefore, the electronic interaction of the M, M’ and O orbitals along the M–O–M’–O–M pathways is strongly influenced by symmetry reduction and tilting of the MO_6 and $M'O_6$ octahedra. In the course of this work, A will be restricted to alkaline earth metals. M and M’ consist mainly of 3*d* and 4*d*/5*d* transition metals or their charge and size equivalent main group metal cations, respectively. Moreover, only oxidic double perovskites will be considered in this study.

The first example of an ordered double perovskite (Fig. 5) exhibiting a large low-field magnetoresistance at room temperature is Sr_2FeMoO_6 which experiences a continuous structural phase transition around 400 K. Above 400 K the compound crystallizes in the cubic space group $Fm\bar{3}m$, a tetragonal distortion to space group $I4/m$ (a = 5.57 Å, c = 7.90 Å) is determined below 400 K. [18,25-30] This structural phase transition is in good agreement to the symmetry behaviour anticipated from the perovskite tolerance factor. Perovskites with $t = 0.899$ are supposed to show transitions from cubic to tetragonal symmetry. Owing to the small size difference between Fe^{3+} and Mo^{5+} cations ($r(Fe^{3+})$ = 65 pm, $r(Mo^{5+})$ = 61 pm [31]), antisite disorder on the Fe and Mo sites strongly influences the structural and magnetic properties of Sr_2FeMoO_6. Under carefully controlled synthesis conditions, antisite disorder can be reduced to approx. 10 %, but standard samples often exhibit up to 30 % of Fe/Mo disorder. [32-35]

From the point of view of electronic structure, ordered Sr_2FeMoO_6 is reported to be a typical ferrimagnetic half-metal. As the stoichiometry dictates that the oxidation numbers of Fe and Mo sum up to +8, two different distributions of the *d* electrons over the Fe and Mo sites are feasible: $Fe^{3+} \leftrightarrow Mo^{5+}$ and $Fe^{2+} \leftrightarrow Mo^{6+}$. Thus, six valence electrons need to be distributed over the Mo and Fe *d* orbitals. The density of states (DOS) reveals that five of these six electrons are localized in the Fe 3*d* spin up states. (Fig. 6) The corresponding Mo 4*d* spin up states do not host any electrons, i.e. the spin up direction is insulating. In contrast, the remaining electron is delocalized over the Mo 4*d* t_{2g} and Fe 3*d* t_{2g} spin down states which consequently form the conduction band. The corresponding e_g states are empty. In other words, the spins of the electrons localized at the Fe atoms couple ferromagnetically to each other and antiferromagnetically to the spins of the itinerant electrons distributed over the Fe and Mo sites. Therefore, the ferrimagnetism of the compound stems from the antiferromagnetic interaction of localized and itinerant electrons. The spin down electrons are delocalized by means of a Zener double exchange mechanism mediating the charge transfer of the 100 % spin polarized charge carriers from Mo to Fe over their common oxygen atoms. [18,25,36-39] However, the concept of half-metallic ferrimagnetism is only valid for ordered Sr_2FeMoO_6. Antisite disorder destroys the half-metallicity but the ferrimagnetism persists in spite of disorder. [35]

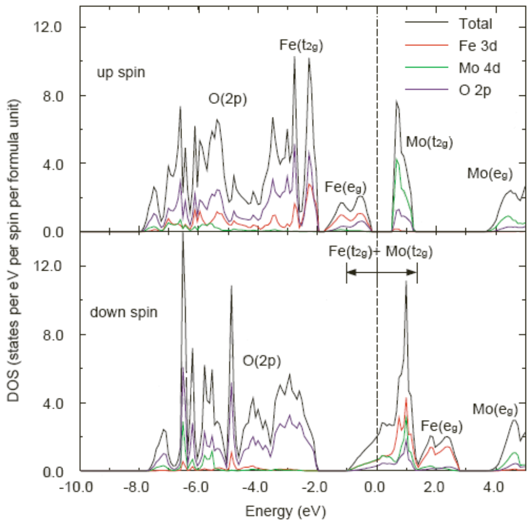

Fig. 6 DOS of Sr_2FeMoO_6 [18].

As a consequence of the charge transfer from Fe to Mo, the charge distribution over the Fe and Mo sites is difficult to determine and values between $\mu_{Fe} = 4.1\ \mu_B \leftrightarrow \mu_{Mo} = 0\ \mu_B$ and $\mu_{Fe} = 4.6\ \mu_B \leftrightarrow \mu_{Mo} = -0.6\ \mu_B$ leading to Fe valence states between 2+ and 3+ are reported. [25-27,32,40-42] However, within the ferrimagnetic model, any charge distribution between $Fe^{3+} \leftrightarrow Mo^{5+}$ and $Fe^{2+} \leftrightarrow Mo^{6+}$ leads to a theoretical saturation magnetization of M_S(theo.) = 4 μ_B/f.u. [18] Owing to the antisite disorder problem of Sr_2FeMoO_6, which leads to an antiferromagnetic alignment of the neighbouring Fe atoms via Fe–O–Fe superexchange pathways, the saturation magnetization is often limited to values of $M_S = 2.7\ \mu_B$/f.u. [28-30,34,38] The Curie temperature of ordered Sr_2FeMoO_6 (T_C = 420 K) is also reduced by the effects of the antisite disorder. [34,36,38]

The low field (< 10 kOe) magnetoresistance (MR) of Sr_2FeMoO_6 originates from a spin dependent tunneling process at the grain boundaries of the polycrystalline samples. (PMR effect) The introduction of insulating $SrMoO_4$ into the grain boundaries (onto the crystallite surface) by oxygenation of the sample strongly improves the insulating properties of the grain boundaries. Therefore, the negative low field MR, caused by intergrain tunnelling, increases. MR values between 42 % at 4.2 K and 70 kOe, 10 % at 15 K and 0 kOe and 10 % at 300 K and 70 kOe are reported.

The conductivity of Sr_2FeMoO_6 strongly depends on the annealing process of the corresponding sample because it is also dominated by intergrain spin polarized tunneling. The predicted metallic as well as semiconducting and insulating behaviour can be obtained by different annealing procedures. [18,25-27]

In order to improve the MR effect of Sr_2FeMoO_6 without influencing the magnetic sublattices directly, several ways of A site substitution were investigated. The simple substitution of Sr^{2+} by La^{3+} leads to a tetragonal to monoclinic (pseudo-orthorhombic) distortion for substitution levels between $0.2 < x < 0.4$ owing to the large size difference between Sr^{2+} and La^{3+} ($r(Sr^{2+}) = 140$ pm, $r(La^{3+}) = 103$ pm). The structural transition is accompanied by a strong increase of the antisite disorder. [43] It originates from a partial localization of the additional electrons at the Mo sites which reduces the charge difference between Fe and Mo and thus reduces the amount of antisite order. Thus, the coexistence of ferrimagnetic Fe–O–Mo–O–Fe and antiferromagnetic Fe–O–Fe interaction pathways enables a spin frustration and leads to a decrease of M_S. Moreover, $Sr_{2-x}La_xFeMoO_6$ converges from a soft to a hard magnet.

The highly ordered cubic compound $Ba_{1.6}Sr_{0.4}FeMoO_6$ was chosen to stabilize the symmetry of the double perovskite upon La^{3+} substitution. [44] As expected, symmetry and degree of antisite disorder are retained upon La substitution of the A site. Lattice constant c and unit cell volume V decrease because of the size difference between La^{3+} and Sr^{2+}. The additional electrons provided by the substitution of an alkaline earth 2+ cation by La^{3+} are injected into the valence band which leads to an increase of T_C upon increasing x. The value of the saturation magnetization is in accordance to a highly ordered structure. Nevertheless, resistivity and MR decrease because of an impurity assisted tunneling effect enabled by impurities containing La which are located in the grain boundaries.

A slight improvement of the magnetoresistive properties of Sr_2FeMoO_6 can be achieved by substituting the A site with small amounts of Ba^{2+} ($x \leq 0.4$). [45] Owing to the highly ordered, ideal cubic ($Fm\bar{3}m$) structure the half-metallicity of the double perovskite is optimized which leads to a rise of T_C, M_S and MR effect.

A second double perovskite found to exhibit a large PMR at room temperature is Sr_2FeReO_6. The structure of the compound is difficult to determine because the small differences in symmetry, which exist between double perovskites crystallizing in space groups $Fm\bar{3}m$, $I4/mmm$ and $I4/m$, are difficult to detect by powder X-ray diffraction. Therefore, Sr_2FeReO_6 is reported to crystallize in space group $Fm\bar{3}m$ (c = 7.89 Å) [15,19,46-48], $I4/mmm$ (a = 5.58 Å, c = 7.89 Å) [48] or $I4/m$ (a = 5.56 Å, c = 7.90 Å) [49,50,51]. This finding is in good accordance to the structural properties expected from the calculated perovskite tolerance factor $t = 0.905$, i.e. at the borderline from the ideal cubic to the tetragonally distorted double perovskite structure. In space groups $Fm\bar{3}m$ and $I4/mmm$ the Fe–O–Re bond angle amounts 180 °, in space group $I4/m$ it is smaller (167 °). Owing to the size difference of the Fe and Re cations ($r(Fe^{3+}) = 65$ pm, $r(Re^{5+}) = 58$ pm) [31] antisite disorder does not play an important role in Sr_2FeReO_6.

Just like Sr_2FeMoO_6, Sr_2FeReO_6 is reported to be a half-metallic ferrimagnet with 100 % spin polarized charge carriers. [15,19,46-48] Owing to the boundary condition n + m = 8 for the valence states Fe^{n+} and Re^{m+}, seven electrons are distributed within the Fe and Re *d* states. In spin up direction, the Fe 3*d* states are filled with five electrons, the corresponding Re 5*d* states are empty. (Fig. 7) In contrast to the band gap in spin up direction, the spin down direction reveals metallic properties. The two remaining electrons are delocalized within the Fe/Re t_{2g} conduction band. Analogous to Sr_2FeMoO_6 the electrons localized at the Fe atoms and the itinerant electrons distributed over the Fe and Re sites couple antiferromagnetically. This arrangement is mediated by means of a Zener double exchange along the Fe–O–Re–O–Fe units forming an overall ferrimagnetic behaviour. [39] Consequently, the valence states of Fe and Re are difficult to determine, but NMR and Mössbauer spectroscopy report unanimously that the valence state of Fe is between 2.5+ and 3+. [15,19,46-48,51,52,55] The experimental saturation magnetization (M_S = 2.7 μ_B/f.u.) is in good agreement to the expected M_S based on the antiparalell arrangement of itinerant and localized electrons (M_S = 3 μ_B/f.u.). The ferromagnetic to paramagnetic transition occurs at T_C = 401 K.

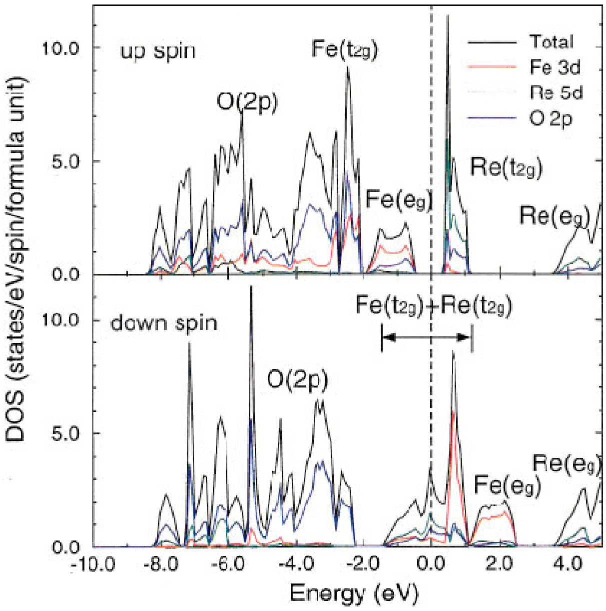

Fig. 7 DOS of Sr_2FeReO_6 [19].

The low-field magnetoresistance effect of Sr_2FeReO_6 is based on a PMR effect in perfect analogy to Sr_2FeMoO_6, i.e. the properties of the grain boundaries determine the properties of the sample. Maximum MR values of 21 % at 4.2 K and 70 kOe are reported. The conductivity of Sr_2FeReO_6 can be metallic and semiconducting depending on the synthesis procedure. [15,19,46-48,51,52]

As expected from an analysis by means of the perovskite tolerance factor (t = 0.965), Ba_2FeReO_6 is reported to crystallize in the cubic space group $Fm\bar{3}m$ with a lattice constant c = 8.054 Å. [14,15,51,52,54] Therefore, the Fe–O–Re bond angle is retained at 180 °. Owing to the larger A cation compared to Sr_2FeReO_6, antisite disorder is reduced to 2 %. Ba_2FeReO_6, in analogy to Sr_2FeReO_6, is predicted to be a half-metallic ferrimagnet by means of band structure calculations. The subsequent delocalization of two electrons over the spin down states of the Fe and Re atoms causes the variety of iron valence states (from Fe^{2+} to Fe^{3+}) determined by NMR and Mössbauer spectroscopy. [14,15,40,51,52,53,54] The reported conductivity (metallic) and saturation magnetization ($M_S = 3.04\ \mu_B$/f.u.) are in good accordance to the predicted half-metallic ferrimagnet. The experimental low-field magnetoresistance is 3 % at 10 K and 2 kOe. The Curie temperature of Ba_2FeReO_6 is published to be 315 K.

In contrast to the similarity of Sr_2FeMoO_6, Sr_2FeReO_6 and Ba_2FeReO_6 concerning crystal structure, electronic band structure and magnetism, Ca_2FeReO_6 is a monoclinic distorted, ordered double perovskite as expected from the perovskite tolerance factor ($t(Ca_2FeReO_6) = 0.842$). Above $T_C \approx$ 520 K - 540 K the compound consists of one monoclinic phase M1 ($P2_1/n$). Below approx. 300 K - 400 K, Ca_2FeReO_6 separates into two different monoclinic phases (M1 and M2). The relative phase fractions are 90 % for phase M1 and 10 % for phase M2. Below the metal to insulator transition temperature at approx. 100 K – 150 K, the relative phase fraction of M1 and M2 changes significantly accompanied by the appearance of a third monoclinic phase (M2 ≈ 60 %, M1 ≈ 35 %, M3 ≈ 5 %). The average Fe–O–Re bond angle is reported to be 156 °. [14,15,51,52,55-57] From an electronic point of view, the antiparalell arrangement of Fe and Re is preserved in spite of the monoclinic crystal structure but the two Fe/Re *d* electrons, which are itinerant in the spin down conduction band of $(Sr/Ba)_2FeReO_6$, are located at the Re sites in Ca_2FeReO_6. Therefore, the valence states of Fe and Re are 3+ and 5+, respectively. [14,15,51-53,56]

Moreover, Ca_2FeReO_6 exhibits a ferrimagnetic ordering below $T_C \approx$ 520 K - 540 K. At room temperature the compound is a ferrimagnetic metal. A metal to insulator transition appears at T_{MI} = 100 K - 150 K. The compound does not exhibit a magnetoresistance effect. [14,15,51,52,55]

The symmetry and lattice constants as well as magnetic properties of the members of the solid solution series $Ba_{2-x}Sr_xFeReO_6$ ($0 < x < 2$) and $Sr_{2-y}Ca_yFeReO_6$ ($0 < y < 2$) vary linearly with the substitution level. [58-61] Ba^{2+} containing samples crystallize in space group $Fm\bar{3}m$, Ca^{2+} containing samples crystallize in monoclinic symmetry ($P2_1/n$). Only Sr_2FeReO_6 adopts the tetragonal symmetry ($I4/m$). The lattice constants a and c decrease from $Ba^{2+} \rightarrow Sr^{2+} \rightarrow Ca^{2+}$ as expected from their ionic radii ($r(Ba^{2+})$ = 135 pm, $r(Sr^{2+})$ = 118 pm, $r(Ca^{2+})$ = 100 pm). [31] However, the decrease of the lattice constants is faster from Sr^{2+} to Ca^{2+} than from Ba^{2+} to Sr^{2+} because of the tilting of the FeO_6 and ReO_6 octahedra, which occurs with increasing Ca^{2+} content. The simultaneous structural and metal/insulator transition (T_{MI}) which is reported for unsubstituted Ca_2FeReO_6 can be observed for samples with $y \geq 1$. Within the series of solid solutions $Sr_{2-y}Ca_yFeReO_6$, T_{MI} decreases with decreasing Ca^{2+} content.

The increase of T_C ($T_C(Ba_2FeR\ eO_6) = 315$ K, $T_C(Sr_2FeReO_6) = 401$ K, $T_C(Ca_2FeReO_6) \approx 520$ K - 540 K) can be explained by considering the influence of the lattice parameters and MO_6 tilt angles on the electronic band width. [58-61] For compounds with straight FeO_6 and ReO_6 octahedra a shortening of the A cation size leads to a decrease of the Fe–O–Re bond length which increases the electronic band width and consequently T_C. [58] The Fe–O–Re bond angle reduction taking place upon Ca^{2+} substitution weakens the Fe–O–Re–O–Fe interaction, but enables direct Re–Fe interaction which additionally increases T_C.

The second consequence of the tilt of the MO_6 octahedra is the metal → insulator transition occurring along the series $Ba^{2+} \rightarrow Sr^{2+} \rightarrow Ca^{2+}$. [58-61] The Ba^{2+} as well as the Ca^{2+} containing samples up to a substitution level of $y \leq 0.3$ are metallic in the whole temperature range of ferrimagnetic behaviour. Samples containing more Ca^{2+} exhibit a metal to insulator transition at low temperature.

From the point of view of spintronic applications, the low Curie temperature of Ba_2FeReO_6 excludes an application of this compound in spintronic devices. On the other hand, the compound with the highest T_C, Ca_2FeReO_6, does not exhibit a magnetoresistance effect. Consequently, Sr_2FeReO_6 is a promising candidate for future spintronic application exhibiting a large negative low-field magnetoresistance at room temperature enabled by a ferromagnetic to paramagnetic transition temperature well above 300 K.

In order to enhance the MR effect of Sr_2FeReO_6, the Fe and Re sites of this compound were substituted by different transition metals. Kim et al. partially substituted the Re site by Fe. [62] $Sr_2Fe(Re_{2/3}Fe_{1/3})O_6$ crystallizes in space group $Fm\bar{3}m$ with a lattice constant $c = 7.87$ Å. Stoichiometry forces the valence states of Fe and Re to be 3+ and 6+, respectively. The expected saturation magnetization of approx. 2.6 μ_B/f.u. is not confirmed by experimental results ($M_S = 0.9$ μ_B/f.u.). However, the metallic nature of Sr_2FeReO_6 is preserved upon this series of solid solutions and the paramagnetic to ferromagnetic transition temperature is even increased ($T_C = 475$ K). Nevertheless, the MR effect is decreased to 1.5 % at 15 kOe.

Substitution of Re by W bleaches the metallic properties of Sr_2FeReO_6. [63] $Sr_2FeRe_{1-x}W_xO_6$ experiences a continuous transition from a ferrimagnetic metal for $x = 0$ to an antiferromagnetic insulator for $x = 1$.

Replacing Re by small amounts of Nd, Nb or Ta (substitution levels < 0.1) mainly leads to a strong increase of the antisite disorder up to 25 %. [48,64] The experimental saturation magnetization can be verified by considering the normal antiferromagnetic arrangement of localized and itinerant electrons, if the large amount of antisite disorder is taken into account. Nd substitution up to 10 % retains the tetragonal symmetry of the parent compound Sr_2FeReO_6 ($I4/mmm$) whereas Nb and Ta on the M' site enforce a structural phase transition from tetragonal ($I4/mmm$) to monoclinic ($P2_1/n$) at T_C = 410 K. In these compounds the half-metallic ferrimagnetism is destroyed because of the large amount of antisite disorder.

An approach reported only for $Ba_2FeM'O_6$ based compounds is the substitution of Re by Mo. [65] $Ba_2FeMo_{1-x}Re_xO_6$ ($0 < x < 1$) is a complete series of solid solutions without any phase separation. As expected for Ba^{2+}-based double perovskites, all compounds are cubic. Curie temperature and saturation magnetization show a discontinuous behaviour with highest values for the samples with 50 % Re content. Nevertheless, the semiconducting properties of all samples accompanied by a maximum low temperature MR effect of 1.34 % at 70 kOe exclude a possible application in spintronic devices.

Fe site substitution by Mn lowers the symmetry of the parent double perovskite so that Sr_2MnReO_6 crystallizes in the monoclinic space group $P2_1/n$. [66] The Mn–O–Re bond angle is reduced to 162 °. This tilting of the MnO_6 and ReO_6 octahedra leads to a canting of the Mn^{2+} and Re^{6+} magnetic moments which causes the appearance of antiferromagnetic impurities in the ferromagnetic main phase. Moreover, the Curie temperature is lowered to T_C = 120 K.

$Sr_2Fe_{1-x}Sc_xReO_6$ ($0 < x \leq 0.1$) exhibits orthorhombic symmetry ($Immm$). [48,67] The antisite order on the M and M' sites is drastically reduced from > 95 % for the parent compound to 75 % for $Sr_2Fe_{0.9}Sc_{0.1}ReO_6$. The experimental saturation magnetization (M_S (x = 0.1) = 0.9 μ_B/f.u.) is in good accordance to the estimated value of 1.25 μ_B/f.u. for a double perovskite with 75 % antisite disorder. Thus, the antiparalell arrangement of the localized and itinerant electrons is retained upon Sc substitution. The Curie temperature rises to 450 K for $Sr_2Fe_{0.9}Sc_{0.1}ReO_6$. Again, antisite disorder prevents the application of $Sr_2Fe_{1-x}Sc_xReO_6$ in spintronic devices.

A more promising approach in terms of spintronic application is the substitution of Fe by Cr. Sr_2CrReO_6 is a double perovskite crystallizing in the tetragonal space group $I4/mmm$. The smaller lattice constants (a = 5.52 Å, c = 7.82 Å) compared to Sr_2FeReO_6 (a = 5.56 Å, c = 7.90 Å) are related to the ionic radii of Fe^{3+} and Cr^{3+} ($r(Fe^{3+})$ = 65 pm, $r(Cr^{3+})$ = 62 pm). [31] The antisite disorder amounts to 84 %. [60] The experimental saturation magnetization of 0.86 μ_B/f.u. corresponds to an antiparalell arrangement of the transition metal cations in combination with a considerable amount of antisite disorder. [60,67] Band structure calculations reveal half-metallic properties. [60,68] The insulating spin up direction consists of completely filled Cr 3*d* t_{2g}^{3} states below E_F and empty Cr 3*d* e_g and Re 5*d* states above E_F. The conduction band in spin down direction is formed by the hybridized Cr 3*d* t_{2g} and Re 5*d* t_{2g} bands which host two electrons. (Fig. 8) Thus, the spin down electrons are delocalized over the Cr and Re sites enforcing mixed valence states for Cr and Re. Moreover, Sr_2CrReO_6 is a hard metal on the vicinity to a metal → insulator transition like Sr_2FeReO_6. The ferrimagnetic to paramagnetic transition occurs at 635 K.

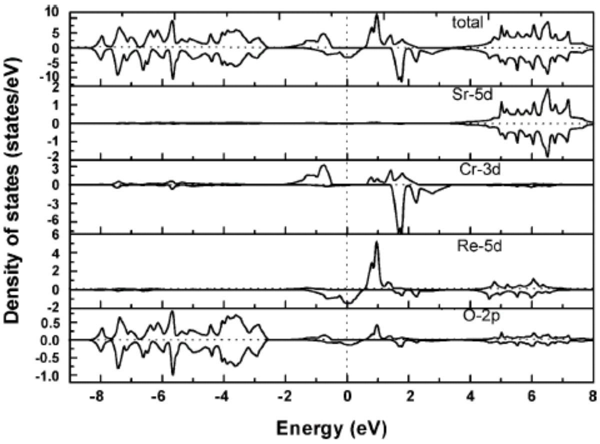

Fig. 8 DOS of Sr_2CrReO_6 [68]

A neutron diffraction study of the solid solution series $Sr_2Fe_{1-x}Cr_xReO_6$ reveals that only the end members are single phase compounds. [69] A structural phase transition from a cubic high temperature phase to a tetragonal low temperature phase occurs at a transition temperature ($T_T(Sr_2FeReO_6)$ = 490 K, $T_T(Sr_2CrReO_6)$ = 260 K) depending on the Cr^{3+} content. The magnetic transition temperature T_C increases with increasing Cr^{3+} content from 401 K for Sr_2FeReO_6 to 635 K for Sr_2CrReO_6. Therefore, the structural and the magnetic transition of the compounds with lower Cr^{3+} substitution level take place at approx. the same temperature. For higher values of x, the temperature difference between T_T and T_C increases, enabling the existence of a cubic ferrimagnetic phase at room temperature. Moreover, the refinement of the magnetic structure proves the spins of Fe(Cr) on the one hand and Re on the other hand to be arranged in an antiferromagnetic manner.

In the course of this work, Sr_2FeReO_6 will be chosen as model compound in order to study the influence of different metal cations on the M and M' sites on the structural and magnetic properties of the parent double perovskite. The objective of these substitutions is two-fold. First, the band model will be used to select a metal cation which will probably improve the magnetic and magnetoresistive properties of Sr_2FeReO_6 by adjusting the electron count of $Sr_2Fe_{1-x}M_xRe_{1-y}M'_yO_6$ to its optimum value. At the same time, the element composition should be compatible with the requirement of an enhancement of the compound symmetry. Additionally, a second solid solution system will be investigated in order to study the contrary effect, i.e. strong structural distortion and electronic doping toward high energy separation of E_F and van Hove-singularity. The second objective of this work is the understanding of the principles behind the magnetic interaction between Fe and Re. Therefore, the M and M' sites of Sr_2FeReO_6 will be substituted by valence invariant, closed shell metal cations which do not enable a double exchange mechanism.

References

[1] P. Grünberg, R. Schreiber, Y. Pang, M. B. Brodsky and H. Sowers, *Phys. Rev. Lett.*, 1986, **57**, 2442.

[2] M. N. Baibich, J. M. Broto, A. Fert, F. Nguyen van Dau, F. Petroff, P. Etienne, G. Creuzet, A. Friedrich and J. Chazelas, *Phys. Rev. Lett.*, 1988, **61**, 2472.

[3] M. Johnson, *J. Phys. Chem. B*, 2005, **109**, 14278.

[4] A. Fert and C. Vouille, *Schriften des Forschungszentrums Jülich, Materie und Material*, 1999, **2** (Magnetische Schichtsysteme), D1.

[5] J. Wecker, R. Kinder and R. Richter, *PhiuZ*, 2002, **5**, 210.

[6] J. Wecker and J. Bangert, *Schriften des Forschungszentrums Jülich, Materie und Material*, 1999, **2** (Magnetische Schichtsysteme), D6.

[7] G. Reiss, H. Brückl and A. Hütten, *Schriften des Forschungszentrums Jülich, Materie und Material*, 1999, **2** (Magnetische Schichtsysteme), D3.

[8] J. Schelten, *Schriften des Forschungszentrums Jülich, Materie und Material*, 1999, **2** (Magnetische Schichtsysteme), D7.

[9] J. M. D. Coey, Phil. Trans. R. Soc. Lond. A, 1998, 356, 1519.

[10] J. M. D. Coey, *J. Appl. Phys.*, 1999, **85**, 5576.

[11] H. Y. Hwang, S.-W. Cheong, N. P. Ong and B. Batlogg, Phys. Rev. Lett., 1996, 77, 2041.

[12] H. Y. Hwang and S.-W. Cheong, Science, 1997, 278, 1607.

[13] (a) A. P. Ramirez, *J. Phys.: Condens. Matter*, 1997, **9**, 8171; (b) C. N. R. Rao and B. Raveau, *Colossal magnetoresistance and other related properties in 3d oxides*, Eds; World Scientific: Singapore, 1998.

[14] W. Prellier, V. Smolyaninova, A. Biswas, C. Galley, R. L. Greene, K. Ramesha and J. Gopalakrishnan, *J. Phys.: Condens. Matter*, 2000, **12**, 965.

[15] J. Gopalakrishnan, A. Chattopadhyhay, S. B. Ogale, T. Venkatesan, R. L. Greene, A. J. Millis, K. Ramesha, B. Hannover and G. Marest, *Phys. Rev. B*, 2000, **62**, 9538.

[16] C. Felser, Habilitationsschrift an der Johannes Gutenberg-Universität Mainz, 2000.

[17] C. Felser, R. Seshadri, A. Leist and W. Tremel, *J. Mater. Chem.*, 1998, **8**, 787.

[18] K.-I. Kobayashi, T. Kimura, H. Sawada, K. Terakura and Y. Tokura, *Nature*, 1998, **395**, 677.
2004, **85**, 266.

[19] K.-I. Kobayashi, T. Kimura, Y. Tomioka, H. Sawada, K. Terakura and Y. Tokura, *Phys. Rev B*, 1999, **59**, 11159.

[20] J. Longo and R. Ward, *J. Am. Chem. Soc.*, 1961, **83**, 2816.

[21] A. W. Sleight, J. Longo and R. Ward, *Inorg. Chem.*, 1962, **1**, 245.

[22] A. W. Sleight and J. F. Weiher, *J. Phys. Chem. Solids*, 1972, **33**, 679.

[23] M. T. Anderson, K. G. Greenwood, G. A. Taylor and K. R. Poeppelmeier, *Prog. Solid St. Chem.*, 1993, **22**, 197.

[24] U. Müller, *Anorganische Strukturchemie*; Teubner Studienbücher: Stuttgart, 1996.

[25] B. García-Landa, C. Ritter, M. R. Ibarra, J. Blasco, P. A. Algarabel, R. Mahendiran and J. García, *Sol. State Commun.*, 1999, **110**, 435.

[26] O. Chmaissem, R. Kruk, B. Dabrowski, D. E. Brown, X. Xiong, S. Kolesnik, J. D. Jorgensen and C. W. Kimball, *Phys. Rev. B*, 2000, **62**, 14197.

[27] B. Fisher, K. B. Chashka, L. Patlagan and G. M. Reisner, *J. Magn. Magn. Mater.*, 2004, **272-276**, 1790.

[28] D. Niebieskikwiat, A. Caneiro, R. D. Sánchez and J. Fontuberta, *Phys. Rev. B*, 2001, **64**, 180406(R).

[29] D. Niebieskikwiat, A. Caneiro, R. D. Sánchez and J. Fontuberta, *Physica B*, 2002, **320**, 107.

[30] K. Wang and Y. Sui, *Physica B*, 2004, **344**, 423.

[31] R. D. Shannon, *Acta Crystallogr.*, 1976, **A32**, 751.

[32] K. Kuepper, I. Balasz, H. Hesse, A. Winiarski, K. C. Prince, M. Matteucci, D. Wett, R. Szargan, E. Burzo and M. Neumann, *Phys. Stat. Sol. A*, 2004, **201**, 3252.

[33] A. Sharma, A. Berenov, J. Rager, W. Branford, Y. Bugoslavsky, L. F. Cohen and J. L. MacManus-Driscoll, *Appl. Phys. Lett.*, 2003, **83**, 2384.

[34] (a) D. Sánchez-Soria, J. A. Alonso, M. García-Hernández, M. J. Martínez-Lope, J. L. Martínez and A. Mellergard, *Appl. Phys. A*, 2002, **74**, S1752; (b) D. Sánchez, M. García-Hernández, J. L. Martínez, J. A. Alonso, M. J. Martínez-Lope, M. T. Casais and A. Mellergard, *J. Magn. Magn. Mater.*, 2002, **242-245**, 729.

[35] D. D. Sarma, E. V. Sampathkumaran, S. Ray, R. Nagarajan, S. Majumdar, A. Kumar, G. Nalini and T. N. Guru Row, *Sol. State Commun.*, 2000, **114**, 465.

[36] B. Martínez, J. Navarro, L. I. Balcells and J. Fontcuberta, *J. Phys.: Condens. Matter*, 2000, **12**, 10515.

[37] M. Tovar, M. T. Causa, A. Butera, J. Navarro, B. Martínez, J. Fontcuberta and M. C. G. Passeggi, *Phys. Rev. B*, 2002, **66**, 024409.

[38] T.-Y. Cai and Z.-Y. Li, *J. Phys.: Condens. Matter*, 2004, **16**, 3737.

[39] C. Zener, *Phys. Rev.*, 1951, **81**, 440; C. Zener, *Phys. Rev.*, 1951, **82**, 403; C. Zener, *Phys. Rev.*, 1951, **83**, 299; C. Zener, *Phys. Rev.*, 1952, **85**, 324.

[40] Cz. Kapusta, D. Zajac, P. C. Riedi, M. Sikora, C. J. Oates, J. Blasco and M. R. Ibarra, *J. Magn. Magn. Mater.*, 2004, **271-279**, e1619.

[41] P. A. Agarabel, L. Morellon, J. M. De Teresa, J. Blasco, J. García, M. R. Ibarra, T. Hernández, F. Plazaola and J. M. Barandiarán, *J. Magn. Magn. Mater.*, 2001, **226-230**, 1089.

[42] M. S. Moreno, J. E. Gayone, M. Abbate, A. Caneiro, D. Niebieskikwiat, R. D. Sánchez, A. de Siervo, R.

[43] D. Sánchez, J. A. Alonso, M. García-Hernández, M. J. Martínez-Lope, M. T. Casais and J. L. Martínez, *J. Mater. Chem.*, 2003, **13**, 1771.

[44] D. Serrate, J. M. De Teresa, J. Blasco, M. R. Ibarra, L. Morellón and C. Ritter, *Appl. Phys. Lett.*, 2002, **80**, 4573.

[45] X. M. Feng, G. H. Rao, G. Y. Liu, W. F. Liu, Z. W. Ouyang and J. K. Liang, *Sol. State Commun.*, 2004, **129**, 753.

[46] M. Abe, T. Nakagawa and S. Nomura, *J. Phys. Soc. Jpn.*, 1973, **35**, 1360.

[47] S. Nakmura, M. Tanaka, H. Kato and Y. Tokura, *J. Phys. Soc. Jpn.*, 2003, **72**, 424.

[48] J. J. Blanco, T. Hernandez, L. M. Rodriguez-Martinez, M. Insausti, J. M. Barandiaran, J.-M. Greneche and T. Rojo, *J. Mater. Chem.*, 2001, **11**, 253.

[49] S. Nakamura and K. Oikawa, *J. Phys. Soc. Jpn.*, 2003, **72**, 3123.

[50] H. Kato, T. Okuda, Y. Okimoto, Y. Tomioka, K. Oikawa, T. Kamiyama and Y. Tokura, *Phys. Rev. B*, 2004, **69**, 184412.

[51] N. Auth, G. Jakob, W. Westerburg, C. Ritter, I. Bonn, C. Felser, W. Tremel, *J. Magn. Magn. Mater.*, 2004, **272-276**, e607.

[52] K. G. Bramnik, H. Ehrenberg, J. K. Dehn and H. Fuess, *Sol. State Sci.*, 2003, **5**, 235.

[53] J. Herrero-Martin, G. Subías, J. Blasco, J. García and M. C. Sánchez, *J. Phys.: Condens. Matter*, 2005, **17**, 4963.

[54] N. Rammeh, K. G. Bramnik, H. Ehrenberg, C. Ritter, H. Fuess and A. Cheikh-Rouhou, *Phys. Stat. Sol. (C)*, 2004, **1**, 1669.

[55] W. Westerburg, O. Lang, C. Ritter, C. Felser, W. Tremel and G. Jakob, *Sol. State Commun.*, 2002, **122**, 201.

[56] E. Granado, Q. Huang, J. W. Lynn, J. Gopalakrishnan, R. L. Greene and K. Ramesha, *Phys. Rev. B*, 2002, **66**, 064409.

[57] H. Iwasawa, T. Saitoh, Y. Yamashita, D. Ishii, H. Kato, N. Hamada, Y. Tokura and D. D. Sarma, *Phys. Rev. B*, 2005, **71**, 075106.

[58] J. M. De Teresa, D. Serrate, J. Blasco, M. R. Ibarra and L. Morellon, *Phys. Rev. B*, 2004, **69**, 144401.

[59] J. M. De Teresa, D. Serrate, J. Blasco, M. R. Ibarra and L. Morellon, *J. Magn. Magn. Mater.*, 2005, **290-291**, 1043.

[60] (a) H. Kato, T. Okuda, Y. Okimoto, Y. Tmioka, Y. Takenoya, A. Ohkubo, M. Kawasaki and Y. Tokura, *Appl. Phys. Lett.*, 2002, **81**, 328; (b) H. Kato, T. Okuda, Y. Okimoto, Y. Tomioka, K. Oikawa, T. Kamiyama and Y. Tokura, *Phys. Rev. B*, 2002, **65**, 144404.

[61] T. Alamelu, U. V. Varadaraju, M. Venkatesan, A. P. Douvalis and J. M. D. Coey, *J. Appl. Phys.*, 2002, **91**, 8909.

[62] T. H. Kim, M. Uehara, S.-W. Cheong and S. Lee, *Appl. Phys. Lett.*, 1999, **74**, 1737.

[63] A. Poddar and S. Das, *Physica B*, 2004, **344**, 325.

[64] J. J. Blasco, M. Insausti, L. Lezama, J. P. Chapman, I. Gil de Muro and T. Rojo, *Sol. State Chem.*, 2004, **177**, 2749.

[65] F. Sriti, N. Nguyen, C. Martin, A. Ducouret and B. Raveau, *J. Magn. Magn. Mater.*, 2002, **250**, 123.

[66] G. Popov, M. Lobanow, E. V. Tsiper, M. Greenblatt, E. N. Caspi, A. Borissov, V. Kiryukhin and J. W. Lynn, *J. Phys.: Condens. Matter*, 2004, **16**, 135.

[67] P. Majewski, S. Geprägs, O. Sanganas, M. Opel, R. Gross, F. Wilhelm, A. Rogalev and L. Alff, *Appl. Phys. Lett.*, 2005, **87**, 202503.

[68] C. Q. Tang, Y. Zang and J. Dai, *Sol. State Commun.*, 2005, **133**, 219.

[69] J. M. De Teresa, D. Serrate, C. Ritter, J. Blasco, M. R. Ibarra, L. Morellon and W. Tokarz, *Phys. Rev. B*, 2005, **71**, 092408.

2. Structural and magnetic properties of the solid solution series $Sr_2Fe_{1-x}M_xReO_6$ (M = Cr, Zn)

2.1 Introduction

The discovery of tunnelling magnetoresistance at room temperature and at low magnetic fields in powder samples (PMR) of the ferrimagnetic double perovskites Sr_2FeMoO_6 and Sr_2FeReO_6 has indicated the potential of compounds from the so-called double perovskite group for magnetic sensor applications. [1-4] The essential features of materials exhibiting a large PMR effect are (i) halfmetallic spin-polarized conductivity and (ii) a ferromagnetic ordering at Curie temperatures as high as possible, ideally above a value of two times room temperature. [1,3,5] From a band electronic point of view the first requirement corresponds to a saddle point (the so-called van Hove-instability) close to the Fermi level and a spin density wave instability. [6] The band model provides a practical tool for a systematic variation of magnetization, Curie temperature and the TMR effect by “doping”, i.e. adjusting the electron count of the target compounds to their optimum values. In this contribution we have applied this approach to the double perovskites.

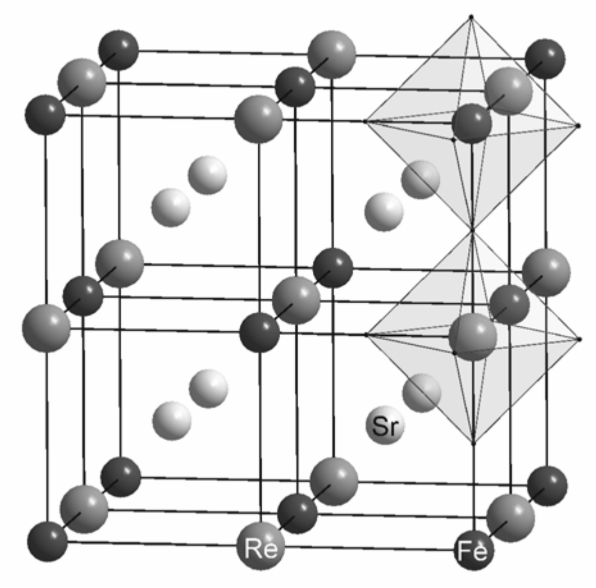

Fig. 1a Crystal structure of Sr_2FeReO_6.

Double perovskites of the general formula $A_2MM'O_6$, where M and M′ sites are occupied alternatively by different transition metal cations (M = first row transition metal; M′ = Mo, W, Re) are known since more than forty years. [7,8] The ideal structure of these compounds can be considered as a regular arrangement of corner sharing MO_6 and $M'O_6$ octahedra alternating along the three directions of the crystal with the large A cations situated in the voids between the octahedra.

(Fig. 1a) The crystal structure and physical properties of the double perovskite oxides strongly depend on the size and valencies of the cations A, M and M′. An early study of the A = Ba and M′ = Re members by Sleight and collaborators [8] revealed that several members of the series (M = Mn, Fe, Ni) are ferrimagnetic, [9] Sr_2FeReO_6, [2] Ba_2FeReO_6 [3,9] and Sr_2CrReO_6 [8,10] are unique in that they are both metallic and ferrimagnetic, Sr_2CrReO_6 having an exceptionally large Curie temperature of 635 K.

In an attempt to probe the influence of the M site cations on the structure and properties of Sr_2FeReO_6 we have investigated the substitution series $Sr_2Fe_{1-x}Cr_xReO_6$ and $Sr_2Fe_{1-x}Zn_xReO_6$. Based on the available theoretical results, [2a,2b,11-13] it could be assumed that saturation magnetization and PMR effect increase upon hole “doping” (M = Cr) or - strictly speaking - increase with the degree of substitution in the solid solution series $Sr_2Fe_{1-x}Cr_xReO_6$, whereas it decreases upon electron “doping” (M = Zn). However, the role of the van Hove-singularity in the vicinity of the Fermi energy (E_F) was not considered in the original paper. [2b] Therefore, we intend to maximize the density of states at the Fermi level by tuning the electron concentration in the conduction band by means of “doping”. On the other hand, there appears to be a correlation between the crystal symmetry (which is dictated on the cation radii) and the saturation magnetization: the higher the symmetry of the system, the larger the saturation magnetization. [14] In this contribution we report the synthesis, structures and properties of the $Sr_2Fe_{1-x}Cr_xReO_6$ and $Sr_2Fe_{1-x}Zn_xReO_6$ series. The aim of this work is twofold. Firstly, we want to test the validity of the theoretical working model. Although one might assume that the magnetic properties vary in a linear manner with the substitution level, this is not obviously the case as the example $Ba_2FeMo_{1-x}Re_xO_6$ indicates. [15] Secondly, we want to characterize the representatives of the substitutional series in order to understand their physical properties and relate them to the results of electronic band structure calculations.

2.2 Experimental

Starting materials were reagent grade SrO (Aldrich, 99.9 % purity), Fe_2O_3 (Alfa Aesar, 99.99 % purity), Re metal, Re_2O_7 (Alfa Aesar, 99.9 % purity), ZnO (Alfa Aesar, 99.99 % purity) and Cr_2O_3 (Alfa Aesar, 99.997 % purity). All starting materials are stored in a glove box under argon (Braun Labmaster) and examined by X-ray powder diffraction prior to use.

The $Sr_2Fe_{1-x}M_xReO_6$ samples were prepared by high-temperature solid state reactions. Because of the strongly hygroscopic properties of SrO and the large vapour pressure of Re_2O_7 the samples were prepared under inert gas atmosphere in a glove-box. Stoichiometric amounts of SrO, Fe_2O_3, Re, Re_2O_7, ZnO and Cr_2O_3 (2 SrO : (1-x)/2 Fe_2O_3 : 0.3 Re : 0.35 Re_2O_7 : x ZnO (x/2 Cr_2O_3)) were ground in an agate mortar and pressed into pellets. In order to avoid Sr attack on the quartz tubes these pellets were transferred into corundum containers and finally sealed in evacuated quartz tubes. The samples were annealed for seven days at 1000°C. Thereafter they were rapidly cooled to room temperature by quenching in ice.

X-ray powder diffraction patterns were recorded using a Siemens D5000 diffractometer with monochromatized (Ge (111)) Cu $K_{\alpha 1}$ radiation.

The variable - temperature magnetic susceptibility measurements of $Sr_2Fe_{1-x}M_xReO_6$ were performed using the Quantum Design MPMS-XL SQUID magnetometer, equipped with a high-temperature furnace. Experimental data were corrected for diamagnetism using Pascal's constants. [16]

^{57}Fe Mössbauer spectra were measured with a constant acceleration type Mössbauer spectrometer operated in a multichannel scaling mode. A 10 mCi ^{57}Co/Rh source was employed which was maintained at ambient temperature. The isomer shifts reported here are relative to metallic iron. Spectra were collected at variable temperatures between 293 and 4.2 K by means of a combined He continuous flow/bath cryostat. The Mössbauer spectra were analyzed with the computer program EFFINO [17] using Lorentzian line shapes.

Band structure calculations were performed within the potential augmented plane-wave (FLAPW) framework within the generalized gradient approximation (GGA). [18] The crystal structure of the parent compound Sr_2FeReO_6 was approximated by the ideal cubic structure of a double perovskite with the lattice parameter a = 7.89 Å. The number of k points in the irreducible Brillouin zone is 20 and the convergence criteria was fixed to 0.0001 Ry.

2.3 Results and discussion

2.3.1 Structural characterization

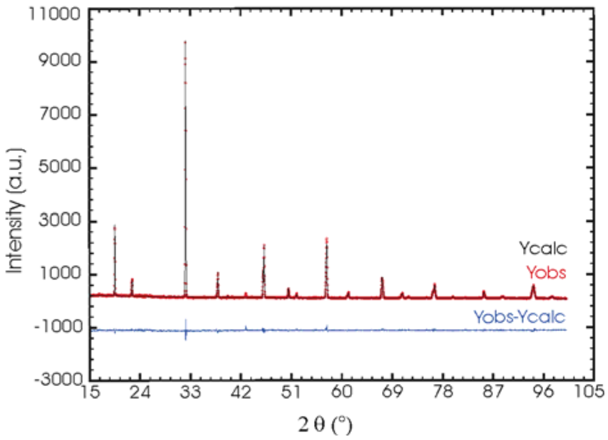

Fig. 1b X-ray pattern (red) of $Sr_2Fe_{0.9}Zn_{0.1}ReO_6$ together with the Rietveld fit (black) and the corresponding difference curve (blue).

The crystal structure of the parent compound Sr_2FeReO_6 was determined by neutron diffraction and refined in space group $P4_2/m$. [19] The X-ray patterns of twelve Zn and Cr containing samples reveal that they adopt the double perovskite structure like the original unsubstituted Sr_2FeReO_6. [2,7,8,19] Lattice parameters of Sr_2FeReO_6, $Sr_2Fe_{1-x}Cr_xReO_6$ and $Sr_2Fe_{1-x}Zn_xReO_6$ as obtained by Rietveld refinements using the program FULLPROF [20] are compiled in Table 1. An X-ray pattern of $Sr_2Fe_{0.9}Zn_{0.1}ReO_6$ together with the Rietveld fit and the corresponding difference curve is given in Fig. 1b, X-ray patterns of $Sr_2Fe_{0.6}Zn_{0.4}ReO_6$ (a), Sr_2FeReO_6 (b), and $Sr_2Fe_{0.6}Cr_{0.4}ReO_6$ (c) are provided in Fig. 2, the most informative part of the X-ray powder diffraction pattern in the range $45° < 2\theta < 47°$ is highlighted as an insert in the Figure. The distribution of three elements Fe, Cr, and Re on two available lattice sites brings about the question of cation and antisite disorder. As Fe and Cr are almost indistinguishable by X-ray diffraction because of their similar scattering factors, their distribution on the lattice sites could hardly be determined. However, in contrast to the corresponding molybdates $Sr_2Fe_{1-x}Cr_xMoO_6$ [21,22] we found only a minor extent (< 16 %) of antisite disorder for the Fe/Cr and Re atoms which increases slightly to 16 % with increasing Cr content, which may be related to the difference in the ionic radii of Cr^{3+} and Re^{5+}. These findings are in line with the results of the Mössbauer spectroscopy given below. For the Zn containing compounds, the splitting of reflections increases with increasing Zn content, whereas the Cr substituted compounds show the opposite behaviour. The dependence of lattice parameters a and c on the substitution level for the Zn containing samples is almost linear, confirming the existence of a continuous solid solution series in the range $0 \leq x \leq 1$. The lattice parameters and unit cell volume increase with increasing Zn content as illustrated in Fig. 3a. The increase of the cell volume can be explained from the ionic radii of Zn^{2+} and Fe^{3+} ($r(Zn^{2+}) = 88$ pm, $r(Fe^{3+}) = 78.5$ pm). [23] For the series of Cr substitution the lattice parameters as well as the unit cell volume monotonically decrease with increasing Cr content (Fig. 3b). This finding may be explained by the relation of the ionic radii of Fe^{3+} and Cr^{3+}, which are 78.5 pm and 75.5 pm, respectively.

Table 1 Lattice parameters (standard deviation <0.0005 Å), *c*/*a* relations, and cell volumes of $Sr_2Fe_{1-x}Zn_xReO_6$ and $Sr_2Fe_{1-x}Cr_xReO_6$ solid solution.

	$Sr_2Fe_{1-x}Zn_xReO_6$				$Sr_2Fe_{1-x}Cr_xReO_6$			
x	*a* (Å)	*c* (Å)	*c*/*a*	V (Å^3)	*a* (Å)	*c* (Å)	*c*/*a*	V (Å^3)
0	5.5596	7.8981	1.4206	244.12	5.5596	7.8981	1.4206	244.12
0.10	5.5619	7.9063	1.4215	244.56	5.5587	7.8936	1.4200	243.96
0.20	5.5633	7.9142	1.4226	244.95	5.5578	7.8892	1.4195	243.69
0.25	-	-	-	-	5.5562	7.8798	1.4182	243.26
0.40	5.5667	7.928	1.4242	245.67	5.5504	7.8510	1.4145	241.87
0.60	5.5703	7.9444	1.4262	246.50	5.5445	7.8410	1.4142	241.04
0.80	5.5734	7.9566	1.4276	247.15	5.5376	7.8313	1.4142	240.15
0.90	5.5749	7.9657	1.4289	247.57	5.5345	7.8271	1.4142	239.75
1	5.5771	7.9734	1.4297	248.00	5.5319	7.8233	1.4142	239.41

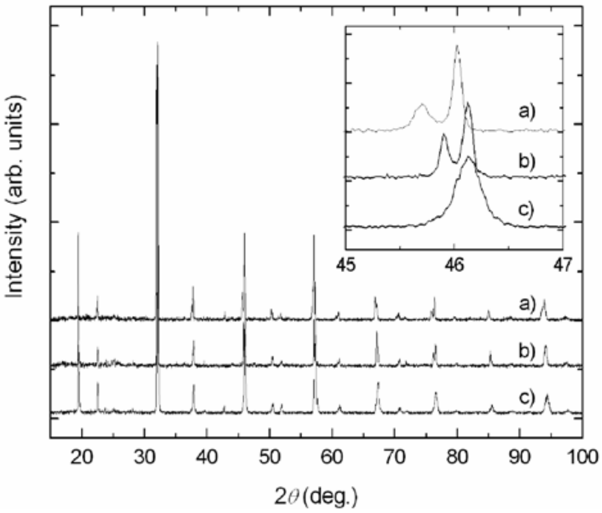

Fig. 2 X-ray patterns of (a) $Sr_2Fe_{0.6}Zn_{0.4}ReO_6$, (b) Sr_2FeReO_6, (c) $Sr_2Fe_{0.6}Cr_{0.4}ReO_6$; insert: range 45° < 2θ < 47° highlighted.

The continuous increase of the tetragonal distortion of the Zn containing samples can be seen from the plot of *c*/*a* ratio which is almost linear (Fig. 3c). In contrast, the concentrational dependence of the *c*/*a* ratio for the Cr containing samples (Fig. 3c) shows a transition from tetragonal to cubic symmetry. From the relation $c/a = \sqrt{2}$ for the cubic phase one can conclude that the cubic structure exists above x ≈ 0.4. Refinement of the lattice parameters based on the powder X–ray data shows a continuous decrease of tetragonal distortion for substitution levels $0 \leq x \leq 0.4$. The data in Fig. 3c indicate the presence of a continuous solid solution associated with a tetragonal – cubic transition. Studies on the temperature dependent tetragonal – cubic transition are in progress.

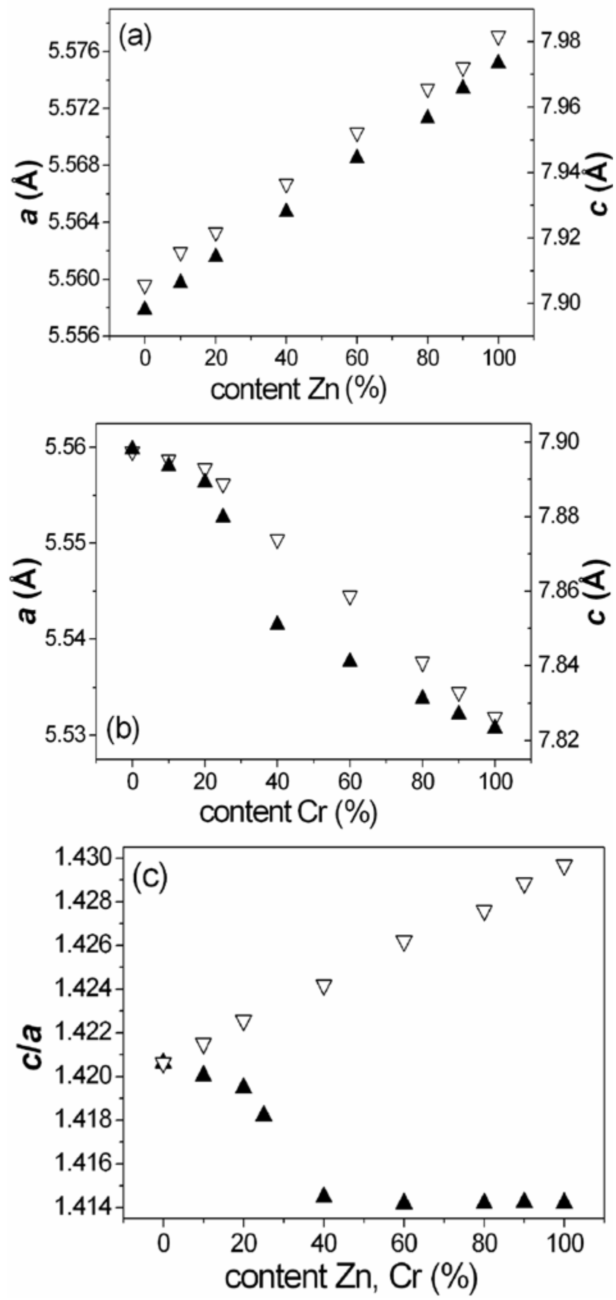

Fig. 3 Lattice parameter *a* (∇) and *c* (▲) of $Sr_2Fe_{1-x}M_xReO_6$ versus M content in tetragonal setting for (a) M = Zn and (b) M = Cr, (c) lattice parameter relation c/a versus Zn (∇) and Cr (▲) content.

The above results qualitatively agree with the structural behaviour expected from an analysis of the tolerance factor *t*

$$t = \frac{r(A) + r(X)}{\sqrt{2}\left[r(M) + r(X)\right]}$$

for perovskites of the general formula AMX_3 (Fig. 4), where the ionic radii were taken from Shannon et al. [23] The tolerance factor describes the interrelation between the perovskite structure and the associated ionic radii. [24,25]

To plot the concentrational dependence of the tolerance factor, one should know the valence state of ions in the crystal structure. The valence state of iron is of most importance because the ionic radii of Fe^{2+} and Fe^{3+} differ significantly, whereas the ionic radius of Re is practically valence independent. The plot in Fig. 4 uses the results of a detailed study of the iron valence states by means of Mössbauer spectroscopy which are discussed in detail below.

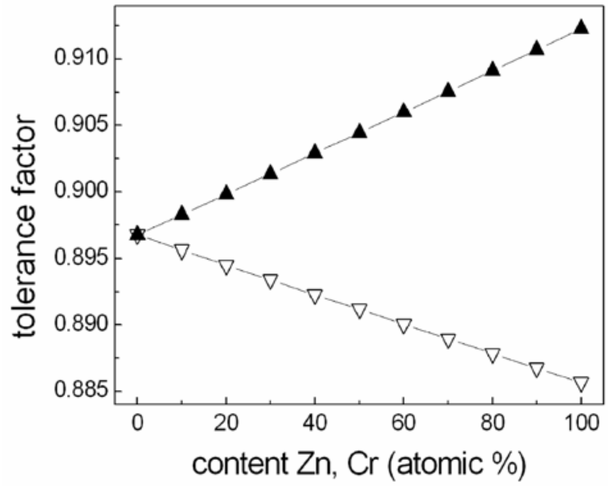

Fig. 4 Perovskite tolerance factor *t* of $Sr_2Fe_{1-x}Cr_xReO_6$ (▲) and $Sr_2Fe_{1-x}Zn_xReO_6$ (∇) for an iron valence state given by Mössbauer experiments ($Fe^{2.7+}$).

For an iron valence state $Fe^{2.7+}$ obtained from Mössbauer measurements the structural behaviour of Sr_2FeReO_6 as a result of Zn and Cr substitution can be analyzed as follows. For the unsubstituted sample the room temperature structure is tetragonal. We note that the value of the tolerance factor $t \approx 0.90$ found in our experiment for the tetragonal – cubic transition agrees well with the empirical value $t \approx 0.89$ mentioned in the literature. For $t > 0.89$ perovskites prefer the cubic structure, below 0.89 the structure is expected to be tetragonal. [24,25] For the Zn substitution series a tetragonal structure is observed for the full range of substitution, whereas for Cr substitution a cubic structure is predicted and actually observed above a Cr content of 40 %. In summary: experimental results and the description based on a space filling model are in good agreement.

2.3.2 Magnetic measurement

Fe-based ordered double perovskites A_2FeMO_6 (A = Ca, Ba; M = Mo, Re) have been reported to be half-metallic with a high T_C [9,26,27] except for Ca_2FeReO_6 which undergoes a metal-insulator transition with decreasing temperature. [10,28] In those compounds Fe^{3+} ($3d^5$, $S = 5/2$) and Mo^{5+} ($4d^1$, $S = 1/2$) or Re^{5+} ($5d^2$, $S = 1$) couple antiferromagnetically, where the conduction band is composed of the $4d/5d$ down spin electrons of Mo^{5+} or Re^{5+}. On the other hand, Sr_2CrReO_6 was found to be a metallic ferromagnet with the highest Curie temperature ever found for the perovskite family. [10] In order to elucidate the nature of the magnetism (itinerant vs. localized) and to determine how it changes as a function of the electron concentration, we studied the solid solution series $Sr_2Fe_{1-x}M_xReO_6$.

The magnetic susceptibility measurements of Zn and Cr containing Sr_2FeReO_6 samples reveal the spontaneous magnetization. (Fig. 5) Because of the small coercive field one can consider both series of samples as soft magnetic materials.

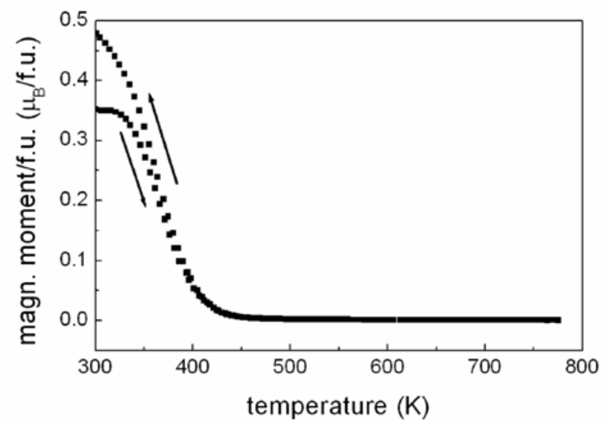

Fig. 5 Temperature dependence of magnetic moment/f.u. of $Sr_2Fe_{0.9}Zn_{0.1}ReO_6$ measured at 0.1 T (FC) both in cooling (↑) and heating modes (↓).

Zn containing samples reveal ferrimagnetic behaviour in the range of concentrations up to x ≅ 0.6. These samples show the similar temperature dependence of the reciprocal susceptibility characteristic for ferrimagnetic compounds in the paramagnetic region. (Fig. 6) At concentrations x ≥ 0.6, the magnetic ordering transforms to the ferromagnetic type. Fig. 6 demonstrates the typical temperature dependence for ferromagnets of χ_M^{-1} for the sample with x = 0.8. Cr containing samples reveal ferrimagnetic type of ordering in the overall range of concentrations.

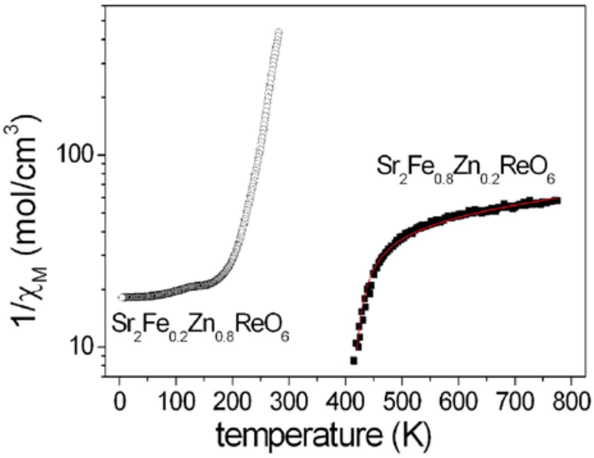

Fig. 6 Temperature dependence of reciprocal susceptibility above Curie temperature for ferrimagnetically ordered $Sr_2Fe_{0.8}Zn_{0.2}ReO_6$ and ferromagnetically ordered $Sr_2Fe_{0.2}Zn_{0.8}ReO_6$; the solid line shows the fitting curve according to the procedure described in the text.

Ferrimagnetic (T_C) and paramagnetic (Θ) Curie temperatures

$$\Theta=-\frac{2\mu C_A C_B}{C_A+C_B}$$

for both series of compounds were determined from the fit of high-temperature magnetic susceptibility measurements. The standard dependence describing the susceptibility χ as function of interaction parameter μ,

$$\chi=\frac{(C_A+C_B)T-2\mu C_A C_B}{T^2-T_C^2}$$

Curie constants of sublattices A and B, [29] C_A and C_B has been applied. The concentrational dependences of Θ extracted from the fit of the temperature dependence of the reciprocal susceptibilities [29] are presented in Fig. 7. The important feature of the Zn containing compounds is its weak overall concentrational dependence of the paramagnetic Curie temperature. An increase of Θ (ca. 100 K) is observed for small Zn concentrations only. For Cr substitution levels smaller than 40 % a large increase of Θ is found, whereas for higher Cr contents (> 40 %) the paramagnetic Curie temperature is practically concentration independent. This behaviour of the paramagnetic Curie temperature for the Zn containing compound is non-trivial and difficult to interpret from the localized magnetism point of view because in this case a simple diamagnetic dilution should lead to a monotonic decrease of the magnetic exchange. Our observation is compatible with itinerant magnetic behaviour. On the other hand, with increasing Zn concentration the exchange interaction within the Fe-based sublattice weakens. At some critical concentration of Zn ($x \cong 0.6$ - 0.8) the long-range magnetic correlations within this sublattice disappear, whereas the long-range magnetic correlations within the Re-sublattice are not influenced by this process. Therefore, heavy Zn dilution leads to the transformation of the ferrimagnetic to the ferromagnetic type of ordering. However, the short-range antiferromagnetic correlations between Re and the remaining magnetic Fe atoms are preserved, which can be confirmed by saturation magnetization values. (Fig. 10) One can expect that the end member of the substitution series Sr_2ZnReO_6 could be ferromagnetic; however, at this point we were unable to prepare a single phase compound with that composition.

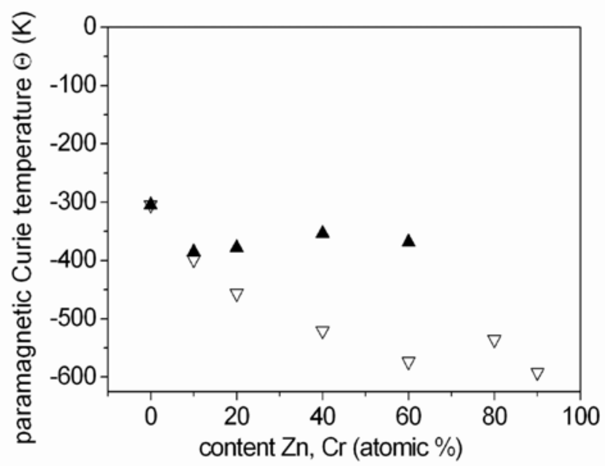

Fig. 7 Paramagnetic Curie temperature Θ of ferrimagnetically ordered samples $Sr_2Fe_{1-x}M_xReO_6$, M = Zn (▲), M = Cr (∇).

The conclusion about the itinerant magnetism approach should be valid for Cr containing compounds because the paramagnetic Curie temperature is practically concentration independent for substitution levels above 40 %. A concentrational dependence of Θ for the Cr containing compounds at levels below 40 % can be related to an expected structural transition from the tetragonal to the cubic modification of $Sr_2Fe_{1-x}Cr_xReO_6$. It is worth mentioning that the Zn substituted compounds are tetragonal for all Zn concentrations. From this fact one can conclude that the crystal structure is an important factor for the magnetic exchange for $Sr_2Fe_{1-x}M_xReO_6$, and the exchange is altered during a structural transition.

A comparison of the band structures of Sr_2FeMoO_6 and Ba_2FeMoO_6 as well as Sr_2FeReO_6 and Ba_2FeReO_6 gives an idea of the effect substitution on the magnetic properties. We have performed spin polarized *ab initio* band structure calculations for these compounds using the WIEN97 software. [18] The most important parts of the band structures are given in Fig. 8. Fig. 8a and b show the majority bands for Sr_2FeMoO_6 and Ba_2FeMoO_6. Fig. 8c and 8d depict the analogous bands for the corresponding Re compounds. The features associated with the van Hove-singularity are circled in all Figures. The spin up channel (not shown) is insulating. For the spin down direction there are several flat bands corresponding to a maximum in the density of states close to E_F associated with a van Hove-singularity in the band structure, i.e. a saddle point of Fe/Re centred band at the L point of the

Brillouin zone. To reach the coincidence of the van Hove-singularity and the Fermi energy, we must fill or deplete the conduction band to some extent. Because of the larger number of electronic states close to E_F this should lead to a larger saturation magnetization, and - concomitantly - to a higher Curie temperature and presumably to a larger MR effect.

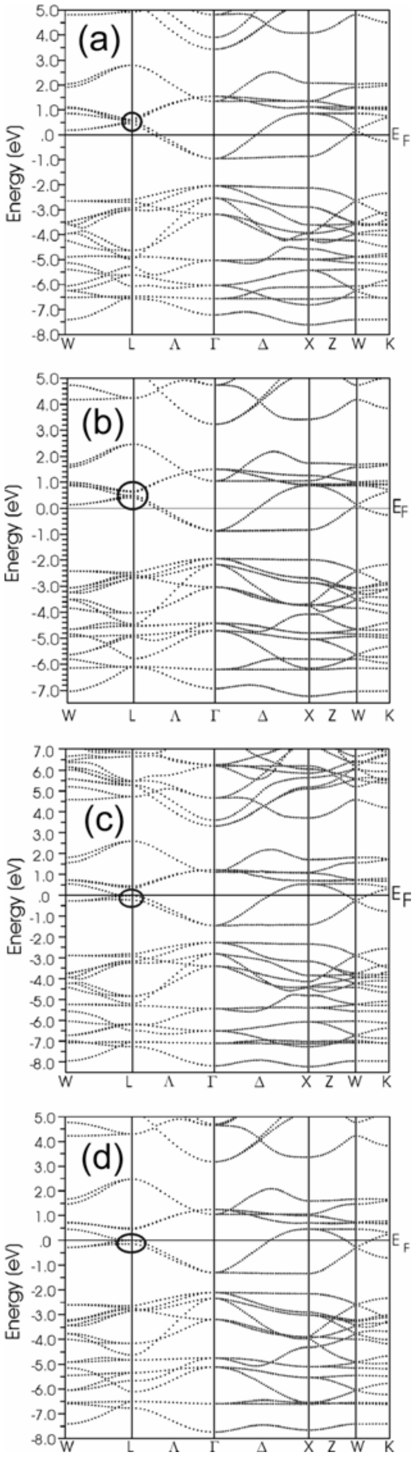

Fig. 8 Band structures of the metallic spin direction of (a) Sr_2FeMoO_6, (b) Ba_2FeMoO_6, (c) Sr_2FeReO_6 and (d) Ba_2FeReO_6.

For Sr_2FeMoO_6 and Ba_2FeMoO_6 the Fermi level is situated below the van Hove-singularity, whereas it is located above the van Hove-singularity for Sr_2FeReO_6 and Ba_2FeReO_6. These results indicate our "doping" approach to be valid. Furthermore, the presence of the degeneracies of the electronic states close to the Fermi level (circled in the Figures) leads to a higher density of states which again causes an increase of the magnetization in these materials. Another way of visualizing the statements is provided by the computed Fermi surface for Sr_2FeReO_6 in Fig. 9. A decrease of the electron concentration leads to a closing of the open parts of the Fermi surface and to a more efficient nesting of its individual sections. Any lowering in the symmetry would induce a higher curvature of the individual segments which - in turn - leads to a less efficient nesting resulting in a smaller magnetization.

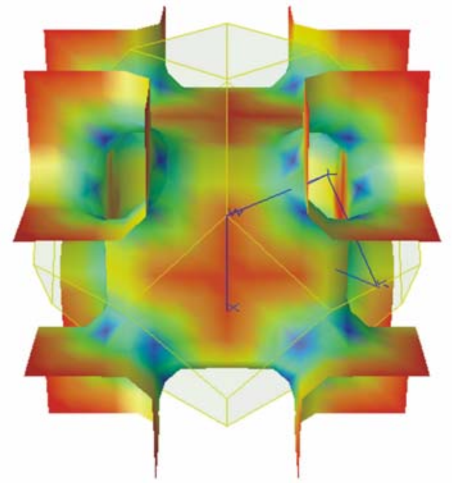

Fig. 9 Fermi surface of the majority (metallic) spin direction of Sr_2FeReO_6.

To achieve optimal Fermi surface nesting, i.e. to drive the compound closer to its electronic instability, one must decrease the electron concentration of the parent compound Sr_2FeReO_6 by replacing Fe with elements containing less valence electrons. A clear example of the opposite situation is given in the series $Sr_{2-x}La_xFeMoO_6$, where an increase of the Curie temperature is observed upon electron "doping" the parent Sr_2FeMoO_6 oxide. [30] This becomes obvious by inspecting Fig. 8a. Alternatively, substituting the compound with more electron-rich transition metals such as Zn will shift E_F further above the van Hove-singularity. In this case both saturation magnetization and Curie temperature should decrease.

The magnetic measurement on $Sr_2Fe_{1-x}Zn_xReO_6$ at 5 K indicates a decrease of the saturation magnetization with increasing Zn content (Fig. 10). According to our high temperature magnetic studies dilution of the magnetic iron sublattice with diamagnetic Zn does not weaken its magnetic interaction with the Re sublattice. (Fig. 7) Therefore, one should attribute the decrease of the saturation magnetization to the decrease of the concentration of magnetic iron atoms. Additionally, an increasing content of electron-rich elements (in our case Zn) leads to a decrease of the saturation magnetization and T_C because electron "doping" causes E_F to move away from the van Hove-singularity.

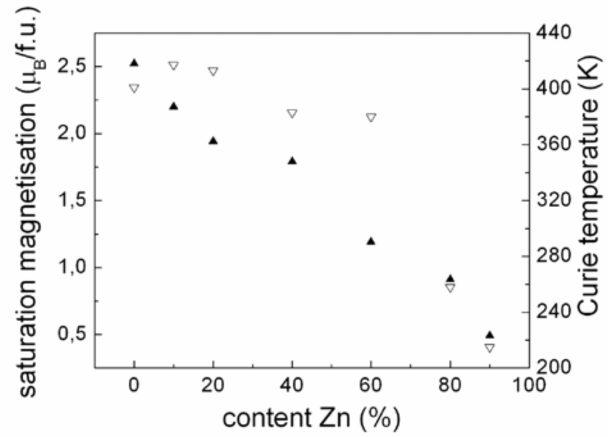

Fig. 10 Saturation magnetization of $Sr_2Fe_{1-x}Zn_xReO_6$ measured at 5 K (▲) and Curie temperatures measured in a magnetic field of 0.1 T (∇) versus Zn content.

For $Sr_2Fe_{1-x}Zn_xReO_6$ the Curie temperature T_C decreases from 417 K to 215 K as illustrated in Fig. 10. The non-monotonic concentrational T_C behaviour might be attributed to different crystal structures at ambient and elevated temperatures (> 300 K). One cannot exclude that for samples with 10 % and 20 % Zn content the transition temperature from the tetragonal to the cubic phase is located below the magnetic ordering temperature T_C. The elucidation of this question should follow from high temperature X-ray studies, which are in progress. As cubic symmetry should lead to enhanced electronic interaction in the crystal, T_C goes up. With increasing Zn content the tetragonal distortion increases. Therefore one can expect the tetragonal-cubic transition to occur at higher temperature. In this case lower T_C values (for Zn substitution levels exceeding 40 %) should be attributed to the tetragonal structure. In the range of concentrations above 80 %, the low values of T_C reflect the transition to the ferromagnetically ordered phase.

For Cr substitution a substantially different behaviour is observed. For small levels of substitution the saturation magnetization increases, reaches a maximum for a substitution level of approximately 10 % and subsequently falls off for higher levels of substitution. This is illustrated in Fig. 11. As the ionic radius of Cr^{3+} is with 75.5 pm slightly smaller than the radius of Fe^{3+} with 78.5 pm, Cr substitution should favour the cubic structure as expected from the computed values for the tolerance factor. As a result, the saturation magnetization should increase with increasing Cr content if electronic effects are not considered. From an electronic point of view, the saturation magnetization should decrease when the bands close to the Fermi level are depleted. The superposition of these two opposite tendencies leads to the non-monotonic behaviour of the magnetization as a function of the Cr content. Cr substitution levels higher than 10 % shift E_F far below the van Hove-singularity. Therefore, the saturation magnetization decreases upon higher Cr substitution levels.

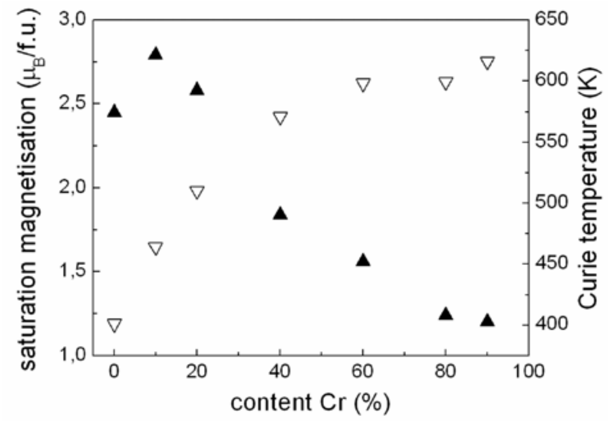

Fig. 11 Saturation magnetization of $Sr_2Fe_{1-x}Cr_xReO_6$ measured at 5 K (▲) and T_C measured at magnetic field of 0.1 T (∇) versus Cr content.

The Curie temperatures of the Cr samples shown in Fig. 11 are generally higher than those of the Zn containing samples because of the magnetic character of the Cr atoms. Additionally the distortions from cubic symmetry at room temperature of the Cr containing samples are smaller that the Zn containing ones. There is no correlation between the saturation magnetization and the Curie temperature. This finding may be explained from the differences of the crystal structures as one cannot exclude a tetragonal → cubic distortion for low Cr substitution levels upon heating as well as a cubic → tetragonal distortion for Cr rich samples upon cooling. The role of the structural factor in the magnetic properties of Cr substituted samples should be clarified in additional studies.

2.3.3 Mössbauer spectroscopy

The Mössbauer spectra of $Sr_2Fe_{0.8}M_{0.2}ReO_6$, with M = Fe, Zn, Cr taken at 130 K are displayed in Fig. 12. The 6-line pattern of the spectra is typical for materials in the magnetically ordered phase and the very sharp lines are indicative of a high degree of Fe(M)--Re order in the structure. A considerable cationic disorder would result in broadened lines due to a distribution of different environments of iron. [31-33] The results of the fit are collected in Table 2.

Table 2 Mössbauer data for $Sr_2Fe_{0.8}M_{0.2}ReO_6$, M = Fe, Zn, Cr and $Sr_2Fe_{1-x}Zn_xReO_6$, x = 0.2 and 0.8.

Compound	δ (mm/s)	H_{hf} (T)
Sr_2FeReO_6	0.67(1)	45.4(1)
$Sr_2Fe_{0.8}Zn_{0.2}ReO_6$	0.71(1)	44.3(1)
$Sr_2Fe_{0.8}Cr_{0.2}ReO_6$	0.67(1)	46.3(1)
$Sr_2Fe_{0.8}Zn_{0.2}ReO_6$	0.71(1)	44.3(1)
$Sr_2Fe_{0.2}Zn_{0.8}ReO_6$	0.75(1)	40.3(1)

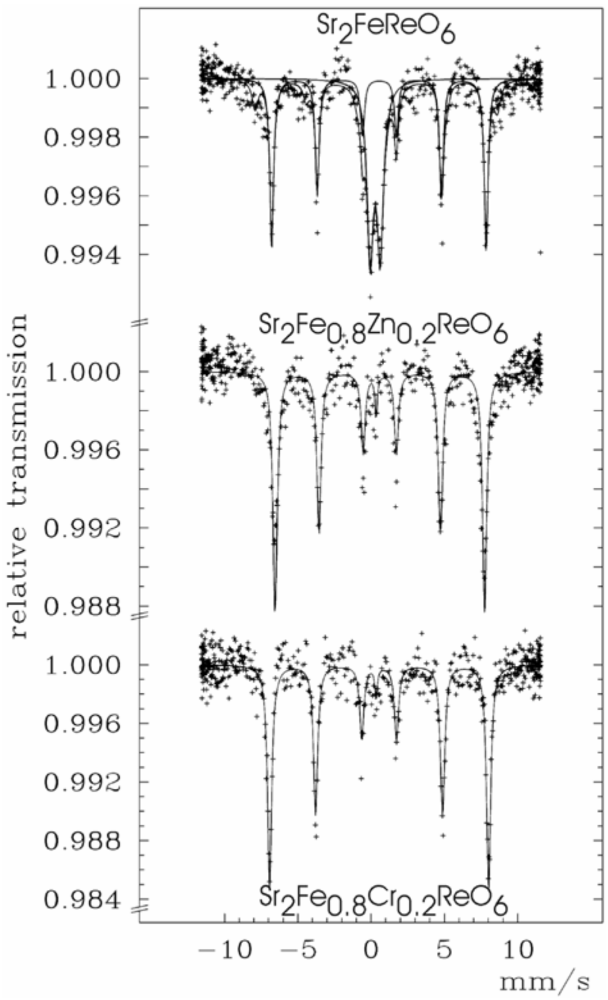

Fig. 12 Mössbauer spectra of $Sr_2Fe_{0.8}M_{0.2}ReO_6$ at 130 K, (a) M = Fe, (b) M = Zn, (c) M = Cr.

From Table 2 it is obvious that the isomer shifts (IS) are higher and the hyperfine fields (H_{hf}) are smaller compared to typical values of Fe^{3+} in iron oxides, but the IS's are too small and the H_{hf}'s too high for Fe^{2+} in oxidic compounds. The IS values of the double perovskites studied here are close to those of B-site Fe of Fe_3O_4, [34] indicating that Fe is in the $Fe^{2.5+}$-state or close to it.

Taking $Cs_2Fe_2(MoO_4)_3$ and $Li_3Fe(MoO_4)_3$ [35] as reference materials for pure Fe^{2+} and Fe^{3+} ions in the double perovskite structure at 130 K, respectively, it is possible to estimate (calculate) the mixed-valence charge state of iron in the title compounds. The derived values of the charge states are listed in Table 2; a valence state of $Fe^{2.69+}$ results for the non-substituted compound Sr_2FeReO_6. Partial substitution of iron by Zn^{2+} and Cr^{3+} induces a slight decrease of the charge on iron in the case of Zn and practically no change in the case of Cr, respectively. Among the members of the series $Sr_2Fe_{1-x}Zn_xReO_6$, the compound with x = 0.8 shows Fe in a valence state close to $Fe^{2.5+}$; this is manifested by a higher IS and an appropriately lower H_{hf} value compared to the non-substituted sample. It is observed that the IS's increase and the H_{hf}'s decrease with increasing Zn substitution according to the diamagnetic nature of Zn^{2+} ions (see Table 2 and Fig. 13).

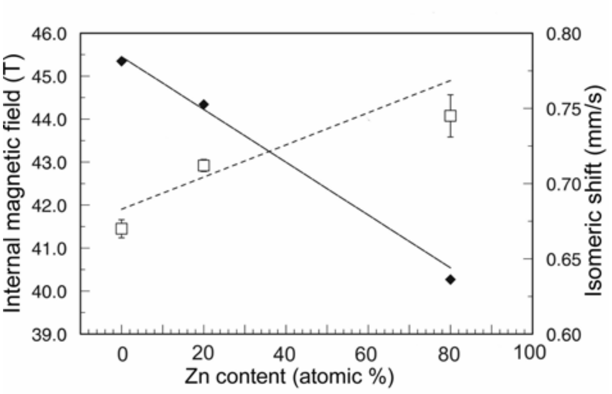

Fig. 13 Isomer shift (□) and internal magnetic field (■) of $Sr_2Fe_{1-x}Zn_xReO_6$ versus Zn content.

The observed H_{hf} values reflect the same trends; substitution by Zn leads to smaller, and substitution by Cr to higher internal fields. Two mechanisms can explain this finding. Firstly, the charge state of iron is changed due to the metal substitution. The limiting values are for $Fe^{2+} \leq 40$ T and for Fe^{3+} ca. 52 T. Secondly, Zn substitution increases the lattice parameters implicating a decrease in the exchange interaction of the iron ions; adding to this is the diamagnetic nature of Zn^{2+} ions which diminishes the exchange coupling. In the case of Cr substitution the lattice experiences a contraction which causes an increase in the exchange interaction.

2.4 Conclusion

We have explored the effect of transition metal substitution on the electronic and magnetic structure of the double perovskites $Sr_2Fe_{1-x}M_xReO_6$ (M = Cr, Zn). The focus of our study was to elucidate the role of the van Hove-scenario, i.e. to systematically use information from electronic band structure calculations for the prediction and targeted design of spintronic materials. The results of band structure calculations for the double perovskite Sr_2FeReO_6 indicated that the Fermi level is situated slightly above the van Hove-singularity. Therefore, one may achieve a coincidence of the Fermi level and the local maximum of the density of states by a decrease of the valence electron concentration. We demonstrated the validity of this model by substituting Sr_2FeReO_6 with Zn and Cr. As predicted, Cr substituion up to the optimal valence electron concentration leads to an enhancement of the magnetic characteristics such as Curie temperature and saturation magnetization. In contrast, Zn substitution leads to the opposite effect by an increase of the valence electron concentration. We also demonstrated that structural factors play an important role by competing with the electronic effects. Quantitative explanation of the structural models by means of the tolerance factor t revealed that the physical properties are influenced by the valence states and ionic radii of the constituting elements. The structural effects may be in line with the electronic effects for the series $Sr_2Fe_{1-x}Zn_xReO_6$ or opposite to the electronic factors as evidenced in the study of the series $Sr_2Fe_{1-x}Cr_xReO_6$. The superposition of structural and electronic effects can be considered the reason for the non-monotonic behaviour of the magnetic properties as a function of the degree of substitution.

2.5 References

[1] (a) A. P. Ramirez, *J. Phys.: Condens. Matter*, 1997, **9**, 8171; (b) C. N. R. Rao and B. Raveau, *Colossal magnetoresistance and other related properties in 3d oxides*, Eds; World Scientific: Singapore, 1998.

[2] (a) K.-I. Kobayashi, T. Kimura, H. Sawada, K. Terakura and Y. Tokura, *Nature*, 1998, **395**, 677; (b) K.-I. Kobayashi, T. Kimura, Y. Tomioka, H. Sawada, K. Terakura and Y. Tokura, *Phys. Rev. B*, 1999, **59**, 11159; (c) T. H. Kim, M. Uehara, S.-W. Cheong and S. Lee, *Appl. Phys. Lett.* 1999, **74**, 1737.

[3] W. Prellier, V. Smolyaninova, A. Biswas, C. Galley, R. L. Greene, K. Ramesha and J. Gopalakrishnan, *J. Phys.: Condens. Matter*, 2000, **12**, 965.

[4] I.V. Solovyev, *Phys. Rev. B*, 2002, **65**, 144446.

[5] J. Gopalakrishnan, A. Chattopadhyhay, S. B. Ogale, T. Venkatesan, R. L. Greene, A. J. Millis, K. Ramesha, B. Hannover and G. Marest, *Phys. Rev. B*, 2000, **62**, 9538.

[6] C. Felser, R. Seshadri, A. Leist and W. Tremel, *J. Mater. Chem.*, 1998, **8**, 787.

[7] J. Longo and R. Ward, *J. Am. Chem. Soc.*, 1961, **83**, 2816.

[8] A. W. Sleight, J. Longo and R. Ward, *Inorg. Chem.*, 1962, **1**, 245.

[9] A. W. Sleight and J. F. Weiher, *J. Phys. Chem. Solids*, 1972, **33**, 679.

[10] H. Kato, T. Okuda, Y. Okimoto, Y. Tomioka, Y. Takenoya, A. Ohkubo, M. Kawasaski and Y. Tokura, *Appl. Phys. Lett.*, 2002, **81**, 328.

[11] D. D. Sarma, P. Mahadevan, T. Saha-Dasgupta, S. Ray and A. Kumar, *Phys. Rev. Lett.*, 2000, **85**, 2549.

[12] D. D. Sarma, *Curr. Opinion Solid State Mater. Sci.*, 2001, **5**, 261.

[13] A. Jung, Diploma Thesis, *Johannes Gutenberg-Universität Mainz*, 2002.

[14] W. A. Harrison, *Electronic Structure and the Properties of Solids*, Dover Publications: New York, 1989.

[15] F. Sriti, N. Nguyen, C. Martin, A. Ducouret and B. Raveau, *J. Magn. Magn. Mater.*, 2002, **250**, 123.

[16] W. Haberditzl, *Magnetochemie*, Akademie-Verlag: Berlin, 1968.

[17] H. Spiering, L. Deák and L. Bottyán, *Hyp. Int.*, 2000, **125**, 197.

[18] P. Blaha, K. Schwarz, G. K. H. Madsen, D. Kvasnicka and J. Luitz, *Wien2k, An augmented plain wave + local orbitals program for calculating crystal properties*, (Karlheinz Schwarz, Techn. Universtität Wien, Austria), 2001.

[19] N. Auth, G. Jakob, W. Westerburg, C. Ritter, I. Bonn, C. Felser and W. Tremel, *J. Magn. Magn. Mater.*, accepted for publication.

[20] J. Rodríguez-Carvajal, *Physica B*, 1993,**192**, 55.

[21] J. Blasco, C. Ritter, L. Morellon, P. A. Algarabel, J. M. De Teresa, D. Serrate, J. García and M. R. Ibarra, *Solid State Sci*, 2002, **4**, 651.

[22] X. M. Feng, G. H. Rao, G. Y. Liu, H. F. Yang, W. F. Liu, Z. W. Ouyang and J. K. Liang, *Physica B*, 2004, **344**, 21.

[23] R. D. Shannon, *Acta Crystallogr.*, 1976, **A32**, 751.

[24] U. Müller, *Anorganische Strukturchemie*; Teubner Studienbücher: Stuttgart, 1996.

[25] G. Popov, M. Greenblatt and M. Croft, *Phys. Rev. B*, 2003, **67**, 024406.

[26] A. Maignan, B. Raveau, C. Martin and M. Hervieu, *J. Solid State Chem.*, 1999, **144**, 224.

[27] J. A. Alonso, M. T. Casais, M. J. Martinez-Lope, J. L. Martinez, P. Velasco, A. Munoz and M. T. Fernandez-Diaz, Chem. Mater., 2000, **12**, 161.

[28] H. Kato, T. Okuda, Y. Okimoto, Y. Tomioka, K. Oikawa, T. Kamiyama and Y. Tokura, *Phys. Rev. B*, 2002, **65**, 144404.

[29] C. Kittel, *Introduction to solid state physics*, VCH Wiley: New York, London, Sydney, Toronto, 1976.

[30] J. Navarro, C. Frontera, L. I. Balcells, B. Martínez and J. Fontcuberta, *Phys. Rev. B*, 2001, **64**, 092411.

[31] T. Alamelu, U. V. Varadaraju, M. Venkatesan, A. P. Douvalis and J. M. D. Coey, *J. Appl. Phys.*, 2002, **91**, 8909.

[32] J. M. Greneche, M. Venkatesan, R. Suryanarayanan and J. M. D. Coey, *Phys. Rev. B*, 2001, **63**, 174403.

[33] D. D. Sarma, E. V. Sampathkumaran, S. Ray, R. Nagarajan, S. Majumdar, A. Kumar, G. Nalini and T. N. Guru Row, *Solid State Commun.*, 2000, **114**, 465.

[34] S. Nakamura, L. Li, M. Tanaka, S. Todo and K. Siratori, *J. Phys. Soc. Jpn.*, 1997, **66**, 472.

[35] I. Bonn, in partial fulfillment of the Ph.D. Thesis, private communication, 2003.

3. Magnetic transitions in the double perovskite Sr_2ZnReO_6

3.1 Introduction

The crystal structure of ordered double perovskites $A_2MM'O_6$ (A = alkaline earth metal, M = 3*d* transition metal and M' = transition metal) can be considered a regular arrangement of corner sharing MO_6 and $M'O_6$ octahedra alternating along the three directions of the crystal. Large A cations are situated in the voids between the octahedra. (Fig. 1) Size and valence of the cations A^{2+}, M^{n+} and M'^{m+} determine the structural properties of these double perovskites. [1-3] In general, double perovskites with A = Ba^{2+} are cubic, whereas the smaller A = Sr^{2+} cation leads to a tetragonal distortion, and the even smaller Ca^{2+} cation enforces a monoclinic structure. For Sr_2ZnReO_6 and $Sr_2Fe_{1-x}Zn_xReO_6$ tetragonally as well as monoclinic distorted crystal structures have been reported. The Zn–O–Re angles adopt values between 167 ° and 180 °. In case of a 180 ° Zn–O–Re angle, the atoms Zn, O and Re are aligned on the edge of the cubic unit cell whereas smaller angles lead to a tilting of the ZnO_6 and ReO_6 octahedra about the common oxygen atom. Most importantly, this bending of the octahedra leads to a change in the through bonds Zn–O–Re interactions. [4,5]

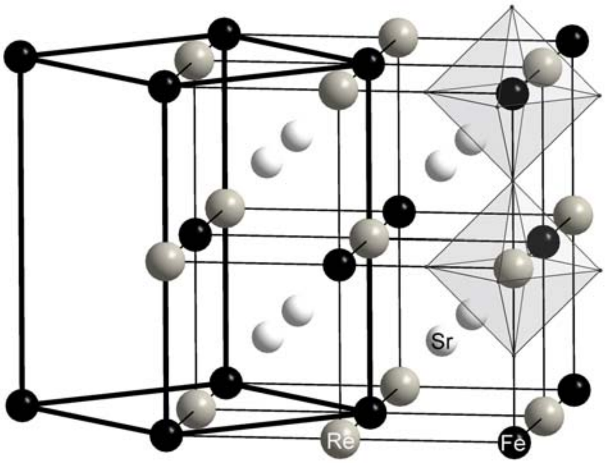

Fig. 1 Crystal structure of the double perovskite Sr_2FeReO_6; Fe (black), Re (dark grey), Sr (light grey), and O (corners of the octahedra); the cubic unit cell is drawn in thin black lines, the tetragonal unit cell in thick black lines.

The parent double perovskite Sr_2FeReO_6 receives a lot of attention due to its low-field tunneling type magnetoresistance at room temperature (PMR) and its possible application in spintronic devices. The effect of substitution of the Fe position by a diamagnetic valence-invariant metal has been probed on the basis of different series of solid solutions, e.g. $Sr_2Fe_{1-x}Zn_xReO_6$, $Sr_2Fe_{1-x}Mg_xMoO_6$ and A_2MgReO_6 (A = Ca, Sr, Ba). [5-7] Sr_2FeReO_6 is reported to be an itinerant ferrimagnetic compound owing to the linear sequence of Fe–O–Re–O–Fe units which enables the mediation of the electronic interaction via Zener double exchange. [8] Therefore, the magnetic structure of the parent compound can be considered as two different ferromagnetic sublattices – one Fe-based and one Re-based – which couple antiferromagnetically via the oxygen atoms bridging the Re and Fe atoms. [1-3,5,9,10] Sher et al., Bramnik et al. and Jung et al. report congruently the substitution of Fe by a diamagnetic metal to bleach only the long-range ferromagnetic order within the Fe sublattice whereas the long-range ferromagnetic order within the Re/Mo sublattice is retained over the whole range of substitution. Thus, dilution of the ferromagnetic metal Fe by a non-magnetic metal such as Zn or Mg causes a change from itinerant ferrimagnetic to ferromagnetic behaviour for higher Zn/Mg contents. Moreover, the end members of the solid solution series $A_2Fe_{1-x}Mg_xReO_6$, i.e. Ca_2MgReO_6, Sr_2MgReO_6 and Ba_2MgReO_6, can still be judged as soft magnets. Magnetic measurements at 5 K indicate a coexistence of paramagnetic and ferromagnetic regions. [5-7]

In contrast Kato et al. assume Sr_2ZnReO_6 to be antiferromagnetic with slight ferromagnetic impurities which stem from a spin-glass like ground state or a spin canting of the Re^{6+} ions due to a tilting of the ZnO_6 and ReO_6 octahedra. [4]

In order to elucidate these contradictory results, we studied the crystal and magnetic structures of Sr_2ZnReO_6. The results are presented in this contribution.

3.2 Experimental

Starting materials were reagent grade SrO (Aldrich, 99.9 % purity), ZnO (Aldrich, 99.99 % purity) and ReO_3 (Alfa Aesar, 99.9 % purity). All starting materials are stored in a glove box under argon (Braun Labmaster) and examined by X-ray powder diffraction prior to use.

Sr_2ZnReO_6 samples were prepared by high-temperature solid state reactions. Because of the strongly hygroscopic character of SrO, the samples were prepared under inert gas atmosphere in a glove-box. Stoichiometric amounts of SrO, ZnO and ReO_3 with a 2 % excess of ZnO were ground in an agate mortar and pressed into pellets. In order to avoid Sr^{2+} attack on the quartz tubes these pellets were transferred into corundum containers and finally sealed in evacuated quartz tubes. The samples were annealed for seven days at 1000°C. Thereafter they were rapidly cooled to room temperature by quenching in ice.

X-ray powder diffraction patterns were recorded using a Siemens D5000 diffractometer with monochromatized (Ge (111)) Cu $K_{\alpha 1}$ radiation equipped with a Braun DM50 linear PSD in transmission mode. Lattice constants obtained by Rietveld refinement using the program FULLPROF [11] were refined relative to Si as internal standard.

Temperature dependent magnetic susceptibility measurements of Sr_2ZnReO_6 were performed using the Quantum Design MPMS-XL SQUID magnetometer. Experimental data were corrected for diamagnetism using Pascal's constants. [12]

3.3 Results and discussion

3.3.1 Crystal Structure

The crystal structure of Sr_2ZnReO_6 was determined by X-ray powder diffraction in transmission mode. The XRD pattern of the compound under study (with Si as internal standard) together with the reflection positions and the difference curve of the Rietveld fit is given in Fig. 2. The X-ray pattern reveals that Sr_2ZnReO_6 adopts the tetragonally distorted double perovskite structure as reported for the solid solutions series $Sr_2Fe_{1-x}Zn_xReO_6$ ($0.1 < x < 0.9$). [5] The best agreement parameter (R_{Bragg} = 4.43) resulted from refinement in space group *I*4/*mmm* with Sr situated on site 4*d*, Zn on site 2*a*, Re on site 2*b*, O1 on site 8*h* and O2 on site 4*e*. (Table 1) The lattice constants and the unit cell volume were refined to a = 5.578615(6) Å, c = 7.99892(1) Å and V = 248.93 Å^3. (Table 1) The mean bond lengths of Re–O and Zn–O (1.78 Å and 2.19 Å, respectively) as well as the volumes of the corresponding MO_6 and $M'O_6$ octahedra ($V(ZnO_6)$ = 20.11 Å^3, $V(ReO_6)$ = 11.69 Å^3) are comparable to the ionic radii given by Shannon et al. ($r(Zn^{2+})$ = 74 pm, $r(Re^{6+})$ = 55 pm). [13] The Zn–O–Re bond angle is 180 °, i.e. the crystal structure does not exhibit any tilting of the ReO_6 and ZnO_6 octahedra. Thus, the linear Zn–O–Re–O–Zn units corresponding to a Zener double exchange are preserved. [8]

However, Kato et al. report a phase separation of Sr_2ZnReO_6 at room temperature. 85 % of the compound crystallizes in the tetragonal space group *I*4/*m*, 15 % in the monoclinic space group *P*2$_1$/*n*. [4] In contrast to our structural model, the tetragonal space group *I*4/*m* allows a tilting of the ReO_6 and ZnO_6 octahedra. Kato et al. determined the Zn–O–Re bond angles along [110] to be approx. 166 °. Therefore, a direct Re–Zn–Re interaction is feasable.

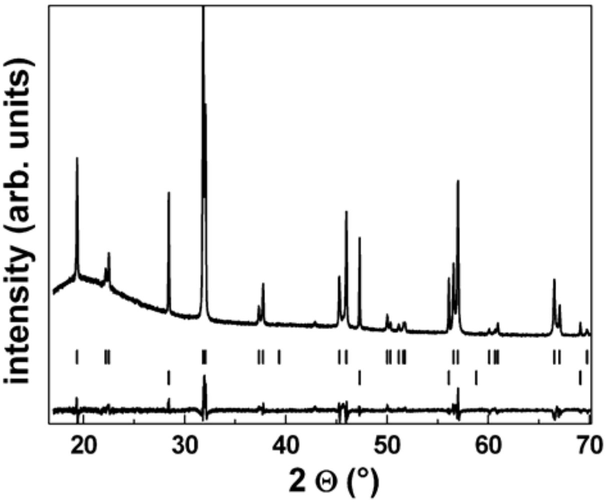

Fig. 2 X-ray pattern of Sr_2ZnReO_6 mixed with Si as internal standard (upper black line), the positions of the reflections of Sr_2ZnReO_6 (upper black bars) and Si (lower black bars) and the corresponding difference curve (lower black line).

Table 1. Atomic coordinates for Sr_2ZnReO_6 at room temperature (space group *I*4/*mmm*). Agreement parameter of the refinement R_{Bragg} = 4.43.

atom	site	*x*	*y*	z	SOF
Sr	4*d*	0	½	¼	1
Zn	2*a*	0	0	0	0.999
Re	2*a*	0	0	0	0.001
Re	2*b*	0	0	½	0.999
Zn	2*b*	0	0	½	0.001
O1	8*h*	0.26536	0.26536	0	1
O2	4*e*	0	0	0.28680	1

The perovskite tolerance factor *t* for perovskites of the general formula AMX_3 describes the interrelation between the perovskite structure and the associated ionic radii. [13,14]

$$t = \frac{r(A) + r(X)}{\sqrt{2}\left[r(M) + r(X)\right]}$$

For the solid solution series $Sr_2Fe_{1-x}Zn_xReO_6$ (0.1 < x < 0.9) the monotonous decrease of the *t* values with increasing x is in good agreement to the increasing tetragonal distortion of the crystal structure monitored by the relation $c/a = \sqrt{2}$ for a cubic phase. [5] Consequently, *t* = 0.892 for Sr_2ZnReO_6 indicates a tetragonal distortion of the sample. The *c*/*a* ratio calculated from the refined values for *c* and *a* (*c*/*a* = 1.4339) is in accordance with the structural behaviour based on a space filling model (cf. *c*/*a* = 1.429 for $Sr_2Fe_{0.1}Zn_{0.9}ReO_6$).

3.3.2 Magnetic measurements

The parent double perovskite Sr_2FeReO_6 is a soft ferrimagnetic half-metal with a Curie temperature (T_C) of 401 K and an expected saturation magnetization (M_S) of 3 μ_B/f.u. The magnetic structure consists of a Fe-based and a Re-based ferromagnetic sublattice which are bridged in an antiferromagnetic manner by means of the common oxygen atoms of the corner sharing FeO_6 and ReO_6 octahedra. Therefore, the Zener double exchange along the –Fe–O–Re–O–Fe– pathways leads to overall ferrimagnetic behaviour of Sr_2FeReO_6. [5,9,10,14-17] Along the series of solid solutions $Sr_2Fe_{1-x}Zn_xReO_6$ ($0 \leq x \leq 0.9$) a non-monotonous decrease of T_C (T_C (x = 0.9) = 215 K) and a monotonous decrease of the saturation magnetization (M_S (x = 0.9) = 0.5 μ_B/f.u.) was demonstrated. [5] Moreover, magnetic susceptibility measurements reveal a transition of ferri- to ferromagnetism due to the disappearance of the long-range ferromagnetic interactions within the Fe-based sublattice upon high Zn concentration. As the long-range magnetic interactions within the Re-based sublattice are not influenced by the Zn substitution the members in the range $0.6 \leq x \leq 0.9$ of the solid solution series are itinerant ferromagnets. The decrease of M_S upon increasing the Zn content confirms the antiferromagnetic interaction between the two sublattices along the whole range of substitutions.

Fig. 3 shows the molar susceptibility of Sr_2ZnReO_6 as a function of the temperature. The run of the curve exhibits the typical temperature dependence of a ferromagnetic or ferrimagnetic compound with a paramagnetic to ferromagnetic transition at 18 K. The existence of ferromagnetic impurities in the sample can be excluded as any ferromagnetic impurity would disturb the temperature independence of χ_M (T) in the temperature range above 50 K. However, the temperature dependence of $1/\chi_M$ (inset of Fig. 3) does not only show the Curie temperature at 18 K but two more transitions (at 27 K and 120 K). Thus, the ferromagnetic behaviour of the $1/\chi_M$ (T) curve is found only below approx. 27 K. The paramagnetic region begins at the transition temperature at 27 K and is superimposed by a -probably- structural transition at 120 K.

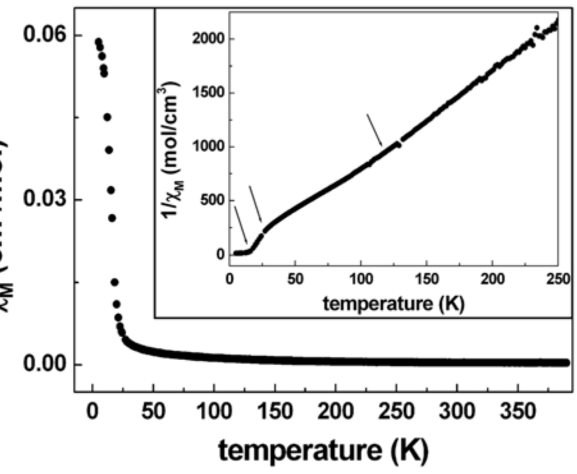

Fig. 3 Molar susceptibility of Sr_2ZnReO_6 as a function of temperature; inset: inverse molar susceptibility vs. temperature. The arrows indicate the estimated transition temperatures.

To gain more insight into the magnetic structure of Sr_2ZnReO_6, field dependence curves of the magnetization were measured within the three different temperature regions defined above ($T < 18$ K, $18 \text{ K} < T < 27$ K and $T > 27$ K). The data at 40 K (Fig. 4 ▲) do not show a magnetic hysteresis, but a straight line indicating paramagnetic behaviour above the unspecified transition at 27 K. At 20 K (Fig. 4 ●) the superposition of a small magnetic hysteresis loop and a straight line suggests a coexistence of ferromagnetic and paramagnetic clusters between 18 K and 27 K. At 5 K, a hysteresis loop typical for Zn-substituted double perovskites denotes a state of complete magnetic order. (Fig. 4 ■) However, the saturation magnetization determined at 5 K and 50 kOe ($M_S = 0.13$ μ_B/f.u.) is not in accordance with the estimated value of $M_S = 1$ μ_B/f.u. which is expected by considering the standard Zn–O–Re–O–Zn double exchange leading to an antiferromagnetic arrangement of Zn^{2+} ($3d^{10}$) and Re^{6+} ($5d^1$).

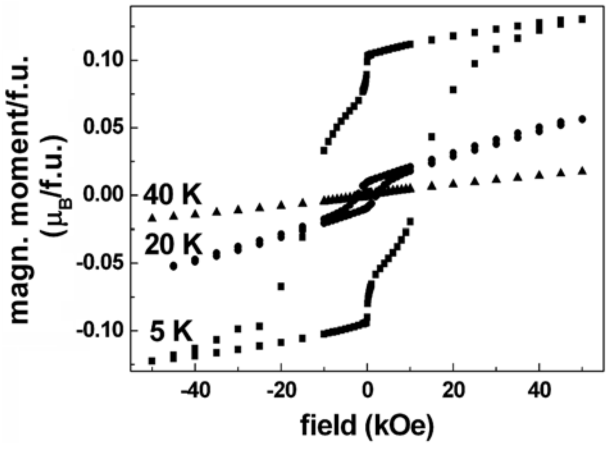

Fig. 4 Field dependence of the magnetization of Sr_2ZnReO_6 at 5 K, 20 K and 40 K.

The type of magnetic interaction between the metal cations in the paramagnetic temperature region (T > 27 K) can be determined by examining the χ_MT *versus* T curve. (Fig. 5) The negative slope from 92 K to 250 K indicates ferromagnetic interaction within the paramagnetic region whereas the positive slope below 92 K proves antiferromagnetic interaction in the paramagnetic region.

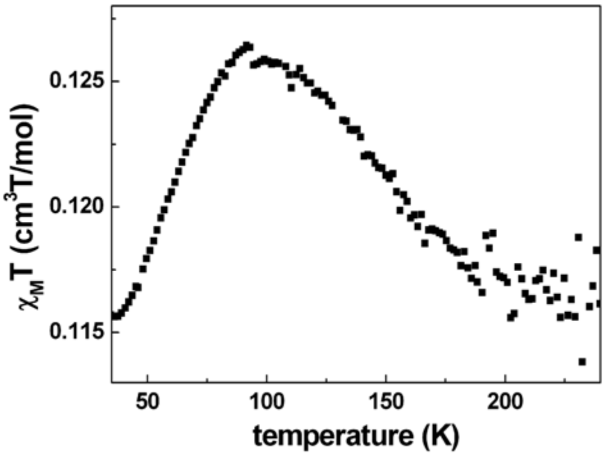

Fig. 5 Molar susceptibility of Sr_2ZnReO_6 multiplied by the temperature as a function of the temperature.

Kato et al. [4] concluded Sr_2ZnReO_6 to consist of a mainly antiferromagnetic phase (T_N = 20 K) with slight ferromagnetic impurities. This assumption was based exclusively on the temperature dependence of the inverse molar susceptibility. However, the detailed investigations of the temperature and field dependence of the molar susceptibility presented in this work, exhibit Sr_2ZnReO_6 to be ferromagnetic or ferrimagnetic below 18 K and paramagnetic above 27 K. The type of magnetic interaction in the temperature region between 18 K and 27 K can not be determined by magnetic susceptibility measurements only. The magnetic structure of Sr_2ZnReO_6 will be elucidated in more detail by means of X-ray and neutron diffraction measurements at low temperature.

3.4 Conclusion

In this study, the crystallographic and magnetic properties of Sr_2ZnReO_6 were explored by means of X-ray structural analysis at room temperature and temperature as well as field dependent magnetic measurements. The single phase compound Sr_2ZnReO_6 crystallizes in a tetragonally distorted, ordered double perovskite structure (space group *I*4/*mmm*). The lattice constants *a* and *c* as well as the volumes of the ZnO_6 and ReO_6 octahedra are in good agreement with the ionic radii reported in the literature. [13] The different sizes of the ZnO_6 and ReO_6 octahedra prevent antisite disorder. Moreover, the straight alignment of Zn, O and Re on the edges of the cubic unit cell without any tilting of the MO_6 and $M'O_6$ octahedra preserves the Zn–O–Re–O–Zn pathways of the Zener double exchange which mediates the electronic interaction in double perovskites. Therefore, a direct Zn-Re-

Zn interaction without the bridging oxygen atoms, as suggested by Kato et al. [4] is in contradiction to our structural model.

Temperature and field dependent susceptibility measurements hint at (i) the absence of ferromagnetic impurities, (ii) a ferro- or ferrimagnetic order of the Re^{6+} ($5d^1$) spins below 18 K and (iii) a paramagnetic state above 27 K. The magnetic structure between T_C = 18 K and the transition at 27 K is subject to ongoing investigations.

3.5 References

[1] J. Longo and R. Ward, *J. Am. Chem. Soc.*, 1961, **83**, 2816.

[2] A. W. Sleight, J. Longo and R. Ward, *Inorg. Chem.*, 1962, **1**, 245.

[3] A. W. Sleight and J. F. Weiher, *J. Phys. Chem. Solids*, 1972, **33**, 679.

[4] H. Kato, T. Okuda, Y. Okimoto, Y. Tomioka, K. Oikawa, T. Kamiyama and Y. Tokura, *Phys. Rev. B*, 2004, **69**, 184412.

[5] A. Jung, I. Bonn, V. Ksenofontov, G. Melnyk, J. Ensling, C. Felser and W. Tremel, *J. Mater. Chem.*, 2005, **15**, 1760.

[6] K. G. Bramnik, H. Ehrenberg, J. K. Dehn and H. Fuess, *Solid State Sci.*, 2003, **5**, 235.

[7] F. Sher, A. Venimadhav, M. G. Blamire, B. Dabrowski, S. Kolesnik and J. P. Attfield, *Solid State Sci.*, 2005, **7**, 912.

[8] C. Zener, *Phys. Rev.*, 1951, **81**, 440; C. Zener, *Phys. Rev.*, 1951, **82**, 403; C. Zener, *Phys. Rev.*, 1951, **83**, 299; C. Zener, *Phys. Rev.*, 1952, **85**, 324.

[9] K.-I. Kobayashi, T. Kimura, Y. Tomioka, H. Sawada, K. Terakura and Y. Tokura, *Phys. Rev. B*, 1999, **59**, 11159.

[10] T. H. Kim, M. Uehara, S.-W. Cheong and S. Lee, *Appl. Phys. Lett.*, 1999, **74**, 1737.

[11] J. Rodríguez-Carvajal, *Physica B*, 1993,**192**, 55.

[12] W. Haberditzl, *Magnetochemie*, Akademie-Verlag: Berlin, 1968.

[13] R. D. Shannon, *Acta Crystallogr.*, 1976, **A32**, 751.

[14] U. Müller, *Anorganische Strukturchemie*, Teubner Studienbücher: Stuttgart, 1996.

[15] H. Kato, T. Okuda, Y. Okimoto, Y. Tomioka, K. Oikawa, T. Kamiyama and Y. Tokura, *Phys. Rev. B*, 2002, **65**, 144404.

[16] A. Jung, V. Ksenofontov, S. Reiman, H. A. Therese, U. Kolb, C. Felser and W. Tremel, *Phys. Rev. B*, 2006, in print.

[17] E. Carvajal, O. Navarro, R. Allub, M, Avignon and B. Alascio, *Phys. Stat. Sol. B*, 2005, **242**, 1942.

[18] A. Poddar and S. Das, *Physica B – Cond. Mat.*, 2004, **344**, 325.

4. Magnetic transitions in double perovskite $Sr_2FeRe_{1-x}Sb_xO_6$ ($0 \leq x \leq 0.9$)

4.1 Introduction

The double perovskites Sr_2FeReO_6 and Sr_2FeMoO_6 reveal half-metallic ferrimagnetic behaviour at room temperature. Both compounds obey a relatively high Curie temperature (401 K and 415 K, respectively) which is an important condition for a high degree of spin polarization at room temperature. The conceptual basis for half- metallic ferromagnetism is a large density of states of one spin direction at the Fermi level whilst the other spin direction is insulating. The origin of the large density of states in the vicinity of the Fermi level can be related to a van Hove singularity in the band structure of these compounds as it was suggested in a previous study. [1] It could be demonstrated by the systematic use of electronic band structure calculations that it is possible to predict and tune the electronic structure of spintronic materials, e.g. by diamagnetic dilution [2-5] (i.e. systematic replacement of ions contributing to the magnetic interactions within the sample by diamagnetic ions) of the Fe-sublattice by Zn^{2+} which leads to a transition of the magnetic properties from ferrimagnetic for slight Zn substitution (up to 60 %) to ferromagnetic for heavy Zn substitution (> 60 %). This conclusion was drawn from the weak overall concentrational dependence of the paramagnetic Curie temperature in the solid solution series $Sr_2Fe_{1-x}Zn_xReO_6$ ($0 < x < 0.9$) which is compatible with itinerant magnetic behaviour. With increasing Zn concentration the exchange interaction within the Fe-based sublattice weakens. At some critical concentration of Zn ($x \cong 0.6 - 0.8$) the long-range magnetic correlations within this sublattice disappear, whereas the long-range magnetic correlations within the Re sublattice remain unchanged. Therefore, heavy Zn dilution leads to the transformation of the ferrimagnetic to the ferromagnetic type of ordering. [1]

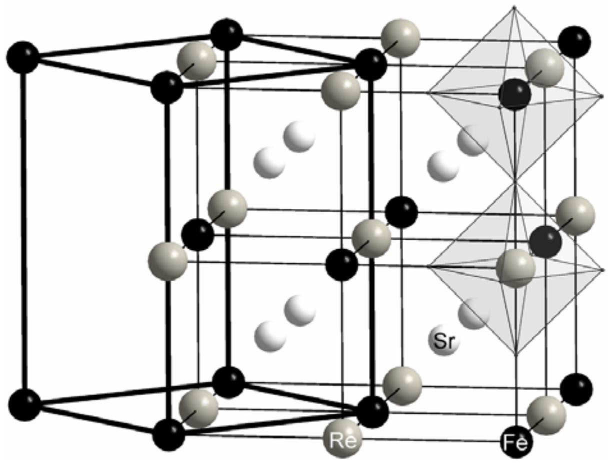

Fig. 1 Crystal structure of the double perovskite Sr_2FeReO_6; Fe (black), Re (dark grey), Sr (light grey), and O (corners of the octahedra); the cubic lattice is drawn in thin black lines, the tetragonal lattice in thick black lines.

Sr_2FeReO_6 as well as Sr_2FeMoO_6 belong to the family of double perovskites of the general formula $A_2MM'O_6$, where the M and M′ sites are occupied alternatively by different transition metal cations (M = first row transition metal; M′ = Mo, W, Re). [6,7] The ideal structure of these compounds can be viewed as a regular arrangement of corner sharing MO_6 and $M'O_6$ octahedra alternating along the three directions of the crystal with large A cations situated in the voids between the octahedra. (Fig. 1) Crystal structure and physical properties of double perovskite oxides strongly depend on size and valencies of the cations A, M and M′. E. g. Sr_2FeReO_6 as well as Sr_2FeMoO_6 show a slight tetragonal distortion from the ideal cubic structure. [8] Sr_2FeReO_6 crystallizes in the space group *I*4/*mmm* as determined by X-ray powder diffraction. (Fig. 2a) Cations Fe^{3+} ($3d^5$, $S = 5/2$) and Re^{5+} ($5d^2$, $S = 1$) order antiferromagnetically and the conduction band is composed of the 5*d* down spin electrons of Re^{5+}. The resulting arrangement of Fe^{3+} and Re^{5+} leads to an overall ferrimagnetic behaviour of Sr_2FeReO_6. [9-12]

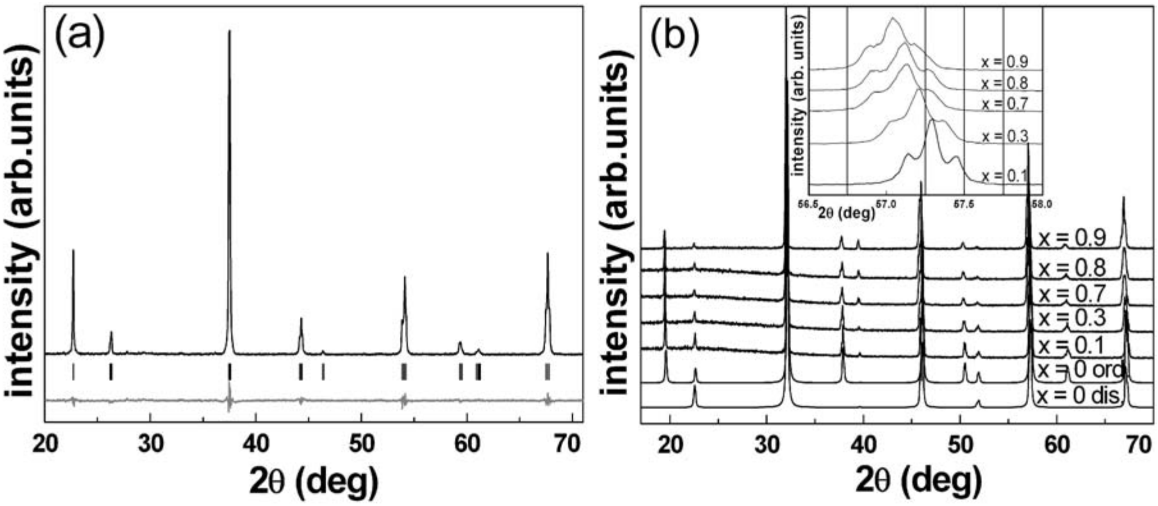

Fig. 2 (a) X-Ray pattern of Sr_2FeReO_6 (black), positions of the reflections (black bars) and the corresponding difference curve (grey); (b) calculated X-Ray pattern of Sr_2FeReO_6 in space group *I*4/*mmm* with fully disordered Fe/Re site (x = 0 dis.), with fully ordered Fe/Re site (x = 0 ord.) and measured X-ray patterns of $Sr_2FeRe_{1-x}Sb_xO_6$; inset: range 56.5 ° < 2θ < 58.0 ° highlighted.

In Ref. 1 it turned out that the 5*d* transition element Re plays an important role in the magnetic coupling between the 3*d* metal atoms. Furthermore, the 5*d* elements act as an electron buffer which stabilizes the valence state of the magnetic element Fe, independent of the substitution level. In the present study we explore the alternative approach to replace the electronic 5*d* buffer element Re by the main group element Sb which formally has the same oxidation state as Re and Mo in the double perovskites Sr_2FeReO_6 and Sr_2FeMoO_6. One can envision that the lack of *d* orbitals requires a fixed valence for Sb and prevents Sb to act as an electron buffer. Furthermore, we expect that the lack of *d* orbitals should have a dramatic influence on the Zener double exchange [13] between the magnetic atoms through the Re *d* orbitals.

In an attempt to probe the influence of the diamagnetic dilution of the Re sublattice we have investigated the solid solution series $Sr_2FeRe_{1-x}Sb_xO_6$ ($0 < x < 0.9$). Here, we report the synthesis, crystal structure and magnetic properties of these compounds.

4.2 Experimental

Starting materials were reagent grade SrO (Aldrich, 99.9 % purity), Fe_2O_3 (Alfa Aesar, 99.99 % purity), Re metal, Re_2O_7 (Alfa Aesar, 99.9 % purity) and Sb_2O_5 (Alfa Aesar, 99.999 % purity). All starting materials are stored in a glove box under argon (Braun Labmaster) and examined by X-ray powder diffraction prior to use.

The $Sr_2FeRe_{1-x}Sb_xO_6$ ($0 \leq x \leq 0.9$) samples were prepared by high-temperature solid state reactions. Because of the strongly hygroscopic properties of SrO and the high vapour pressure of Re_2O_7 the samples were prepared under inert gas atmosphere in a glove-box. Stoichiometric amounts of SrO, Fe_2O_3, Re, Re_2O_7, and Sb_2O_5 (2 SrO : (1-x)/2 Fe_2O_3 : 0.3 Re : 0.35 Re_2O_7 : x/2 Sb_2O_5) were ground in an agate mortar and pressed into pellets. In order to avoid Sr attack on the quartz tubes these pellets were transferred into corundum containers and finally sealed in evacuated quartz glass tubes. The samples were annealed for seven days at 1000°C. Thereafter they were rapidly cooled to room temperature by quenching in ice. Preparations aiming at the fully substituted compound Sr_2FeSbO_6 were unsuccessful.

X-ray powder diffraction measurements were performed using a Seifert XRD 3000 TT diffractometer with a secondary monochromator (Si) equipped with a Cu source and operating in reflection mode and a Bruker D5000 with a secondary monochromator (graphite) equipped with a Co source and operating in reflection mode.

HRTEM analyses were measured by FEI Tecnai F30 ST operated at an extraction voltage of 300kV (equipped with an EDXA energy dispersive X-ray spectrometer) and by selected area electron diffraction techniques (SAED). For transmission electron microscopic (TEM) studies, the sample was dispersed in ethanol ultrasonically first and then a drop of it was placed on a copper grid coated with a carbon film.

The variable - temperature magnetic susceptibility measurements of $Sr_2FeRe_{1-x}Sb_xO_6$ were performed using the Quantum Design MPMS-XL SQUID magnetometer, equipped with a high-temperature furnace. Experimental data were corrected for diamagnetism using Pascal’s constants. [14]

The DC conductivity measurements were done using the four point probe method. The samples were measured using an OXFORD helium bath cryostat operating in the temperature range from 4.2 K to 295 K.

Mössbauer measurements of $Sr_2FeRe_{1-x}Sb_xO_6$ powder samples were performed in transmission geometry using a constant-acceleration spectrometer and a helium bath cryostat. ^{57}Fe Mössbauer spectra were recorded between room temperature and 4.2 K using the 50 mCi source ^{57}Co(Rh). The Recoil 1.03 Mössbauer Analysis Software was used to fit the experimental spectra. [15] Isomer shift values are quoted relative α-Fe at 293 K.

A ^{121m}Sn ($CaSnO_3$) source with activity of 3.0 mCi was placed together with the absorber in the helium bath cryostat. ^{121}Sb Mössbauer spectra were analyzed with the program EFFINO [16] using Lorentzian line shapes. During the fit the source recoil-free fraction value was fixed at 0.6.

Band structure calculations were performed within the potential augmented plane-wave (FLAPW) framework within the generalized gradient approximation (GGA). [17] The crystal structure of the parent compound Sr_2FeReO_6 was approximated by the ideal cubic structure of a double perovskite with the lattice parameter a = 7.89 Å. The number of k points in the irreducible Brillouin zone is 20. The crystal structure of Sr_2FeSbO_6 was approximated from the crystal structures of $Sr_2FeRe_{0.2}Sb_{0.8}O_6$ and $Sr_2FeRe_{0.1}Sb_{0.9}O_6$ to be tetragonal (space group $I4/mmm$) with lattice parameters a = 5.57 Å and c = 7.94 Å. The number of k points in the irreducible Brillouin zone is 28. The convergence criterion was fixed to 0.0001 Ry for both calculations.

4.3 Results and discussion

4.3.1 Structural characterization

The crystal structures of the series $Sr_2FeRe_{1-x}Sb_xO_6$ ($0 \le x \le 0.9$) were determined by powder X-ray diffraction in reflection mode. The corresponding X-ray patterns reveal that the samples - as the unsubstituted parent compounds - adopt a double perovskite structure. [6,7,18,19] An X-ray pattern of Sr_2FeReO_6 together with the Rietveld fit (refined with the FULLPROF program [20]) and the corresponding difference curve are given in Fig. 2a. X-ray patterns of $Sr_2FeRe_{1-x}Sb_xO_6$ are presented in Fig. 2b together with the most informative part of the X-ray diffractogram in the range 56.75 ° < 2θ < 57.75 ° which is highlighted as an insert in the Figure. The reflection profiles indicate that the symmetry of the lattice does not change as a function of the Sb content. The three elements Fe, Re and Sb have to be distributed on two lattice sites which raises the question of cation disorder. Attempts to account for an Fe/Re antisite disorder with the aid of Rietveld refinement lead to maximum disorder ratios of 2 % independent of the degree of Sb substitution. These findings are supported by the results of the High Resolution Transmission Electron Microscopy (HRTEM) studies (*vide infra*). The observed absence of antisite disorder precludes the presence of Fe–O–Fe clusters. Lattice parameters *a* and *c* of Sr_2FeReO_6 and $Sr_2FeRe_{1-x}Sb_xO_6$ as obtained by Rietveld refinements are plotted in Fig. 3. As predicted by Vegard's rule the dependence of the lattice parameters on the Sb content of the solid solution is almost linear, confirming the existence of a continuous solid solution series in the range $0 \le x \le 0.9$. The lattice parameters and unit cell volumes increase with increasing Sb content as illustrated in Fig. 3a-b. The increase of the cell volume can be explained from the ionic radii of Re^{5+} and Sb^{5+} ($r(Re^{5+}) = 58$ pm, $r(Sb^{5+}) = 60$ pm). [21]

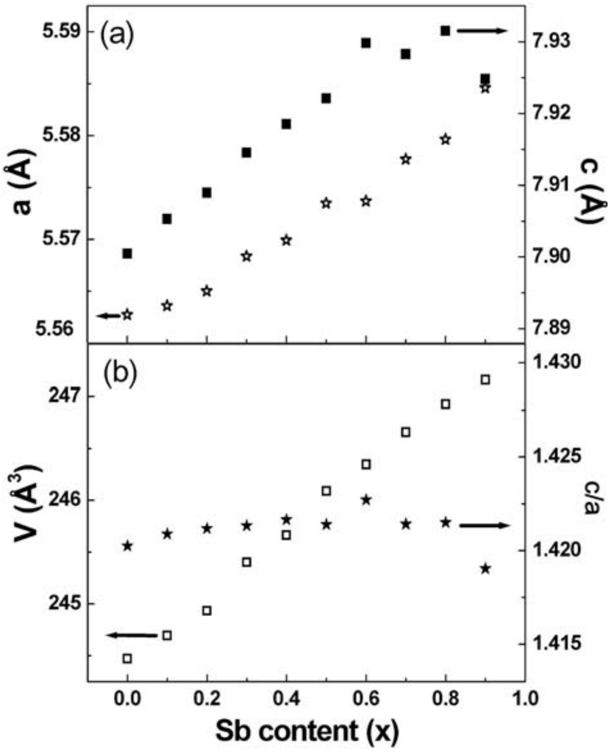

Fig. 3 (a) Lattice parameters a (✯) and c (■) of the tetragonal unit cell and (b) Volume per unit cell (☐) and lattice parameter relation c/a (★) versus Sb content.

The extent of the tetragonal distortion from the ideal cubic structure can be visualized by plotting the ratio of the tetragonal lattice parameters *c*/*a* as a function of the degree of substitution. (Fig. 3b) The condition for a cubic cell is a *c*/*a* ratio of $\sqrt{2}$. A deviation from cubic symmetry leads to a change of the *c*/*a* ratio. A *c*/*a* ratio of 1.421 observed for members of the series $Sr_2FeRe_{1-x}Sb_xO_6$ does not show any significant dependence on the Sb content and is indicative of a tetragonal distortion.

The above results qualitatively agree with the structural behaviour expected from an analysis of the tolerance factor *t* for perovskites of the general formula AMX_3, where the ionic radii were taken from Shannon. [21] The tolerance factor describes the interrelation between the perovskite structure and the associated ionic radii. [22,23]

$$t = \frac{r(A) + r(X)}{\sqrt{2}\left[r(M) + r(X)\right]}$$

To point out the concentrational dependence of the tolerance factor, one should know the valence state of the ions in the crystal structure. The valence states of iron and antimony are important because the ionic radii of Fe^{2+} and Fe^{3+} and Sb^{3+} and Sb^{5+} which appear in the above equation, differ significantly, whereas the ionic radius of Re is practically valence independent. The following results of a detailed study of the iron and antimony valence states by means of ^{57}Fe and ^{121}Sb Mössbauer spectroscopy (discussed in detail below) are used to calculate the perovskite tolerance factor t for the substitution series: the antimony valence state remains constant at +5 for the whole substitution range, whereas the iron valence state changes from $Fe^{2.7+}$ for the parent compound to $Fe^{2.9+}$ for $Sr_2FeRe_{0.1}Sb_{0.9}O_6$.

To determine t for the whole substitution range, one has to consider two different effects. First, the replacement of Re by Sb^{5+} forces the tolerance factor to decrease slightly from 0.896 to 0.890. However, this first effect is overcompensated by a second effect, the change of the iron valence state from +2.7 to +2.9 as determined by Mössbauer spectroscopy. Summarizing both effects, t increases from 0.8965 to 0.8985.

Thus, the structural behaviour of $Sr_2FeRe_{1-x}Sb_xO_6$ as a function of the Sb substitution grade can be analyzed as follows. For the unsubstituted sample the room temperature structure is tetragonal. As the tolerance factor t remains essentially constant, a tetragonal structure is expected and observed for the full range of Sb substitution.

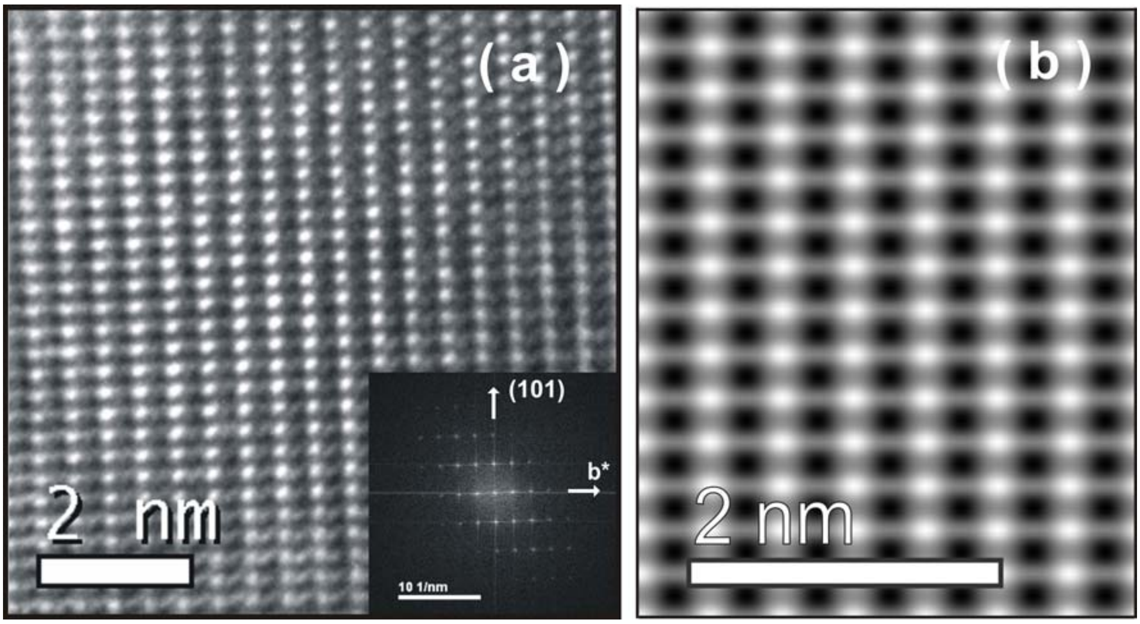

Fig. 4 (a) Experimental High Resolution Transmission Electron Micrograph of $Sr_2FeRe_{0.1}Sb_{0.9}O_6$, inset: selected area electron diffraction (SAED) pattern of the [1 0 -1] zone; (b) image of zone [1 0 -1] simulated by multi-slice method. [24,25]

Fig. 4 shows the experimental HRTEM image and the simulated High Resolution Transmission Electron Micrographs. The high resolution image (Fig. 4a) is in good agreement with the image of zone [1 0 -1] (Fig. 4b) simulated by multi-slice method [24,25] (thickness of 504.27 Å, defocus -222 Å) using the Cerius program suite. [26] The lattice spacings of 0.458 nm and 0.283 nm are in good agreement with (101) and (020) d-spacings of $Sr_2FeRe_{0.1}Sb_{0.9}O_6$.

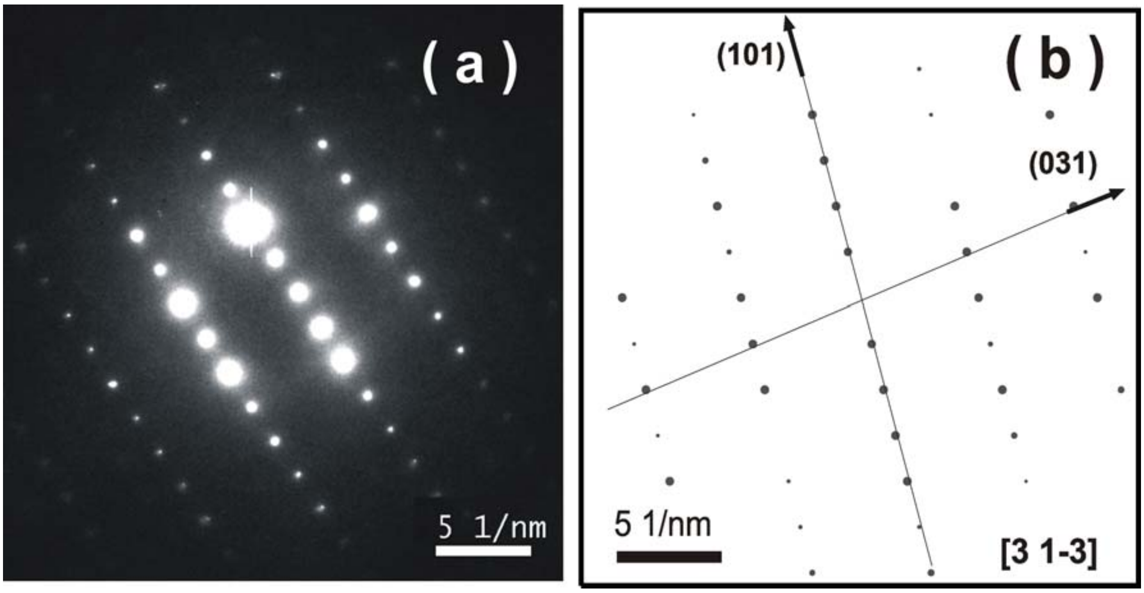

Fig. 5 (a) Selected area electron diffraction (SAED) pattern of $Sr_2FeRe_{0.1}Sb_{0.9}O_6$ and (b) dynamically calculated diffraction pattern of zone [3 1 -3].

The selected area electron diffraction (SAED) pattern of a $Sr_2FeRe_{0.1}Sb_{0.9}O_6$ particle of about 500 nm in diameter is given in Fig. 5a. This is consistent with the kinematically calculated diffraction along [3 1 -3] (Fig. 5b.) indicating the long range ordering of Fe, Re and Sb within this particle.

4.3.2 Magnetic measurement

The magnetic susceptibility measurements of Sr_2FeReO_6 samples reveal spontaneous magnetization below $T_C = 401(1)$ K. According to previous studies this compound can be considered a soft magnetic material. It contains ferromagnetically aligned magnetic moments of Fe atoms in the Fe-sublattice and ferromagnetically aligned magnetic moments of Re atoms in the Re-sublattice which leads to an overall ferrimagnetic behaviour by Zener double exchange via the oxygen atoms. [1,9-12,18] The double exchange pathways Fe–O–Re–O–Fe critically depend on the properties of the elements involved. A replacement of the Re atoms by a non-magnetic, main group element with fixed valence such as Sb should have a dramatic influence on the double exchange pathways of the compound because of the lack of *d* orbitals of Sb. The concentrational dependence of the saturation magnetization of $Sr_2FeRe_{1-x}Sb_xO_6$ ($0 \leq x \leq 0.9$) at 5 K supports this assumption. (Fig. 6) The saturation magnetizations were obtained by measuring hysteresis loops of all samples at 5 K. (Fig. 7e)

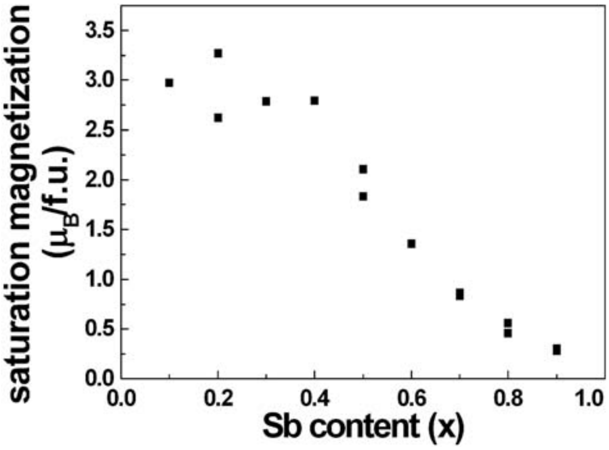

Fig. 6 Concentrational dependence of the saturation magnetization of $Sr_2FeRe_{1-x}Sb_xO_6$ ($0 \leq x \leq 0.9$) at 5 K.

As the concentration of Sb increases ($x > 0.6$) the saturation magnetization decreases and the susceptibility curves show a maximum corresponding to an antiferromagnetic type of ordering. (Fig. 7a) At a maximum Sb content of 90 % the field dependence of the magnetization approaches a straight line and shows almost no hysteresis in comparison to the samples with higher Re concentration. (Fig. 7b) The results of the susceptibility measurements of Sb containing samples reveal ferrimagnetic behaviour in the range of concentrations up to $x \cong 0.3$ as soon as the paramagnetic regions of the high-temperature magnetic susceptibility measurements could only be fitted by a ferrimagnetic model. (Fig. 8b)

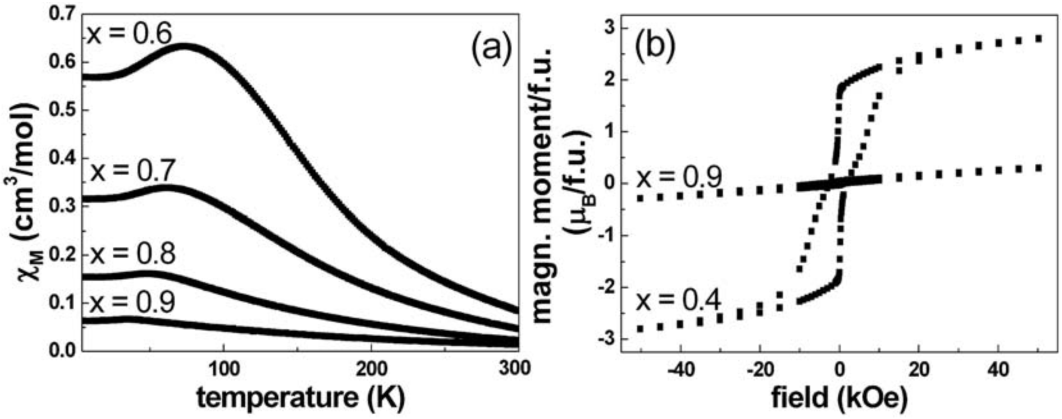

Fig. 7 (a) Molar susceptibility measured at 5 kOe in dc mode of $Sr_2FeRe_{1-x}Sb_xO_6$ and (b) field dependence of the magnetization of $Sr_2FeRe_{1-x}Sb_xO_6$ at 5 K.

The compounds with 10 %, 20 % and 30 % of Sb order ferrimagnetically at T_C = 388 K, 367 K and 366 K, respectively. (Fig. 8b) Reciprocal susceptibilities of these samples in the paramagnetic regions were used to extract the parameters of magnetic interaction. Ferrimagnetic (T_C), paramagnetic (Θ_C) Curie temperatures, interaction parameter (μ) as well as Curie constants (C_A, C_B) for the two sublattices A and B for $Sr_2FeRe_{1-x}Sb_xO_6$ ($0.1 < x < 0.3$) were determined from the fit of the high-temperature magnetic susceptibility measurements. (Fig. 8b) The standard dependence describing the molar susceptibility χ_M in molecular field approximation has been applied: $\chi_M = \frac{(C_A+C_B)T-2\mu C_A C_B}{T^2-T_C^2}$

with $T_C^2=\mu^2 C_A C_B$ and $\Theta_C=-\frac{2\mu C_A C_B}{C_A+C_B}$.

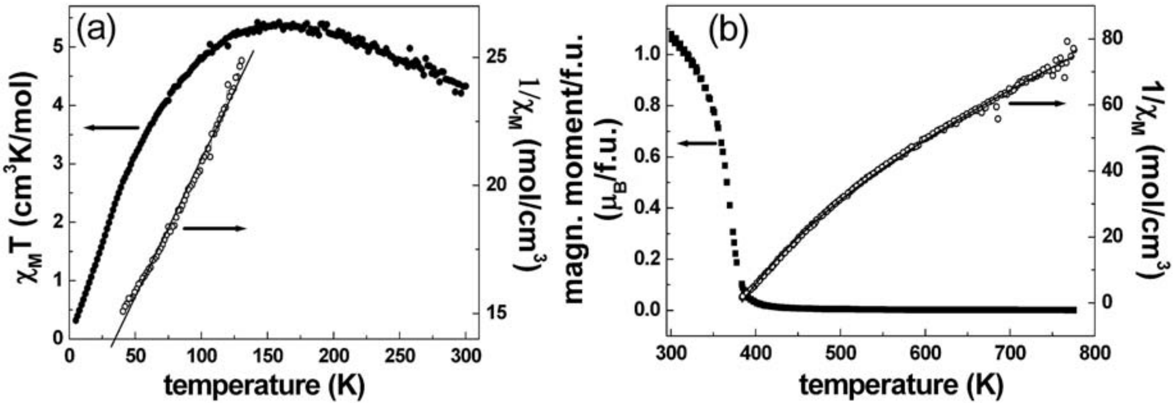

Fig. 8 (a) Molar susceptibility of $Sr_2FeRe_{0.1}Sb_{0.9}O_6$ multiplied by the temperature (●) and inverse molar susceptibility of $Sr_2FeRe_{0.1}Sb_{0.9}O_6$ (○) versus temperature and (b) magnetization of $Sr_2FeRe_{0.9}Sb_{0.1}O_6$ (■) and inverse molar susceptibility of $Sr_2FeRe_{0.9}Sb_{0.1}O_6$ (○) versus temperature.

The fit in the paramagnetic region gives the following set of parameters for $Sr_2FeRe_{0.9}Sb_{0.1}O_6$: Θ_C = -169(6) K, μ = 173(8) mol/cm^3, C_A = 9.5(3) cm^3 K/mol and C_B = 0.5(3) cm^3 K/mol. From the expression for the Curie constant $C = 0.125g^2 S(S+1)$ with $g = 2$ and the effective spin S, it follows that C_A is a Curie constant of the Fe based sublattice ($S(S+1) = 19$) whereas C_B can be attributed to the Re based sublattice ($S(S+1) = 1$).

Mössbauer data discussed hereafter indicate that only $Sr_2FeRe_{0.1}Sb_{0.9}O_6$ can be considered in terms of a “pure” antiferromagnetic phase from the microscopic point of view. The range of concentrations between $0.3 < x < 0.8$ can be considered an intermediate case, comprising antiferro- and ferrimagnetic type of domains. The fit of the magnetic susceptibility data in this range of substitution qualitatively confirmed this model. It follows from the fit that the antiferromagnetic fraction increases as Sb content increases. However, we found that the quantitative interpretation of the intermediate region is problematic because of unknown temperature dependence of ferri- and antiferromagnetic region fractions.

The temperature dependence of $\chi_M T$ (Fig. 8a) for $Sr_2FeRe_{0.1}Sb_{0.9}O_6$ shows ferromagnetic interactions above 150 K which changes to antiferromagnetic interaction for lower temperatures. Antiferromagnetic ordering occurs at T_N = 36 K. Magnetic susceptibility data for the sample with 90 % Sb content were fitted using the expression for the magnetic susceptibility in the temperature range 40 K < T < 130 K corresponding to antiferromagnetic interactions: $\chi_M = \frac{C}{T\text{-}\Theta_N}$ with a paramagnetic Néel temperature $\Theta_N = \frac{1}{2}C(\alpha_{AA} + \alpha_{AB})$ and a Néel temperature $T_N = \frac{1}{2}C(\alpha_{AA} - \alpha_{AB})$. The constants $\alpha_{AA} = \alpha_{BB}$ and α_{AB} consider the exchange and dipole interactions within and between the sublattices A and B, respectively. The fit gives Θ_N = -96(2) K, C = 9.3(1) cm^3K/mol, α_{AA} = -6.4(1) mol/cm^3 and α_{AB} = -99.8(4) mol/cm^3. It is important to notice that the values of the Curie constants C and C_A for the Fe based sublattice are remarkably equal in both compounds. It means that a diamagnetic dilution of the Re-sublattice only slightly perturbs the properties of the magnetic ions of the Fe-based sublattice. In other words, the amount of magnetic centres and their local magnetic moments of the Fe-based sublattice do not change significantly upon Sb substitution. Furthermore, one can conclude that Sb atoms do not replace Fe atoms and vice versa in antisiting fashion. These findings are in agreement with the structural results presented above as an essential antisite disorder Fe–O–Fe would lead to magnetic moments for the two sublattices significantly different from the experimentally observed ones.

4.3.3 Band structure calculation

The double perovskite Sr_2FeReO_6 reveals half-metallic ferrimagnetic behaviour at room temperature. [18] The conceptual basis for this behaviour is a large density of states of one spin direction at the Fermi level E_F while the other spin direction is insulating. (Fig. 9a) Of the seven electrons which are distributed over the Fe and Re atoms five are fixed in Fe *d* orbitals in spin up direction whereas the Re *d* orbitals in this spin direction do not host electrons. The remaining two electrons are located in the Fe and Re *d* t_{2g} orbitals in spin down direction. The origin of the large density of states in the vicinity of the Fermi level can be related to a van Hove-singularity in the band structure of these compounds as it was suggested in a previous study. [1,27] To investigate the influence of the diamagnetic dilution with a main group element on the Re sublattice, we have performed spin polarized *ab initio* band structure calculations for Sr_2FeSbO_6 using the WIEN2k software package.

[17] The density of states given in Fig. 9b shows Sr_2FeSbO_6 to be a semiconductor or an insulator in spite of its spin polarization. The Fe *d* orbitals are completely filled in spin up direction whereas in spin down direction they do not contain any electrons. This situation corresponds to high spin Fe^{3+} ($3d^5$). In contrast, Sb does not show any significant participation to the DOS near E_F as expected from its lack of *d* orbitals. Therefore one can expect a fixed valence for antimony (Sb^{5+}). Finally, Sb substitution “switches off” the itinerant magnetism of the parent compound.

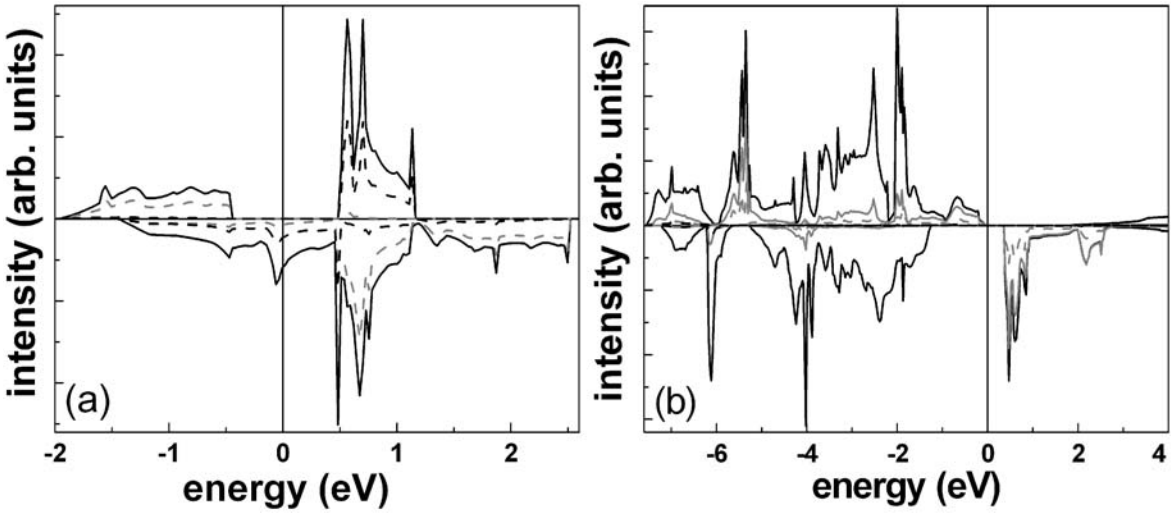

Fig. 9 Density of states of (a) Sr_2FeReO_6, in spin up direction: total DOS (solid black), partial DOS Fe *d* (grey dashed), Re *d* (black dashed); in spin down direction: total DOS (solid black), partial DOS Fe *d* (grey dashed), Re *d* (black dashed) and (b) Sr_2FeSbO_6, in spin up direction: total DOS (solid black), partial DOS Fe *d* e_g (grey dashed), Fe *d* t_{2g} (solid grey), Sb *p* (black dashed); in spin down direction: total DOS (solid black), partial DOS Fe *d* e_g (grey dashed), Fe *d* t_{2g} (solid grey), Sb *p* (black dashed).

4.3.4 Conductivity measurement

The results of the conductivity measurement of four selected samples ($Sr_2FeRe_{1-x}Sb_xO_6$, x = 0, 0.1, 0.4, 0.6) are presented in Fig. 10. In accordance with previous results [18] the unsubstituted sample reveals a metallic behaviour in the whole temperature range. In contrast, Sb containing samples are semiconducting. The room temperature resistance of the sample with highest substitution level of 60 % Sb is several orders of magnitude higher than that of the unsubstituted one and it becomes almost insulating upon cooling in agreement with band structure calculations.

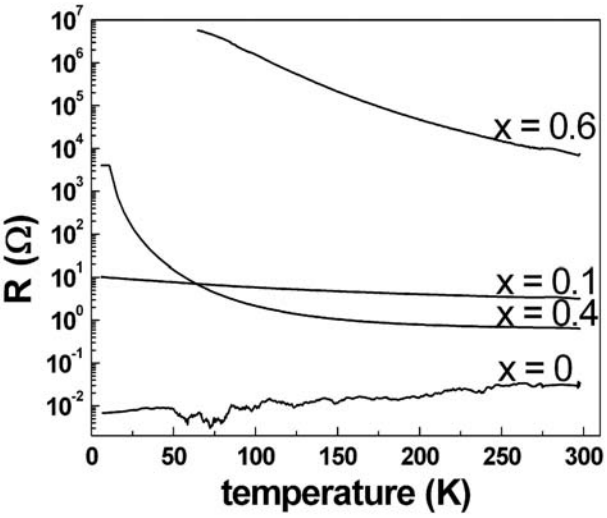

Fig. 10 Conductivity measurements without application of an external magnetic field of (a) $Sr_2FeRe_{0.4}Sb_{0.6}O_6$, (b) $Sr_2FeRe_{0.9}Sb_{0.1}O_6$, (c) $Sr_2FeRe_{0.6}Sb_{0.4}O_6$ and (d) Sr_2FeReO_6.

4.3.5 Mössbauer spectroscopy

^{57}Fe- and ^{121}Sb-Mössbauer experiments give deeper insight into the magnetic structure of $Sr_2FeRe_{1-x}Sb_xO_6$. In the original ferrimagnetically ordered, unsubstituted Sr_2FeReO_6, local magnetic moments of iron atoms are aligned in parallel. Mössbauer spectra reveal only one Fe site with a hyperfine magnetic field of 468.6(5) kOe at 4.2 K. (Fig. 11a) The 6-line pattern of the spectra is typical for materials in the magnetically ordered phase and the very sharp lines are indicative of a very high degree of Fe-Re(Sb) order in the structure. A considerable cationic disorder would result in additional (broadened) spectral lines due to a distribution of different environments of iron. (Fig. 11a) Measurements on Sr_2FeReO_6 in an external magnetic field of 50 kOe at 4.2 K show a decrease of the hyperfine magnetic field to 421(2) kOe which clearly indicates a ferromagnetic type of ordering within the Fe-sublattice. 10 to 80 % of Sb substitution leads to at least two Fe sites which can be seen from the line splitting in the Mössbauer spectra. (Fig. 11b) As follows from the magnetic susceptibility measurements, the transformation from ferri- to antiferromagnetic type of ordering occurs in this range of concentrations. In contrast, the spectra of $Sr_2FeRe_{0.1}Sb_{0.9}O_6$ at room temperature and 4.2 K exhibit only one crystallographic Fe position with a hyperfine magnetic field of 506.8(2) kOe. (Fig. 11c-d) The application of an external magnetic field of 50 kOe causes splitting of the Mössbauer spectrum into two subspectra with hyperfine magnetic fields of 481(4) and 533(4) kOe. (Fig. 11e) This fact indicates an antiferromagnetic arrangement of the Fe cations and confirms the antiferromagnetic ordering found in the magnetic susceptibility measurements. However, as one can judge from the non satisfactory fit of the Mössbauer spectra taken in an external magnetic field, the magnetic structure could be even more complex. From Mössbauer studies on samples with an intermediate degree of Sb substitution (30 to 80 %) in an external magnetic field one can conclude that different types of magnetic clusters either ferri- or antiferromagnetic coexist.

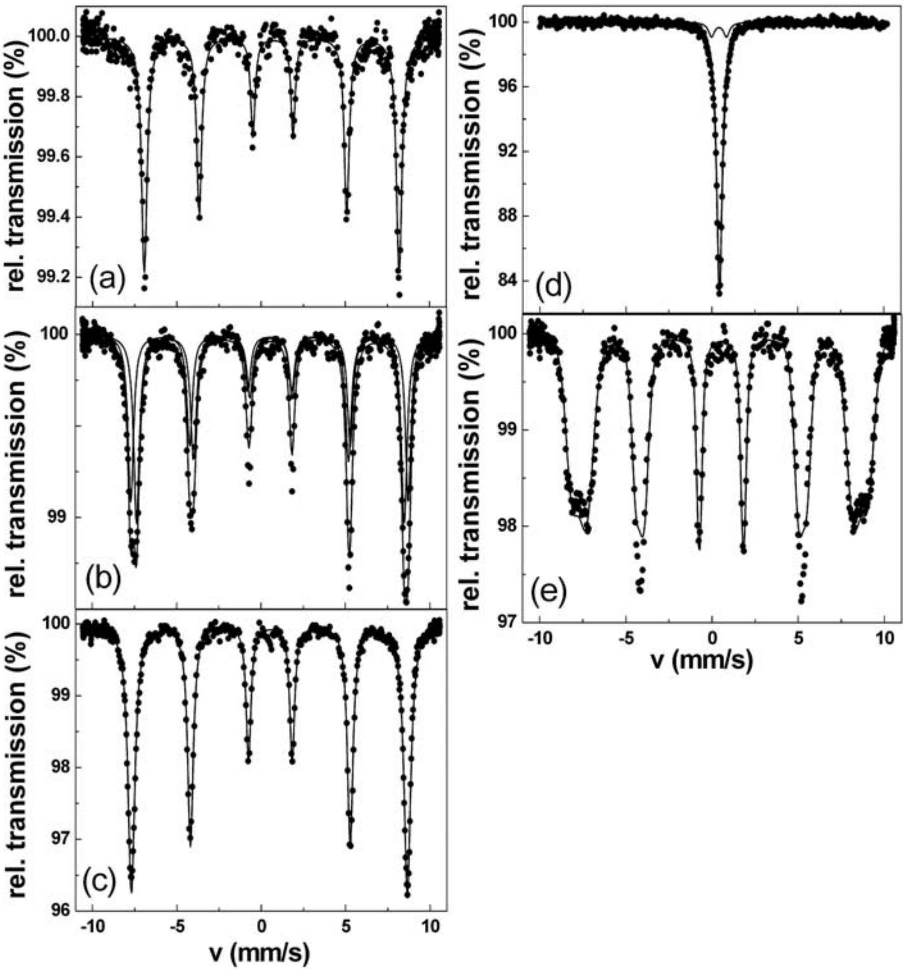

Fig. 11 ^{57}Fe Mössbauer spectra of (a) Sr_2FeReO_6 (4.2 K), (b) $Sr_2FeRe_{0.4}Sb_{0.6}O_6$ (4.2 K), (c) $Sr_2FeRe_{0.1}Sb_{0.9}O_6$ (4.2 K), (d) $Sr_2FeRe_{0.1}Sb_{0.9}O_6$ (300 K) and (e) $Sr_2FeRe_{0.1}Sb_{0.9}O_6$ (4.2 K) in an external magnetic field of 50 kOe.

The ^{121}Sb Mössbauer spectroscopic study at 4.2 K exhibits paramagnetic spectra with an isomer shift $\delta(Sb) = 0.20(5)$ mm/s for the total range of Sb concentration. (Fig. 12) This isomer shift indicates a

5+ Sb valence state. The spectra of compounds with an intermediate Sb content are slightly more broadened in comparison to those of the unsubstituted and 90 % substituted samples, which is in agreement with the presence of ferri- and antiferromagnetic domains as discussed above.

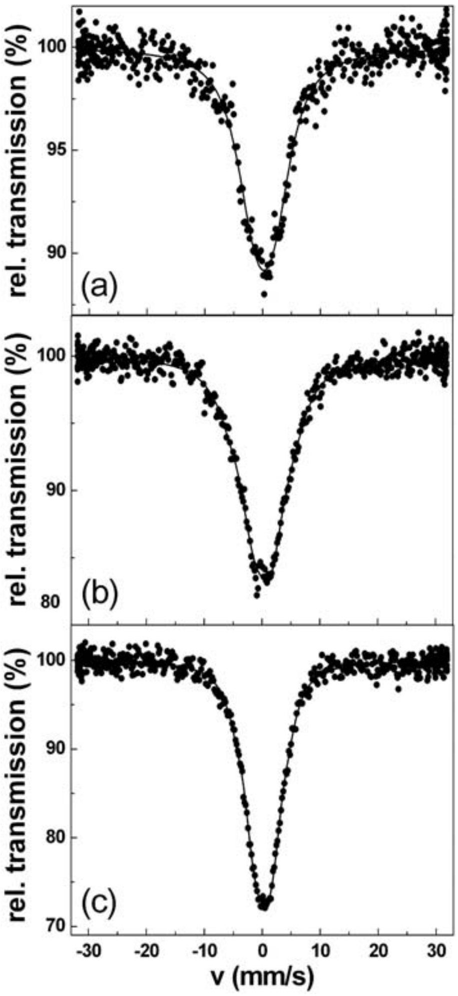

Fig. 12 ^{121}Sb Mössbauer spectra measured at 4.2 K of (a) $Sr_2FeRe_{0.9}Sb_{0.1}O_6$, (b) $Sr_2FeRe_{0.4}Sb_{0.6}O_6$ and (c) $Sr_2FeRe_{0.1}Sb_{0.9}O_6$.

A general advantage of ^{121}Sb Mössbauer spectroscopy is the high sensitivity of the isomer shift on the Sb valence state. The fact that the isomer shift of Sb is constant for the total range of concentrations is remarkable because Sb^{5+} substitutes Re atoms with valence states varying from +5 to +6. From a study of the $Sr_2Fe_{1-x}Zn_xReO_6$ and $Sr_2Fe_{1-x}Cr_xReO_6$ series we concluded that the iron valence state is constant over the whole solid solution series whereas the Re atoms can be considered as a redox buffer with a valence state depending on the substitution level. [1] Following this idea, we can conclude that the valence state of the iron atoms should be concentrationally dependent. In other words, iron atoms must play the role of a redox buffer.

The average Fe valence state for $Sr_2FeRe_{0.1}Sb_{0.9}O_6$ can be estimated by comparing the isomer shift of $Sr_2FeRe_{1-x}Sb_xO_6$ (x = 0 and x = 0.9) with the isomer shifts of standard reference compounds $Cs_2Fe_2^{2+}(MoO_4)_3$ and $Li_3Fe^{3+}(MoO_4)_3$ using the same procedure as described previously. [1] From the values of the isomer shifts δ(Fe, x = 0.9) = 0.504(5) mm/s and δ(Fe, x = 0) = 0.670(5) mm/s it follows that the valence state of Fe is 2.9+. This is in good agreement with the Sb^{5+} valence state following from the chemical composition of the 90 % Sb containing sample $Sr_2Fe^{2.9+}Re_{0.1}^{6+}Sb_{0.9}^{5+}O_6$.

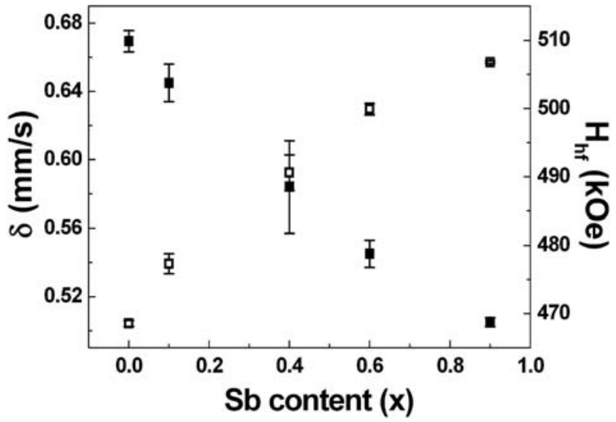

Fig. 13 Isomer shifts δ (■) and hyperfine magnetic fields H_{hf} (□) of the Fe atoms as a function of the Sb content.

The concentrational dependence of the isomer shifts and hyperfine magnetic fields of iron atoms in both types of clusters (ferri-, antiferro-) is shown in Fig. 13. Both values strongly depend on the Sb concentration. Average values of the isomer shifts and hyperfine magnetic fields exhibit an almost linear concentrational dependency. This linear correlation indicates that (i) the samples are chemically and structurally homogeneous and (ii) ferri- and antiferromagnetic clusters coexist within the same crystal structure.

4.4 Conclusion

The interpretation of the magnetic structure of the compounds under study follows from the crystal structure determination, magnetic characterization, band structure calculations, conductivity measurements and Mössbauer experiments. Ferromagnetic alignment of the magnetic moments of the Fe atoms in the Fe sublattice and the Re atoms in the Re sublattice of Sr_2FeReO_6 is mediated by Zener double exchange via oxygen atoms leading to an overall ferrimagnetic behaviour. This situation is valid up to a replacement level of 30 % of Sb for Re as shown at a microscopic level by Mössbauer spectroscopy and at a macroscopic level by magnetic susceptibility measurements. In contrast, large Sb contents lead to antiferromagnetic behaviour. X-ray diffraction and Mössbauer spectroscopy studies revealed the absence of Fe/Re antisite disorder. This supports a double exchange via Fe–O–Re–O–Fe which requires an ordered arrangement of Fe and Re/Sb on their respective lattice sites. The substitution of Re by Sb destroys the itinerant magnetism as Sb (i) is lacking *d* orbitals involved in states at the Fermi level, (ii) shows no magnetic splitting in the Mössbauer spectra and (iii) carries no magnetic moment according to the results of a neutron diffraction study by Cussen et al. [28] (Fig. 14) At the moment, we cannot ultimately conclude whether Sb atoms take part instead of Re atoms in the double exchange pathway Fe–O–Sb–O Fe or alternatively the antiferromagnetic order is determined by direct Fe–Fe exchange. Cussen et al. [28] suggested a model of magnetic interaction which is in agreement with the experimental findings of the present work. Although the Fe–Fe separations of about 4 Å in the title compounds are fairly large, a case of ferromagnetic exchange between layers containing transition elements over distances of about 40 Å has been reported, [29] lends support to the idea of direct ferromagnetic exchange between the Fe atoms in the double perovskites $Sr_2FeRe_{1-x}Sb_xO_6$ ($0.6 < x < 0.9$).

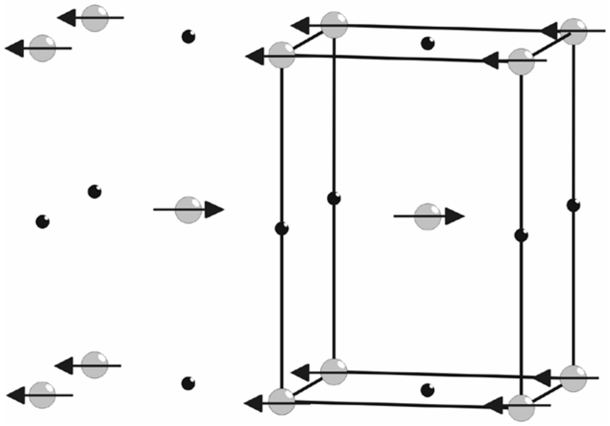

Fig. 14 Magnetic structure of Sr_2FeSbO_6 based on neutron diffraction studies by Cussen et al. [28] Within the tetragonal unit cell, only M (Fe, grey) and M' (Sb, black) positions are shown.

4.5 References

[1] A. Jung, I. Bonn, V. Ksenofontov, G. Melnyk, J. Ensling, C. Felser and W. Tremel, *J. Mater. Chem.,* 2005, **15**, 1760.

[2] A. I. Smirnov, N. V. Glazkov, H.-A. Krug von Nidda, A. Loidl, L. N. Demianets and A. Y. Shapirov, *Phys. Rev. B*, 2002, **65**, 174422.

[3] X. Chen, Ch. Binek, A. Hochstrat and W. Kleemann, *Phys. Rev. B*, 2002, **65**, 012415.

[4] P. Hansen and K. Witter, *Phys. Rev. B*, 1983, **27**, 1498.

[5] Ch. Binek, W. Kleemann and D. P. Belanger, *Phys. Rev. B*, 1998, **57**, 7791.

[6] J. Longo and R. Ward, *J. Am. Chem. Soc.*, 1961, **83**, 2816.

[7] A. W. Sleight, J. Longo and R. Ward, *Inorg. Chem.*, 1962, **1**, 245.

[8] O. Chmaissem, R. Kruk, B. Dabrowski, D. E. Brown, X. Xiong, S. Kolesnik, J. D. Jorgensen, and C. W. Kimball, *Phys. Rev. B*, 2000, **62**, 14197.

[9] H. Kato, T. Okuda, Y. Okimoto, Y. Tomioka, K. Oikawa, T. Kamiyama and Y. Tokura, Phys. Rev. B, 2002, **65**, 144404.

[10] S. Nakamura, M. Tanaka, H. Kato and Y. Tokura, *J. Phys. Soc. Jpn.*, 2003, **72**, 424.

[11] E. Carvajal, O. Navarro, R. Allub, M, Avignon and B. Alascio, *Phys. Stat. Sol. B*, 2005, **242**, 1942.

[12] A. Poddar and S. Das, *Physica B – Cond. Mat.*, 2004, **344**, 325.

[13] C. Zener, *Phys. Rev.*, 1951, **81**, 440; C. Zener, *Phys. Rev.*, 1951, **82**, 403; C. Zener, *Phys. Rev.*, 1951, **83**, 299; C. Zener, *Phys. Rev.*, 1952, **85**, 324.

[14] W. Haberditzl, *Magnetochemie*, Akademie-Verlag: Berlin, 1968.

[15] K. Lagarec and D. G. Rancourt, *Nucl. Instrum. Methods Phys. Res. B*, 1997, **129**, 266.

[16] H. Spiering, L. Deák and L. Bottyán, *Hyp. Int.*, 2000, **125**, 197.

[17] P. Blaha, K. Schwarz, G. K. H. Madsen, D. Kvasnicka and J. Luitz, *Wien2k, An augmented plain wave + local orbitals program for calculating crystal properties*, (Karlheinz Schwarz, Techn. Universtität Wien, Austria), 2001.

[18] K.-I. Kobayashi, T. Kimura, Y. Tomioka, H. Sawada, K. Terakura and Y. Tokura, *Phys. Rev. B*, 1999, **59**, 11159.

[19] T. H. Kim, M. Uehara, S.-W. Cheong and S. Lee, *Appl. Phys. Lett.*, 1999, **74**, 1737.

[20] J. Rodríguez-Carvajal, *Physica B*, 1993, **192**, 55.

[21] R. D. Shannon, *Acta Crystallogr., Sect. A: Cryst. Phys., Diffr., Theor. Gen. Cryst.*, 1976, **32**, 751.

[22] U. Müller, *Anorganische Strukturchemie*, Teubner Studienbücher: Stuttgart, 1996.

[23] G. Popov, M. Greenblatt and M. Croft, *Phys. Rev. B: Condens. Matter*, 2003, **67**, 24406.

[24] J.M. Cowley and A.F. Moodie, *Acta Crys.*, 1957, **10**, 609.

[25] W.O.Saxton, M.A. O'Keefe, D.J.H. Cockayne and M. Wilkens, *Ultramicroscopy*, 1983, **12**, 75.

[26] Cerius2 version 4.6MS, Molecular modeling environment from Accelrys Inc. 9685 Scranton Road, San Diego, CA 92121-3752, USA.

[27] C. Felser, R. Seshadri, A. Leist and W. Tremel, *J. Mater. Chem.*, 1998, **8**, 787.

[28] E. J. Cussen, J. F. Vente, P. D. Battle and T. C. Gibb, *J. Mater. Chem.*, 1997, **7**, 459.

[29] M. Drillon, P. Panissod, P. Rabu, J. Souletie, V. Ksenofontov and P. Gütlich, *Phys. Rev. B*, 2002, **65**, 104404**.**

5. The effect of cation disorder on the magnetic properties of $Sr_2Fe_{1-x}Ga_xReO_6$ (0 < x < 0.7) double perovskites

5.1 Introduction

Double perovskites with the general formula $A_2MM'O_6$, A = alkaline earth metal, M = 3*d* transition metal and M' = transition metal, are known for more than 40 years. [1,2] The ideal cubic structure consists of a rock salt arrangement of corner sharing MO_6 and $M'O_6$ octahedra. Large A cations are situated in the voids between the octahedra. (Fig. 1) The crystallographic and magnetic properties of these double perovskite oxides strongly depend on the size and valence of the cation constituents of the crystal. From a structural point of view, double perovskites with A = Ba^{2+} are cubic, whereas the smaller Sr^{2+} cation on the A site leads to a tetragonal distortion, and the smallest Ca^{2+} cation enforces a monoclinic symmetry. Naturally, there are also some exceptions to this general tendency as the sizes of all participating cations need to be taken into account. For example, cubic and tetragonal symmetry has been reported for Sr_2CrReO_6. [2-6]

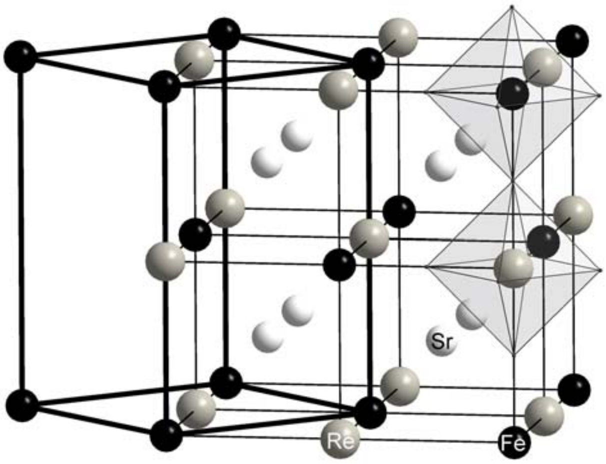

Fig. 1 Crystal structure of the double perovskite Sr_2FeReO_6; Fe (black), Re (dark grey), Sr (light grey), and O (corners of the octahedra); the cubic unit cell is drawn in thin black lines, the tetragonal unit cell in thick black lines.

For a given A^{2+} cation the magnetic properties of double perovskites are mainly determined by the nature of the metals M and M′. Besides ferrimagnetic representatives such as Ba_2MReO_6 (M = Mn, Fe, Ni [2]), antiferromagnetic compounds such as Sr_2FeWO_6, [7] Sr_2MnWO_6, [8] Sr_2CoMoO_6, [9] A_2NiMoO_6 (A = Sr, Ba), [10] Sr_2CrMO_6 (M=Mo, W) [11] have been described. Sr_2FeMoO_6, Sr_2FeReO_6, [12-14] Ba_2FeReO_6 [14,16] and Sr_2CrReO_6 [2,4] are unique in that they are both metallic and ferrimagnetic. Ordered double perovskites A_2FeMO_6 (A = Sr, Ba; M = Mo, Re) have been reported to be half-metallic with high Curie temperature (T_C). [16-18]

The reason for this wide variety of magnetic properties and especially for the half-metallic behaviour of the compounds $A_2FeM'O_6$ (A = Sr, Ba; M' = Mo, Re) [12,13,19-21] lies in the double exchange mechanism [22,23] mediating the electron interaction along the axes of the cubic unit cell along the Fe–O–Re/Mo units via the oxygen bridges forming double exchange pathways Fe–O–Re/Mo–O–Fe. The half-metallic properties of $A_2FeM'O_6$ require a large density of states at the Fermi level ($DOS(E_F)$) for one spin direction, whereas the other spin direction is insulating. In the insulating spin direction five electrons reside in the 3*d* states of Fe, whereas the 5*d*/4*d* states of Re/Mo are empty. As the stoichiometry of $A_2FeM'O_6$ dictates that the combined oxidation states of Fe and Re/Mo sum up to +8, the remaining two/one electrons are located in the conduction band of the metallic spin direction which is composed of the t_{2g} states of Fe and Re/Mo. For Sr_2FeReO_6 the exact distribution of the electrons in the valence states of Fe and Re ($Fe^{2.7+}$ and $Re^{5.3+}$) has been elucidated by means of Mössbauer spectroscopy. [5,24] In summary, $A_2FeM'O_6$ is built up from two different ferromagnetic sublattices - one Fe- and one Re/Mo-sublattice - which couple antiferromagnetically by means of a Zener double exchange mechanism to give rise to an overall ferrimagnetic behaviour.

In an attempt to probe the influence of the M site cation, Jung et al. [5] substituted Fe by Cr and Zn which, as 3*d* metals, possess *d* orbitals to preserve the double exchange mechanism upon Fe substitution. Consequently, the long-range ferromagnetic ordering of the Re sublattice is conserved for the solid solution series $Sr_2Fe_{1-x}Zn_xReO_6$ and $Sr_2Fe_{1-x}Cr_xReO_6$ (0 < x <0.9). With Cr on the M site of $A_2FeM'O_6$ the itinerant ferrimagnetic behaviour of the parent compound Sr_2FeReO_6 is retained over the whole substitution range. In contrast, the closed 3*d* shell of Zn causes a change from itinerant ferrimagnetic to localized ferromagnetic behaviour for Zn contents > 60 % in $Sr_2Fe_{1-x}Zn_xReO_6$. Mössbauer spectroscopy reveals the Fe valence state to remain constant over the whole substitution range. As a result, Re may be considered to act as an electronic buffer element.

To further elucidate the role of the double exchange mechanism the M' cation Re was replaced by the main group metal Sb in $Sr_2FeRe_{1-x}Sb_xO_6$.[24] As expected, the lack of *d* orbitals on the pentavalent main group metal Sb destroys the itinerant magnetism of the parent compound. Furthermore, higher Sb substitution leads to an overall antiferromagnetic behaviour of the corresponding samples. The antiferromagnetic properties may be related either to a direct Fe–Fe interaction or to a double exchange via O–Sb–O units. A decision in favour of one of the two possible models could not be given. Mössbauer spectroscopic data indicated unequivocally that the valence state of iron in $Sr_2Fe_{1-x}M_xReO_6$ (M = Cr, Zn; 0 < x < 0.9) changes upon Sb substitution. [24]

In this contribution we probe the influence of the main group metal Ga on the M site of the double perovskite $A_2FeM'O_6$ on the double exchange mechanism. Results concerning the related double perovskite compounds $A_2Fe_{1-x}Mg_xM'O_6$ (A = Ca, Sr, Ba; M' = Mo, Re) [23,25] point to itinerant ferromagnetic behaviour for the whole solid solution series $Sr_2Fe_{1-x}Ga_xReO_6$ (0 < x <0.7). Sher et al. [23] as well as Bramnik et al. [25] report on the magnetic properties of $A_2Fe_{1-x}Mg_xM'O_6$ which reveal that the long-range ferromagnetism of the compounds is retained even at higher Mg substitution levels. From the room temperature magnetic hysteresis loops one can judge the studied double perovskites to be soft magnets. Magnetic measurements at 5 K indicate a coexistence of paramagnetic and ferromagnetic regions. Unfortunately, we only succeeded in preparing single phase material up to a Ga substitution level of x = 0.7 although the synthesis of Sr_2GaReO_6, the end member of the series, has been claimed. [26] Here we report the synthesis, structures and magnetic properties of the $Sr_2Fe_{1-x}Ga_xReO_6$ series.

5.2 Experimental

Starting materials were reagent grade SrO (Aldrich, 99.9 % purity), Fe_2O_3 (Alfa Aesar, 99.99 % purity), Ga_2O_3 (Aldrich, 99.99 % purity), Re metal and Re_2O_7 (Alfa Aesar, 99.9 % purity). All starting materials are stored in a glove box under argon (Braun Labmaster) and examined by X-ray powder diffraction prior to use.

The $Sr_2Fe_{1-x}Ga_xReO_6$ samples were prepared by high-temperature solid state reactions. Because of the strongly hygroscopic properties of SrO and the large vapour pressure of Re_2O_7 the samples were prepared under inert gas atmosphere in a glove-box. Stoichiometric amounts of SrO, Fe_2O_3, Ga_2O_3, Re and Re_2O_7 (2 SrO : (1-x)/2 Fe_2O_3 : x/2 Ga_2O_3: 0.3 Re : 0.35 Re_2O_7) were ground in an agate mortar and pressed into pellets. In order to avoid Sr attack on the quartz tubes these pellets were transferred into corundum containers and finally sealed in evacuated quartz tubes. The samples were annealed for seven days at 1000°C. Thereafter they were rapidly cooled to room temperature by quenching in ice water.

X-ray powder diffraction patterns were recorded using a Siemens D5000 diffractometer with monochromatized (Ge (111)) Cu $K_{\alpha 1}$ radiation equipped with a Braun DM50 linear PSD in transmission mode. Lattice constants obtained by Rietveld refinement using the program FULLPROF [27] were refined relative to Si as internal standard.

The variable-temperature magnetic susceptibility measure-ments of $Sr_2Fe_{1-x}Ga_xReO_6$ were performed using a Quantum Design MPMS-XL SQUID magnetometer, equipped with a high-temperature furnace. Experimental data were corrected for diamagnetism using Pascal's constants. [28]

Mössbauer measurements of $Sr_2Fe_{1-x}Ga_xReO_6$ powder samples were performed in transmission geometry using a constant-acceleration spectrometer and a helium bath cryostat. ^{57}Fe Mössbauer spectra were recorded between room temperature and 4.2 K using the 50 mCi source $^{57}Co(Rh)$. The

Recoil 1.03 Mössbauer Analysis Software was used to fit the experimental spectra. [29] Isomer shift values are quoted relative α-Fe at 293 K.

Band structure calculations were performed within the potential augmented plane-wave (FLAPW) framework within the generalized gradient approximation (GGA). [30] Sr_2GaReO_6 was reported to be cubic with the lattice parameter c = 7.84 Å. [26,31] Since no further structural details are given in Ref. 26 and 31, the electronic structure of Sr_2GaReO_6 was calculated using the structural model of Kobayashi et. al. [13] The number of k-points in the irreducible Brillouin zone was 20. The convergence criterion was fixed to 0.0001 Ry.

5.3 Results and discussion

5.3.1 Crystal Structure

The crystal structures of the compounds of the series $Sr_2Fe_{1-x}Ga_xReO_6$ ($0 \le x \le 0.7$) were determined by X-ray powder diffraction. The corresponding X-ray patterns presented in Fig. 2 reveal that all samples crystallize in the double perovskite structure type like the parent compound Sr_2FeReO_6. As an example, the X-ray pattern of $Sr_2Fe_{0.65}Ga_{0.35}ReO_6$ (mixed with Si as internal standard), the positions of the reflections and the corresponding difference curve are shown in Fig. 3. For all samples the best agreement parameters (R_{Bragg} values between 1.63 and 3.39) resulted from refinement in space group $I4/mmm$ with Sr situated on site 4d, Fe and Ga on site 2a, Re on site 2b, O1 on site 8h and O2 on site 4e. (Table 1)

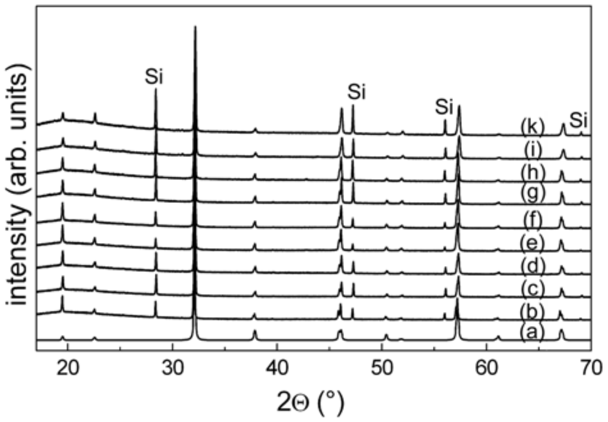

Fig. 2 (a) Calculated X-ray diffraction pattern of Sr_2FeReO_6 in space group $I4/mmm$; measured X-ray diffraction patterns of $Sr_2Fe_{1-x}Ga_xReO_6$ (b) x = 0.1, (c) x = 0.2, (d) x = 0.25, (e) x = 0.3, (f) x = 0.35, (g) x = 0.4, (h) x = 0.5, (i) x = 0.6 and (k) x = 0.7 mixed with Si as internal standard.

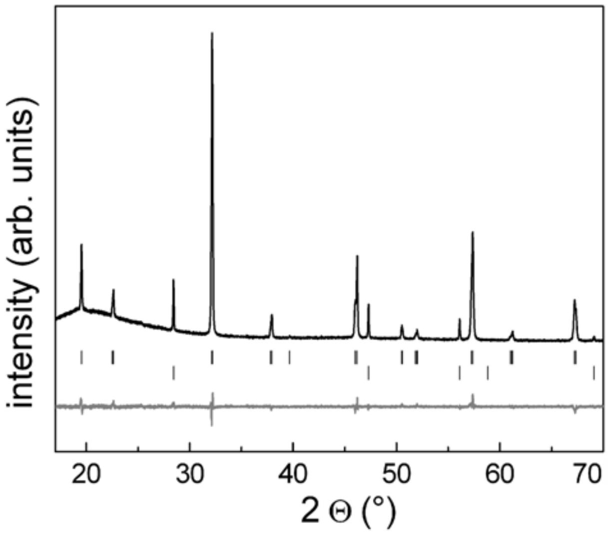

Fig. 3 X-ray pattern of $Sr_2Fe_{0.65}Ga_{0.35}ReO_6$ mixed with Si as internal standard (black line), the positions of the reflections of $Sr_2Fe_{0.65}Ga_{0.35}ReO_6$ (upper black bars) and Si (lower black bars) and the corresponding difference curve (grey).

Table 1 Lattice parameters, *c*/*a* ratios, cell volumes, agreement parameters (R_{Bragg}) and positional parameters of compounds $Sr_2Fe_{1-x}Ga_xReO_6$. ($0 < x < 0.7$). The Rietveld refinement of the series of solid solutions $Sr_2Fe_{1-x}Ga_xReO_6$ was performed in space group *I*4/*mmm* with Sr situated on site 4*d*, Fe and Ga on site 2*a*, Re on site 2*b*, O1 on site 8*h* and O2 on site 4*e*.

Ga content x	*a* (Å)	*c* (Å)	*c*/*a*	V (Å^3)	R_{Bragg}	*x* (O1)	*z* (O2)
0	5.5635	7.9016	1.4203	244.58	2.3	0.2528	0.2527
0.1	5.5594	7.8963	1.4204	244.05	3.2	0.2616	0.2600
0.2	5.5586	7.8919	1,4198	243.84	3.24	0.2641	0.2603
0.25	5.5569	7.8913	1.4201	243.68	2.84	0.2537	0.2575
0.3	5.5560	7.8868	1.4195	243.46	2.76	0.2563	0.2696
0.35	5.5547	7.8857	1.4197	243.31	3.2	0.2567	0.2595
0.4	5.5542	7.8823	1.4191	243.17	3.39	0.2509	0.2652
0.5	5.5532	7.8772	1.4185	242.92	3.15	0.2889	0.2036
0.6	5.5515	7.8697	1.4176	242.54	2.11	0.2888	0.1917
0.7	5.5495	7.8658	1.4174	242.24	1.63	0.2833	0.1790

Table 2 Agreement parameter R_{Bragg} and disorder ratios for the Rietveld refinement of the series of solid solutions $Sr_2Fe_{1-x}Ga_xReO_6$ ($0 \leq x \leq 0.7$).

x	R_{Bragg}	Fe/Re disorder (%)	Ga/Re disorder (%)
0	2.3	0	-
0	2.3	-	0
0.1	3.2	0.6	-
0.1	3.2	-	0.6
0.2	3.24	3	-
0.2	3.24	-	2.6
0.25	2.84	3.2	-
0.25	2.84	-	3.7
0.3	2.76	3.7	-
0.3	2.76	-	1.6
0.35	3.19	3.5	-
0.35	3.2	-	4
0.4	3.35	8.6	-
0.4	3.39	-	5.4
0.5	3.13	11.3	-
0.5	3.15	-	12.8
0.6	3.22	-	-
0.6	2.11	-	16.2
0.7	3.37	-	-
0.7	1.63	-	20.1

However, as the intensities of the reflections could not be modelled in a satisfactory fashion, the distribution of the three elements Fe, Ga and Re on two available lattice sites raises the question of antisite disorder. Two possible types of disorder - Fe/Re and Ga/Re - were taken into account during the course of the structural refinement. The Fe/Re/Ga distribution over the two lattice sites 2*a* and 2*b* was refined within the constraints that the sites remained fully occupied and that the overall Fe : Re : Ga ratio remained at (1-x) : 1 : x for each value of x considered in this study. For both Fe/Re and Ga/Re disorder models a dependence of the disorder ratio on the degree of Ga substitution was determined. The unsubstituted (x = 0) and the low-substituted (x = 0.1) samples show only 0.6 % of disorder for both models of disorder. In contrast, maximum disorder ratios of 11.3 % (Fe/Re disorder) and 20.1 % (Ga/Re disorder) were found for higher Ga substitution levels. (Table 2) Since Fe and Ga are difficult to distinguish by X-ray diffraction because of their similar scattering factors, it is impossible to decide, based on the X-ray data, which type of disorder occurs in the series $Sr_2Fe_{1-x}Ga_xReO_6$.

Lattice parameters *a* and *c* of the solid solution series $Sr_2Fe_{1-x}Ga_xReO_6$ as obtained by Rietveld refinement are compiled in Table 1. As predicted by Vegard's rule the dependence of the lattice parameters on the degree of substitution is almost linear, confirming the existence of a continuous solid solution series in the range $0 \leq x \leq 0.7$. Lattice parameters and unit cell volumes decrease with increasing Ga content as illustrated in Fig. 4a-b. The decrease of both parameters - unit cell volume and lattice parameters - can be rationalized from the ionic radii of Ga^{3+} and Fe^{3+} ($r(Ga^{3+}) = 62$ pm, $r(Fe^{3+}) = 65$ pm). [32]

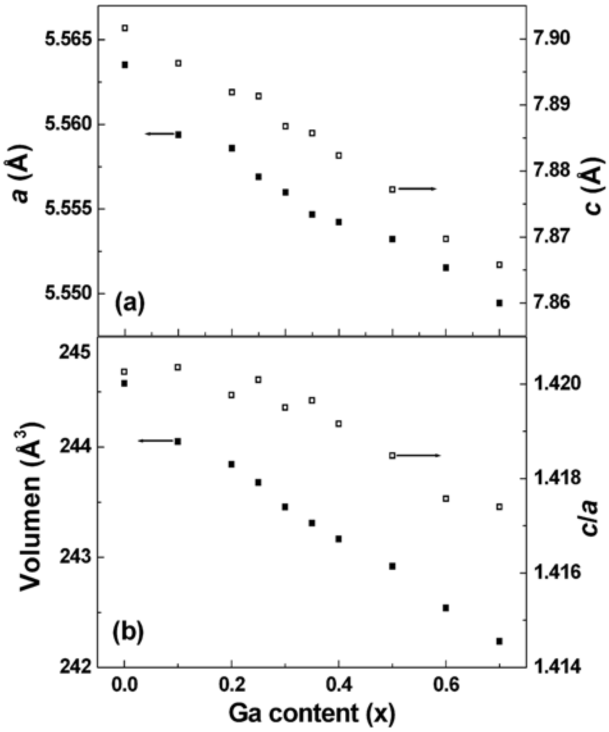

Fig. 4 (a) Lattice constants *a* (■) and *c* (□) of $Sr_2Fe_{1-x}Ga_xReO6$ (0 < x < 0.7) in the tetragonal unit cell and (b) unit cell volume (■) and lattice parameter relation *c*/*a* (□) *versus* Ga content.

A plot of the *c*/*a* ratio (Fig. 4b) is used to gain insight into the dependence of the tetragonal distortion on the substitution level. From the relation $c/a = \sqrt{2}$ for the cubic phase one can conclude that the compounds $Sr_2Fe_{1-x}Ga_xReO_6$ crystallize in a tetragonal unit cell. Nevertheless, the continuous decrease of the *c*/*a* ratio indicates a slow decrease of the tetragonal distortion with increasing Ga content.

The above results qualitatively agree with the structural behaviour expected from an analysis of the tolerance factor *t* for perovskites of the general formula AMX_3 (Fig. 5), where the ionic radii were taken from Shannon et al. [32] The tolerance factor

$$t = \frac{r(A) + r(X)}{\sqrt{2}\left[r(M) + r(X)\right]}$$

describes the interrelation between the perovskite structure and the associated ionic radii. [26,33,34] To plot the concentrational dependence of the tolerance factor, one should know the valence state of the ions in the crystal structure. The valence state of iron is of special importance because the ionic radii of Fe^{2+} and Fe^{3+} differ significantly, whereas the ionic radius of Re is practically valence independent. Fig. 5 is based on an iron valence state $Fe^{2.7+}$ which results from a detailed study of the iron valence states by Mössbauer spectroscopy (*vide infra*). The continuous increase of the tolerance factor t with increasing Ga substitution up to a value $t = 0.9095$ for $Sr_2Fe_{0.3}Ga_{0.7}ReO_6$ supports the experimental results of the c/a plot because perovskites are supposed to crystallize in a cubic unit cell for $t = 1$. An increasing tetragonal distortion is expected for $1 > t > 0.8$, i.e. experimental results and the description based on a space filling model are in good agreement.

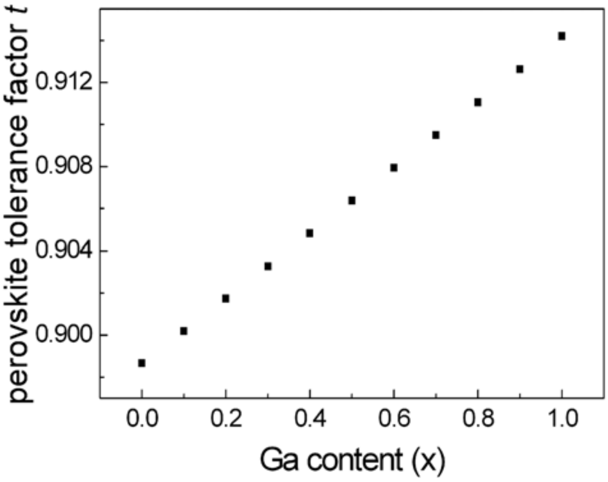

Fig. 5 Perovskite tolerance factor t of $Sr_2Fe_{1-x}Ga_xReO_6$ taking into account $Fe^{2.7+}$ given by Mössbauer experiments.

5.3.2 Magnetic measurements

According to previous studies Sr_2FeReO_6 is a ferrimagnetic half-metal with a Curie temperature T_C = 401 K. From the hysteresis curve it is apparent that Sr_2FeReO_6 is a soft magnetic material. X-ray and neutron diffraction studies are consistent with a tetragonally distorted crystal structure and a negligible degree of antisite disorder. The magnetic structure of Sr_2FeReO_6 can be described based on two ferromagnetic sublattices, an Fe-based and a Re-based one. The overall ferrimagnetic nature of the compound originates from the double exchange of the Fe and Re spins via the oxygen bridges.[1,2,4,5,13,14,24,35,36] In order to determine the effect of the diamagnetic dilution of Sr_2FeReO_6 by a non-magnetic, valence-invariant main group metal, we studied the solid solution series $Sr_2Fe_{1-x}Ga_xReO_6$. We focussed on the alteration of the double exchange in Fe–O–Re–O–Fe units and its effect on the magnetism of the entire series.

The field dependence of the magnetization at 5 K was measured in order to determine the saturation magnetization of the samples. Based on the hysteresis loops with small coercive fields (Fig. 6) materials of all compositions can be classified as soft magnetic.

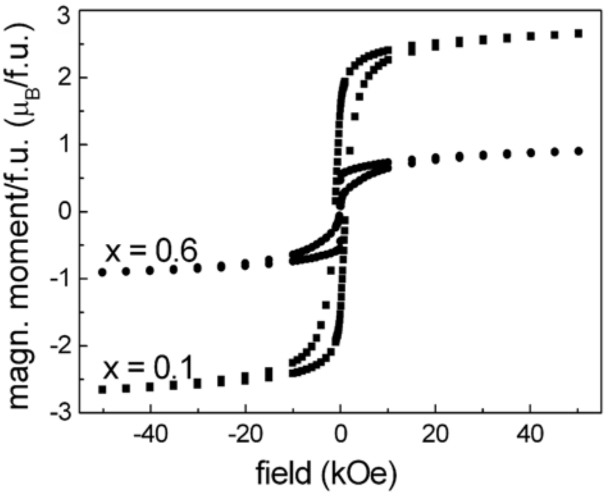

Fig. 6 Magnetic hysteresis loops of $Sr_2Fe_{1-x}Ga_xReO_6$ measured at 5 K.

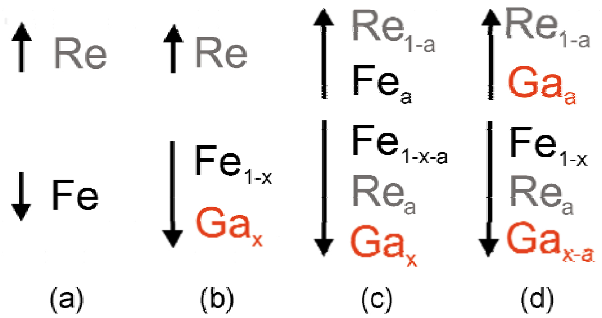

Scheme 1 Distribution of the elements Fe, Ga and Re over the two sublattices as obtained by Rietveld refinement for (a) the unsubstituted Sr_2FeReO_6, (b) the fully ordered $Sr_2Fe_{1-x}Ga_xReO_6$, (c) the Fe/Re disordered $Sr_2Fe_{1-x}Ga_xReO_6$ and (d) the Ga/Re disordered $Sr_2Fe_{1-x}Ga_xReO_6$. x indicates the Ga content, a represents the amount of disorder. The up (↑) and down (↓) arrows indicate the spin direction of the respective magnetic sublattices.

X-ray diffraction data reveal that the parent compound Sr_2FeReO_6 crystallizes without antisite disorder in the tetragonally distorted perovskite structure. (Scheme 1a) The experimental saturation magnetization of the solid solution series $Sr_2Fe_{1-x}Ga_xReO_6$ ($0 < x < 0.7$) monotonously decreases from 2.65 μ_B/f.u. for 10 % Ga substitution to 0.64 μ_B/f.u. for 70 % Ga content. (Fig. 7 □) The assumption of a perfectly ordered sublattice of Fe^{3+}, Ga^{3+}, and Re^{5+} cations (Scheme 1b) with ferromagnetic interactions within each of the two sublattices - Fe/Ga and Re - and antiferromagnetic interactions between the two sublattices leads to the following expectation for the saturation magnetization behaviour: a continuous decrease from 2.5 μ_B/f.u. for 10 % Ga substitution to 0 μ_B/f.u. for 60 % Ga content, with a subsequent increase to 0.5 μ_B/f.u. for 70 % Ga substitution. (Fig. 7 ○) Apparently, the expected trend disagrees with the experimental observation. Moreover, the results of the Rietveld refinement indicate an increasing amount of either Fe/Re or Ga/Re disorder with increasing Ga content.

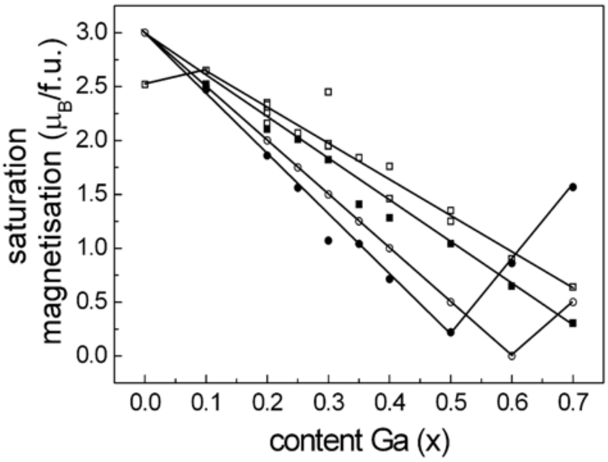

Fig. 7 Experimental saturation magnetization (□) of $Sr_2Fe_{1-x}Ga_xReO_6$ ($o < x < 0.7$) together with the expected saturation magnetization of: (○) the ordered $Sr_2Fe_{1-x}Ga_xReO_6$, (●) $Sr_2Fe_{1-x}Ga_xReO_6$ with an Fe/Re disorder value determined by Rietveld refinement and (■) $Sr_2Fe_{1-x}Ga_xReO_6$ with a Ga/Re disorder value as obtained by Rietveld refinement as a function of the Ga content. The lines serve as guide for the eyes.

The theoretical saturation magnetization of $Sr_2Fe_{1-x}Ga_xReO_6$ is estimated as a function of the Fe/Re disorder based on the following experimental results and assumptions: (i) the Fe sublattice contains the amount of Re that was obtained from the Rietveld refinement (and vice versa), (ii) the spins of all cations within the same sublattice are aligned in parallel and (iii) Ga is located in the Fe sublattice only. (Scheme 1c) The saturation magnetization obtained in this way decreases from 2.47 μ_B/f.u. to 0.2 μ_B/f.u. in the concentration range between 10 % and 50 % Ga. For Ga concentrations between 50 % and 70 % the saturation magnetization increases up to 1.57 μ_B/f.u. (Fig. 7 ●) However, the run of this curve still disagrees with the experimental results. This leads to the conclusion that our assumptions (i) – (iii) are not valid, i.e. Fe and Re do not substitute each other in an antisiting fashion. The calculated saturation magnetization for a Ga/Re type of disorder considering (i) an experimental disorder value obtained by Rietveld refinement, (ii) ferromagnetic interaction within both sublattices and antiferromagnetic interaction between them (Scheme 1d) shows a decrease from 2.52 μ_B/f.u. to 0.3 μ_B/f.u. in the concentration range 10 % < x < 70 %. (Fig. 7 ■)

This result is quite surprising. It is well established that there is virtually no Fe/Re disorder in Re based double perovskites. [4,15,37,38] On the other hand, Fe^{3+} can easily be substituted by Ga^{3+} because of the similarity of the ionic radii. Considering the structural similarity of many Ga^{3+} and Fe^{3+} compounds, a Ga/Re disorder is unexpected. The Ga/Re disorder was derived by a combination of X-ray refinements and magnetic susceptibility measurements: the concentrational dependence of the saturation magnetization could only be modelled correctly by considering a Ga/Re disorder in $Sr_2Fe_{1-x}Ga_xReO_6$ ($0 < x < 0.7$).

The magnetic susceptibility measurements, performed between 780 K and 5 K at 0.1 T, result to Curie temperatures T_C located in the range between 365 K and 401 K. In contrast to the saturation magnetization the T_C values indicate no systematic trend as a function of the Ga content. In order to verify this finding, additional batches of samples were prepared. Magnetic measurements of these samples confirmed the absence of a correlation between T_C and Ga content. This observation indicates that the disorder model presented in Scheme 1d is still not sufficient to fully explain the magnetic behaviour within the substitutional series $Sr_2Fe_{1-x}Ga_xReO_6$. Further insight is provided by Mössbauer spectroscopy, discussed in detail below.

Ga-substituted samples reveal ferrimagnetic behaviour in the total concentration range examined in this study, because the paramagnetic regime of the high-temperature magnetic susceptibility data could only be interpreted using a ferrimagnetic model. The results of the fits were used to extract the ferrimagnetic (T_C) and paramagnetic (Θ_C) Curie temperatures, interaction parameter (μ) as well as Curie constants (C_A, C_B) for the two sublattices A and B for $Sr_2Fe_{1-x}Ga_xReO_6$ (0.1 < x < 0.7). The standard function describing the molar susceptibility χ_M in molecular field approximation has been applied: [39] $\chi_M = \frac{(C_A+C_B)T-2\mu C_A C_B}{T^2-T_C^2}$ with $\Theta_C = -\frac{2\mu C_A C_B}{C_A+C_B}$ and $T_C^2 = \mu^2 C_A C_B$.

The paramagnetic Curie temperature Θ_C changes from -157 K for the parent compound to -340 K for the sample containing 20 % Ga. Between 20 % and 70 % Ga content, Θ_C shows a weak concentrational dependence. (Fig. 8) This observation can be explained by assuming itinerant magnetism, whereas a continuous decrease of Θ_C would be expected for a localized model due to diamagnetic dilution. [5,24]

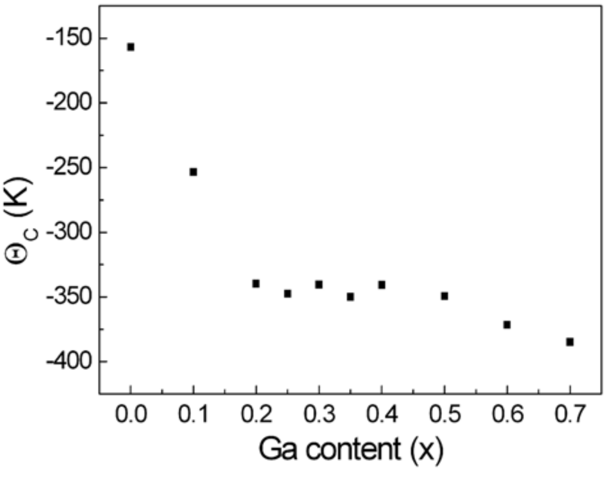

Fig. 8 Paramagnetic Curie temperature Θ_C *versus* Ga content.

The Curie constants C_A and C_B for the two sublattices A and B reveal an opposite dependence on the Ga content. (Fig. 9) Whereas C_A decreases from 8.7 cm^3K/mol to 5.3 cm^3K/mol, C_B increases from 1.2 cm^3K/mol to 3.4 cm^3K/mol with increasing Ga content, i.e. the values for C_A and C_B show a tendency to converge. This behaviour is in line with the change of the chemical compositions of the two sublattices. Together with the decrease of the Fe content for these compounds, the Re/Ga disorder increases with increasing Ga content. (Scheme 1d) In other words, the chemical compositions of the two sublattices - Fe/Ga and Re - become more similar upon Ga substitution. Moreover, the absolute values of C_A and C_B for $Sr_2Fe_{0.9}Ga_{0.1}ReO_6$ are in good agreement with values obtained for $Sr_2FeRe_{0.9}Sb_{0.1}O_6$. [24]

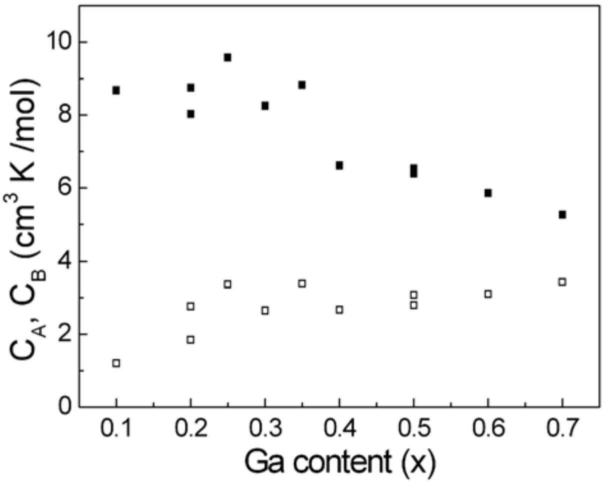

Fig. 9 Curie constants C_A (■) and C_B (□) of the two sublattices A and B *versus* Ga content.

5.3.3 Band structure calculations

The parent compound Sr_2FeReO_6 is reported to be a half-metallic ferrimagnet at room temperature with a large density of states (DOS) of one spin direction at the Fermi level E_F while the other spin direction is insulating. In the insulating spin up direction, five electrons are localized in the Fe 3*d* states whereas the Re 5*d* states are empty. The two remaining electrons are distributed over the Fe and Re *d* t_{2g} orbitals in the metallic spin down direction. [13] Our spin polarized *ab initio* band structure calculations for Sr_2GaReO_6 using the WIEN2k software package [30] show that the diamagnetic dilution of the Fe sublattice with the main group metal Ga preserves the half-metallic nature of Sr_2FeReO_6. (Fig. 10) As expected from the lack of *d* orbitals and in accordance with the fixed 3+ valence state, Ga does not participate to the DOS near E_F. Surprisingly, Sr_2GaReO_6 is calculated to be a half-metallic ferromagnet with highly spin polarized Re *d* t_{2g} - O states. The corresponding magnetic moments are zero for strontium as well as gallium, and 1.17 μ_B/f.u. for rhenium. Finally, the Ga sublattice does not destroy the ferromagnetic properties of the Re sublattice and therefore the overall half-metallic properties of Sr_2GaReO_6.

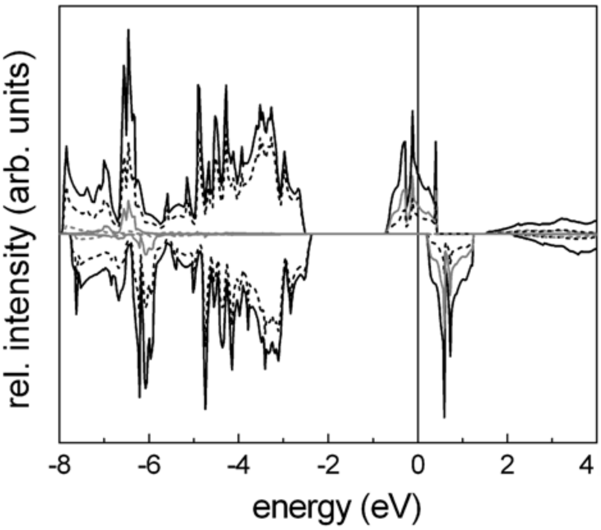

Fig. 10 Density of states of Sr_2GaReO_6, total DOS (solid black), partial DOS Re *d* e_g (grey dashed), Re *d* t_{2g} (solid grey), O (black dashed).

5.3.4 Mössbauer measurements

^{57}Fe-Mössbauer spectra of the samples with x < 0.35 exhibit magnetic sextet patterns with relatively narrow lines corresponding to the only Fe site in symmetrical environment. In the concentration range 0.35 < x < 0.7, a paramagnetic component with relative intensity of about 10 % appears in addition to the magnetic sextet. (Fig.11) The isomer shift value of the sextet δ = 0.66(1) mm/s remains constant over the total range of concentrations. The hyperfine magnetic field of 465(2) kOe is constant up to a Ga content of 35 % and decreases slowly at higher Ga concentrations attaining the value 461(1) kOe at x = 0.7. Taking into account the results of the magnetic measurements, one can conclude that in spite of the paramagnetic component all spectra correspond to magnetically ordered phases. Sharp Mössbauer lines exclude a considerable amount of microscopic disorder involving Fe atoms.

The average valence state of Fe can be estimated by comparing the isomer shift of the series $Sr_2Fe_{1-x}Ga_xReO_6$ with the isomer shift of the parent compound, δ(Fe, x = 0) = 0.67(1) mm/s. [5,24] Thus, the Fe valence state remains constant at +2.7 for the whole series leaving the role of the electronic buffer element to Re.

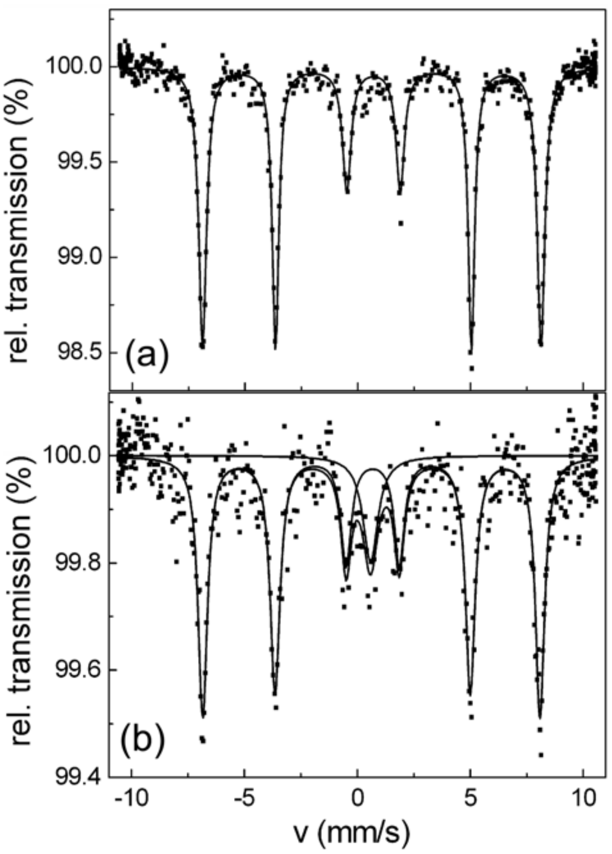

Fig. 11 ^{57}Fe Mössbauer spectra of $Sr_2Fe_{1-x}Ga_xReO_6$ (a) x = 0.2, (b) x = 0.5.

Summarizing the partial results obtained by X-ray diffraction, magnetic susceptibility measurements and Mössbauer spectroscopy, namely (i) the structural homogeneity of the samples, (ii) the concentrational independence of the Curie temperature and (iii) the presence of a magnetically ordered and a paramagnetic phase, we propose the persistence of two different types of clusters, Fe/Re- and Ga/Re-based ones. For small Ga concentrations ($x \leq 0.2$), Ga substitutes Fe in statistical fashion and disturbs the magnetic double exchange between Fe-based and Re-based magnetic sublattices. The value x = 0.2 directly follows from the concentrational dependence of the paramagnetic Curie temperature and manifests the moment where cluster formation begins. Apart from that, the concentration range up to x = 0.2 is characterized by a negligible amount of antisite Ga/Re disorder. The appearance of Ga-rich clusters is visible in the Mössbauer spectra for $x \geq 0.4$. Fe atoms located in these clusters are surrounded by diamagnetic Ga atoms and, as a consequence, reveal no hyperfine magnetic field. Presumably, the process of Ga clusterization can not be traced by means of Mössbauer spectroscopy in the concentrational range below x = 0.4 due to the absence of Fe atoms in Ga-based clusters persisting in this concentration range. The hypothesis of cluster formation also explains the fact that we do not observe Fe species with intermediate values of hyperfine magnetic field originating from configurations with different numbers of diamagnetic Ga neighbours in the first coordination sphere of the Fe atoms. The appearance of paramagnetic species in Mössbauer spectra above $x = 0.4$ coincides with an increasing degree of antisite Ga/Re disorder following from Rietveld refinement. (Table 2)

The interesting fact of hyperfine field constancy independent of the extent of diamagnetic Ga dilution attracts special attention. As mentioned above, Re adopts the role of an electronic buffer and provides the stability of the Fe valence state over the wide range of Ga substitutions. The hyperfine magnetic field on the Fe nuclei mainly depends on the Fermi contact term which depends on the imbalance of the *s* electrons. Therefore, the constant density of *s* electrons detected in the Mössbauer experiments is the reason for the concentrational independence of the hyperfine magnetic field on the Fe atoms. It seems that the static magnetic order is an important precondition, which provides the constancy of the hyperfine magnetic field even in Ga-rich samples.

5.4 Conclusions

In this study we explored the effect of diamagnetic dilution of the Fe sublattice on the structural and magnetic properties of the double perovskite $Sr_2Fe_{1-x}Ga_xReO_6$ ($0 < x < 0.7$) by means of X-ray structural analysis, magnetic characterization, Mössbauer experiments and band structure calculations. An unexpected finding is the observation of Ga/Re antisite disorder. It is a well established fact that the parent compound Sr_2FeReO_6 exhibits virtually no Fe/Re disorder. On the other hand, Fe^{3+} can easily be substituted by Ga^{3+} because of the similarity of the ionic radii, and it is for this reason, that Ga^{3+} is used for the diamagnetic dilution of ferric oxides or sulfides. The Ga/Re disorder was derived by a combination of X-ray refinements and magnetic susceptibility measurements: the concentrational dependence of the saturation magnetization can only be modelled correctly by considering a Ga/Re disorder in $Sr_2Fe_{1-x}Ga_xReO_6$ ($0 < x < 0.7$). The antisite disorder is small below $x = 0.2$, in the $0.2 < x < 0.4$ substitution range disorder is limited to approx. 5 %, whereas a significant amount of antisite disorder (> 12 %) is detected above $x = 0.4$. Although the X-ray data do not reveal any phase separation, sample inhomogeneities caused by a demixing could be observed by a combination of the magnetic characterization and Mössbauer spectroscopy. The experimental data suggest the formation of two types of clusters, ferrimagnetic Fe- and paramagnetic Ga-based ones. Below 20 % Ga content, Ga statistically dilutes the Fe–O–Re–O–Fe double exchange pathways. Cluster formation begins at 20 % Ga substitution, between 20 % and 40 % of Ga content, the paramagnetic Ga-based clusters do not contain any Fe. Fe containing Ga-based clusters which can be detected by Mössbauer spectroscopy firstly appear in $Sr_2Fe_{0.6}Ga_{0.4}ReO_6$.

Due to the Ga content dependent Ga/Re disorder, clusters with itinerant behaviour (as in the parent compound Sr_2FeReO_6) coexist with Ga-rich clusters. Re adopts the role of an electronic buffer element, which keeps the valence state of Fe constant over a wide Ga substitution range. Therefore, Re should be viewed as the basic magnetic element which provides the static ferrimagnetic order for higher Ga substitution levels.

5.5 References

[1] J. Longo and R. Ward, *J. Am. Chem. Soc.*, 1961, **83**, 2816.

[2] A. W. Sleight, J. Longo and R. Ward, *Inorg. Chem.*, 1962, **1**, 245.

[3] J. M. De Teresa, D. Serrate, C. Ritter, J. Blasco, M. R. Ibarra, L. Morellon and W. Tokarz, *Phys. Rev. B*, 2005, **71**, 092408.

[4] H. Kato, T. Okuda, Y. Okimoto, Y. Tomioka, K. Oikawa, T. Kamiyama and Y. Tokura, *Phys. Rev. B*, 2002, **65**, 144404.

[5] A. Jung, I. Bonn, V. Ksenofontov, G. Melnyk, J. Ensling, C. Felser and W. Tremel, *J. Mater. Chem.*, 2005, **15**, 1760.

[6] H. Kato, T. Okuda, Y. Okimoto, Y. Tomioka, K. Oikawa, T. Kamiyama and Y. Tokura., *Phys. Rev. B*, 2004, **69**, 184412.

[7] H. Kawanaka, I. Hase, S. Toyama and Y. Nishihara, *J. Phys. Soc. Jpn.*, 1999, **68**, 2890.

[8] A. K. Azad, S. Ivanov, S.-G. Eriksson, H. Rundlof, J. Eriksen, R. Mathieu and P. Svedlindh, *J. Magn. Magn. Mater.*, 2001, **237**, 124.

[9] M. C. Viola, M. J. Martinez-Lope, J. A. Alonso, P. Velasco, J. L. Martinez, J. C. Pedregosa, R. E. Carbonio and M. T. Fernandez-Diaz, *Chem. Mater.*, 2002, **14**, 812.

[10] M. J. Martinez-Lope, J. A. Alonso and M. T. Casais, *Eur. J. Inorg. Chem.*, 2003, **15**, 2839.

[11] T. S. Chan, R. S. Liu, G. Y. Guo, S. F. Hu, J. G. Lin, J.-F.Lee, L.-Y. Jang, C.-R. Chang and C. Y. Huang, *Solid State Comm.,* 2004, **131**, 531.

[12] K.-I. Kobayashi, T. Kimura, H. Sawada, K. Terakura and Y. Tokura, *Nature*, 1998, **395**, 677.

[13] K.-I. Kobayashi, T. Kimura, Y. Tomioka, H. Sawada, K. Terakura and Y. Tokura, *Phys. Rev. B*, 1999, **59**, 11159.

[14] T. H. Kim, M. Uehara, S.-W. Cheong and S. Lee, *Appl. Phys. Lett.*, 1999, **74**, 1737.

[15] W. Prellier, V. Smolyaninova, A. Biswas, C. Galley, R. L. Greene, K. Ramesha and J. Gopalakrishnan, *J. Phys.: Condens. Matter*, 2000, **12**, 965.

[16] A. W. Sleight and J. F. Weiher, *J. Phys. Chem. Solids*, 1972, **33**, 679.

[17] A. Maignan, B. Raveau, C. Martin and M. Hervieu, *J. Solid State Chem.*, 1999, **144**, 224.

[18] J. A. Alonso, M. T. Casais, M. J. Martinez-Lope, J. L. Martinez, P. Velasco, A. Munoz and M. T. Fernandez-Diaz, *Chem. Mater.*, 2000, **12**, 161.

[19] D. D. Sarma, E. V. Sampathkumaran,; S. Ray, R. Nagarajan, S. Majumdar, A. Kumar, G. Nalini and T. N.G. Row, *Solid State Comm.*, 2000, **114**, 465.

[20] C. Ritter, M. R. Ibarra, L. Morellon, J. Blasco, J. Garcia and J. M. De Teresa, *J. Phys.: Cond. Mat.*, 2000, **12**, 8295.

[21] Z. Fang, K. Terakura and J. Kanamori, *Phys. Rev. B*, 2001, **63**, 180407.

[22] C. Zener, *Phys. Rev.*, 1951, **81**, 440; C. Zener, *Phys. Rev.*, 1951, **82**, 403; C. Zener, *Phys. Rev.*, 1951, **83**, 299; C. Zener, *Phys. Rev.*, 1952, **85**, 324.

[23] F. Sher, A. Venimadhav, M. G. Blamire, B. Dabrowski, S. Kolesnik and J. P. Attfield, *Solid State Sci.*, 2005, **7**, 912.

[24] A. Jung, V. Ksenofontov, S. Reiman, H. A. Therese, U. Kolb, C. Felser and W. Tremel, *Phys. Rev. B*, 2006, in print.

[25] K. G. Bramnik, H. Ehrenberg, J. K. Dehn and H. Fuess, *Solid State Sci.*, 2003, **5**, 235.

[26] T. J. Gray, *J. Power Sources*, 1981, **6**, 121.

[27] J. Rodríguez-Carvajal, *Physica B*, 1993,**192**, 55.

[28] W. Haberditzl, *Magnetochemie*, Akademie-Verlag: Berlin, 1968.

[29] K. Lagarec and D. G. Rancourt, *Nucl. Instrum. Methods Phys. Res. B*, 1997, **129**, 266.

[30] P. Blaha, K. Schwarz, G. K. H. Madsen, D. Kvasnicka and J. Luitz, Wien2k, An augmented plain wave + local orbitals program for calculating crystal properties, (Karlheinz Schwarz, Techn. Universtität Wien, Austria) 2001.

[31] R. Scholder and P. P. Pfeiffer, *Angew. Chem., Int. Ed. Engl.*, 1963, **2**, 265.

[32] R. D. Shannon, *Acta Crystallogr.*, 1976, **A32**, 751.

[33] G. Popov, M. Greenblatt and M. Croft, *Phys. Rev. B*, 2003, **67**, 024406.

[34] U. Müller, *Anorganische Strukturchemie*, Teubner Studienbücher: Stuttgart, 1996.

[35] E. Carvajal, O. Navarro, R. Allub, M, Avignon and B. Alascio, *Phys. Stat. Sol. B*, 2005, **242**, 1942.

[36] A. Poddar and S. Das, *Physica B – Cond. Mat.*, 2004, **344**, 325.

[37] J. Gopalakrishnan, A. Chattopashyay, S. B. Ogale, T. Venkatesan, R. L. Greene, A. J. Millis, K. Ramesha, B. Hannoyer and G. Marest, *Phys. Rev. B*, 2000, **62**, 9538.

[38] N. Rammeh, K. G. Bramnik, H. Ehrenberg, H. Fuess and A. Cheikh-Rouhou, *J. Magn. Magn. Mater.*, 2004, **278**, 14.

[39] C. Kittel, *Introduction to solid state physics*, VCH Wiley: New York, London, Sydney, Toronto, 1976.

6. Conclusion

In the course of this work the effect of metal substitution on the structural and magnetic properties of the double perovskites $Sr_2MM'O_6$ (M = Fe, substituted by Cr, Zn and Ga; M' = Re, substituted by Sb) was explored by means of X-ray diffraction, magnetic measurements, band structure calculations, Mößbauer spectroscopy and conductivity measurements. The focus of this study was the determination of (i) the kind and structural boundary conditions of the magnetic interaction between the M and M' cations and (ii) the conditions for the principal application of double perovskites as spintronic materials by means of the band model approach.

Band structure calculations for the double perovskite Sr_2FeReO_6 indicate the Fermi level to be situated slightly higher in energy than the van Hove-singularity. Therefore, the number of valence electrons guaranteeing a coincidence of the Fermi level and the van Hove-singularity can be achieved by hole "doping", i.e. a decrease of the valence electron concentration. The validity of this model in the preferred hole "doping" as well as the unpreferable electron "doping" mode was demonstrated by substituting the parent compound with Cr (hole "doping") and Zn (electron "doping"), respectively.

Both series of solid solutions $Sr_2Fe_{1-x}Cr_xReO_6$ ($0 \leq x \leq 0.9$) and $Sr_2Fe_{1-x}Zn_xReO_6$ ($0 \leq x \leq 0.9$) adopt the double perovskite structure type. The samples exhibit only a slight amount of antisite disorder. In accordance to the behaviour expected from the geometrical model expressed in terms of the perovskite tolerance factor *t* the strength of the tetragonal distortion increases upon increasing Zn content. On the other hand, the strength of tetragonal distortion decreases upon Cr substitution and samples are cubic for $x \geq 0.4$. The substitution of Fe by Cr up to the optimal valence electron count leads to an enhancement of the saturation magnetization. Further reduction of the valence electron count turns this tendency. The linear decrease of lattice constants and unit cell volume together with the tetragonal to cubic transition leads to an increasing electronic band width and Curie temperature of $Sr_2Fe_{1-x}Cr_xReO_6$. In contrast, Zn substitution enforces a monotonic decrease of the saturation magnetization owing to an increase of the valence electron concentration. The diamagnetic dilution of the Fe-sublattice leads to a transition from an itinerant ferrimagnetic to a localized ferromagnetic material. Thus, Zn substitution inhibits the long-range ferromagnetic interaction within the Fe-sublattice and preserves the long-range ferromagnetic interaction within the Re-sublattice. The temperature dependence of T_C can be explained by the competition of structural and electronic effects. The slow decrease of T_C up to a substitution level of 60 % originates from the increasing amount of tetragonal distortion together with the increase of the lattices constants. The strong decrease for $x > 0.6$ coincides with the transition from itinerant to localized magnetism. However, the end member of the Zn solid solution series, Sr_2ZnReO_6, exhibits a complicated magnetic structure.

Temperature and field dependent susceptibility measurements hint at (i) a ferro- or ferrimagnetic order of the Re^{6+} ($5d^1$) spins below 18 K and (ii) a paramagnetic state above 27 K. The magnetic structure between T_C = 18 K and the transition at 27 K is subject to ongoing investigations.

In order to elucidate the nature of the magnetic interaction between the M and M' cations, Fe and Re were substituted by the valence invariant main group metals Ga and Sb, respectively. As Ga and Sb lack *d* orbitals at the Fermi level, the long-range ferromagnetic interaction within the Fe- and Re-sublattices of $Sr_2Fe_{1-x}Ga_xReO_6$ ($0 \leq x \leq 0.7$) and $Sr_2FeRe_{1-x}Sb_xO_6$ ($0 \leq x \leq 0.9$), respectively, are bleached by inhibiting the Zener double exchange via the M–O–M'–O–M units.

The compounds of the series of solid solutions $Sr_2FeRe_{1-x}Sb_xO_6$ crystallize in the tetragonally distorted double perovskite structure type. Antisite disorder is reduced to 2 %. Up to a substitution level of 30 % the ferromagnetic arrangement of the magnetic moments of Fe and Re in their appropriate sublattices is mediated by a Zener double exchange via oxygen atoms leading to an overall ferrimagnetic behaviour. In contrast, for large Sb contents ($x \geq 0.6$) a macroscopic antiferromagnetic behaviour is observed. The absence of antisite disorder excludes this antiferromagnetism to originate from a superexchange via Fe–O–Fe units. Mössbauer spectroscopy indicates the coexistence of ferri- and antiferromagnetic type of clusters on the microscopic level in all samples, except for Sr_2FeReO_6 and $Sr_2FeRe_{0.1}Sb_{0.9}O_6$, which are purely ferri- and antiferromagnetic, respectively. Sb rich samples are calculated and measured to be semiconductors or insulators by band structure calculations and conductivity measurements. Thus, replacing Re by Sb leads to a transition from an itinerant ferrimagnet for low substitution levels to a localized antiferromagnet for high substitution levels. The antiferromagnetic behaviour in the double perovskites $Sr_2FeRe_{1-x}Sb_xO_6$ ($0.6 < x < 0.9$) seems to originate from a direct antiferromagnetic interaction between the Fe atoms. Sb seems to block the double exchange pathways as it (i) does not contribute to electronic states at the Fermi level and (ii) shows no magnetic splitting in the Mössbauer spectra. As a consequence of the bleaching of the double exchange pathways by substitution of Re by Sb, the magnetic behaviour of $Sr_2FeRe_{1-x}Sb_xO_6$ is determined by Fe^{3+}.

In case of $Sr_2Fe_{1-x}Ga_xReO_6$ ($0 \leq x \leq 0.7$) the inference to the principles of magnetic interaction from the measured magnetic properties is further complicated by the unexpected formation of two types of clusters, ferrimagnetic Fe- and paramagnetic Ga-based ones. The samples of this series of solid solutions crystallize in the tetragonal space group *I*4/*mmm*. As expected from the ionic radii of Ga^{3+} (r = 62 pm) and Fe^{3+} (r = 65 pm), lattice parameters and unit cell volume decrease and the amount of tetragonal distortion is reduced upon Ga^{3+} substitution. X-ray powder diffraction investigations do not point to a phase separation. Yet, a Ga^{3+} content dependent amount of disorder was proven. The antisite disorder is small below x = 0.2 and limited to approx. 5 % in the $0.2 < x < 0.4$ substitution range, whereas a significant amount of antisite disorder (> 12 %) is detected above x = 0.4. The type of disorder was derived by a combination of X-ray powder diffraction and magnetic susceptibility investigations. The concentrational dependence of the saturation magnetization can only be modelled correctly by considering a Ga/Re type of disorder. Moreover, magnetic characterization and Mössbauer spectroscopy data indicate sample inhomogeneities due to a microscopic demixing of the metal cations. The experimental data suggest the formation of two types of clusters, ferrimagnetic Fe- and paramagnetic Ga-based ones. Below 20 % Ga content, Ga statistically dilutes the Fe–O–Re–O–Fe double exchange pathways. Cluster formation is observed above 20 % Ga substitution, between 20 % and 40 % of Ga content, the paramagnetic Ga-based clusters do not contain any Fe. Fe containing Ga-based clusters, which can be detected by Mössbauer spectroscopy, are observed above x = 0.4. Due to the Ga dependent Ga/Re disorder, clusters with itinerant magnetic behaviour (as in the parent compound Sr_2FeReO_6) coexist along with Ga-rich clusters. Re adopts the role of an electronic buffer element, which keeps the valence state of Fe constant over a wide Ga substitution range. Therefore, Re should be viewed as the basic magnetic element which provides the static ferrimagnetic order for higher Ga substitution levels.

A necessary condition for half-metallic ferrimagnetic properties in $Sr_2MM'O_6$ double perovskites is the mediation of the magnetic interaction between the M and M' cations by means of a Zener double exchange mechanism via M–O–M'–O–M units. This condition can be fulfilled only if the M and M' cations are transition metals with open *d* shells. If the open *d* shell metals M and M' are substituted by closed shell metals, two different magnetic behaviours are observed. Substitution of Re (M') results in macroscopic antiferromagnetic behaviour, which has to be explained by direct magnetic coupling of the Fe^{3+} ions. On the other hand, substitution of Fe (M) by closed shell metals leads to different magnetic and structural behaviour depending on the element itself. For Ga substitution, it leads to cluster formation and for Zn substitution to complicated magnetic structures. Thus, in case of solid solution studies on Sr_2FeReO_6, the resulting magnetic structure is determined by the peculiarities of Fe.

The band model approach is a useful tool for the prediction of potential candidates for spintronic applications. $Sr_2Fe_{1-x}Cr_xReO_6$ is selected as a promising series of solid solutions, because Cr fulfils the requirements of a small cationic radius compared to Fe and a smaller valence electron number. Thus, slight amounts of Cr on the M site lead to an improved interaction of the M and M' *d* orbitals due to a reduction of the tetragonal distortion. The partial depletion of the conduction band towards the optimal valence electron concentration enhances the saturation magnetization and the Curie temperature and -probably- the MR effect of the parent compound.